Loss of Asxl1 and Ezh2 cooperates in pathogenesis of haematological malignancies a potential mouse model for CLL pre-clinical study

Tsai, Ray

Awarding institution:
King's College London

Loss of Asxl1 and Ezh2 cooperates in pathogenesis of haematological malignancies: a potential mouse model for CLL pre-clinical study

Chiou-Tsun Tsai

2019

A thesis presented for the degree of

Doctor of Philosophy

Department of Haematological Medicine

King's College London 2019

Declaration

I am hereby declaring this thesis is my own work and not submitted to any other institutes for award. Where other sources of information have been used, they have been acknowledged.

Chiou-Tsun Tsai

2019

Abstract

Loss-of-function mutations of *ASXL1* or/and *EZH2* are frequently found in patients with myeloid neoplasms, and their co-occurrence tends to result in more prognostically detrimental outcomes. While single knockout of *Ezh2* in haematopoietic cells led to development of mild myelodysplastic disorders in the mouse model, double knockout of *Asxl1* and *Ezh2* further provided myeloproliferative features and promoted disease progress, resulting in a severe myelodysplastic/myeloproliferative neoplasm (MDS/MPN) phenotype. Intriguingly, in addition to myeloid malignancies, B-cell lymphoproliferative disorders (B-LPD) were also identified in *Ezh2* cKO mice, and genetic co-inactivation of Asxl1 with Ezh2 enhanced the mono-clonal expansion and bone marrow infiltration of B1α cells, which ultimately progressed to an aggressive chronic lymphocytic leukaemia (CLL) phenotype with short latency and high-risk symptoms in secondary and tertiary transplantation. Meanwhile, while RNA-seq profiling revealed that active B cell receptor (BCR) signalling was crucial for the development of B-cell malignancies in Ezh2 single mutants, more critical genes involved in leukaemogenesis of CLL such as *BCL-2*, *Myc*, *Cxcr5* and *Aicda* were further upregulated in Asxl1/Ezh2 double mutants, accounting for their aggressive properties of high cell division and organ infiltration.

Furthermore, genetic and pharmacological inhibition of Ezh2 enhanced the anti-cancer effects of PARP inhibitors in acute myeloid leukaemia (AML) cells in vitro, providing a new strategy for improving the efficacy of PARP inhibitors in cancer therapy. Meanwhile, the transcriptional profiling displayed active BCR signalosome, base excision repair (BER) and *Aicda* overexpression in *Asxl1*/*Ezh2* cKO CLL mice, further implying BTK and PARP1 as potential targets for the PRC2-deficient CLL. In vivo, while ibrutinib slightly delayed the disease latency with relief of cytopenia, the PARP inhibitor olaparib

significantly prolonged the survival of *Asxl1*/*Ezh2* cKO CLL mice and alleviated splenomegaly, showing therapeutic promises of targeting PARP1 for the treatment of human CLL with loss of PRC2 or the correlated transcriptional profiling.

Acknowledgements

It was merely impossible for me to go through the 4-year PhD study without enough funding from my country. I would like to thank my families for their fullhearted support and Prof. Eric Chi-Wai So for kindly offering me an opportunity to pursue my PhD degree and providing a resourceful research environment for my study. I would never overcome the financial challenges and frustrations without their help. Completing the PhD study is not only approval for my endeavour but also a glory for my life.

I would like to thank Clemence Virely particularly for her help in setting up primary transplantation and collecting samples for the study of early haematopoiesis and Dr Robbert Hoogeboom for his advice in CLL mouse modelling. It is also my honour to work with the senior scientist Bernd Zeisig, Amanda Wilson and other outstanding researchers Ngai Cheung, Tsz Kan Fung, Priscilla Lau, Kar lok Kong, Lu Zhao, Jie Chen and Jennifer Lynch in the laboratory. Thank you so much for your professional direction, suggestions and discussion, all of which give me delight of doing research and shape my expertise during the period.

Also, I want to thank my PhD fellow students as well as kindred spirits Siyi Zhang, Ka Lam Ng, Claire Lynn and Mickey Wong for your mental and physical supports, and it is very lucky to have you in this stage. Our companionship did help me conquer many challenges while studying, and the friendship will last forever.

Table of Contents

List of figures

List of tables

List of abbreviations

Aicda Activation-induced cytidine deaminase

AML Acute myeloid leukaemia

Asxl1 Additional sex combs-like 1

BCR B cell receptor

BER Base excision repair

MMR Mismatch repair

B-LPD B-cell lymphoproliferative disorders

BM Bone marrow

BTKi Bruton's tyrosine kinase inhibitor

CLL Chronic lymphocytic leukaemia

CMML Chronic myelomonocytic leukaemia

CMP Common myeloid progenitor

cKO Conditional knockout

DDR DNA damage response

EMH Extramedullary haematopoiesis

Ezh2 Enhancer of zeste homolog 2

GMP Granulocyte-macrophage progenitor

HCDR Heavy chain complementarity-determining region

Hgb Haemoglobin

HR Homologous recombination

HSCs Haematopoietic stem cells

HSPCs Haematopoietic stem/progenitor cells

H2A119ub1 Histone 2A lysine 9 monoubiquitination

γH2AX Phospho-histone 2AX

H3K27me3 Histone 3 lysine 27 trimethylation

IGHV Immunoglobulin heavy chain variable region

I.V. Intravenous

I.P. Intraperitoneal

LSK Linage^{-}Sca1^{+}c-Kit^{+}

LT-HSC Long term haematopoietic stem cells

ST- HSC Short term haematopoietic stem cells

MBL monoclonal B-cell lymphocytosis

M-CLL (IGHV-mutated CLL)

MDS Myelodysplastic syndrome

MDS/MPN Myelodysplastic/myeloproliferative neoplasm

MEP Megakaryocyte-erythroid progenitor

MPN Myeloproliferative neoplasm

MPP Multipotent progenitor

NHL Non-Hodgkin's lymphoma

PARPi Poly ADP ribose polymerase inhibitor

PB Peripheral blood

Plt Platelet

PMF Primary myelofibrosis

PRC2 Polycomb repressor complex 2

T-ALL T-cell acute lymphoblastic leukaemia

TAM Tamoxifen

TC Thrombocytosis

U-CLL (IGHV-unmutated CLL)

WBC White blood cells

Charter 1: Background

1.1. Overview of haematopoiesis and haematologic malignancies

Haematopoiesis is a highly dynamic developmental process with sophisticated regulation in self-renewal and differentiation of haematopoietic stem cells (HSCs) in order to maintain the lifelong reproduction of blood cells. In mammalian haematopoietic systems, mice for example, the primitive haematopoiesis is originated from embryonic yolk sac in mouse embryonic day 7.5 (E7.5), with production of erythrocytes and limited differentiation of myeloid lineages, to the aorta–gonad–mesonephros (AGM) (E9.5), with definitive haematopoiesis contributing to all haematopoietic lineages in foetus and adult mice. Afterwards, HSCs colonize in foetal livers (E12.5) and ultimately migrate to bone marrow (BM) before birth that support haematopoiesis throughout the whole life (Figure 1.1A) (Hu and Shilatifard, 2016). Therefore, mouse haematopoietic cells are normally collected from BM and foetal livers for experimental transplantation and analysis. While HSCs stay in a quiescent status but retain capability of multipotency and self-renewal, they give rise to all types of distinct mature blood cells through a hierarchical differentiation cascade, from the multipotent progenitors (MPP and LMPP), myeloid progenitors (CMP, GMP and MEP) and lymphoid progenitors (CLP) to the downstream mature red blood cells, platelets and white blood cells involved in innate and adaptive immune system (Figure 1.1B) (Doulatov et al., 2012; Li and Clevers, 2010), and the dynamic equilibrium between self-renewal and multipotent differentiation attributes to a variety of intrinsic and extrinsic factors involved in niche-association, signalling pathways, transcriptional regulation and chromatin modification. Perturbation or dysregulation of the process

potentially leads to various haematopoietic defects from bone marrow failure to haematopoietic malignancies.

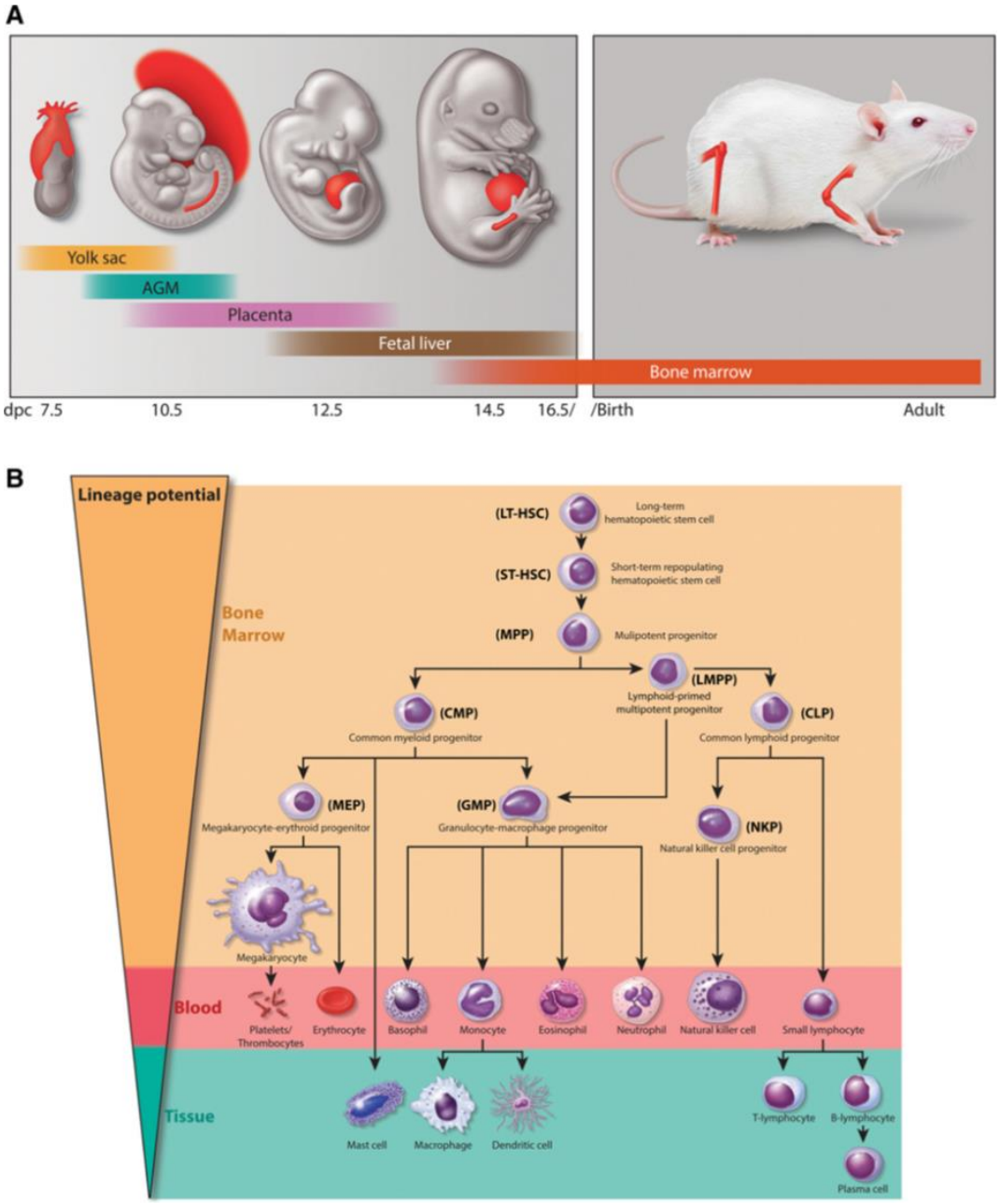

Figure1.1. Haematopoietic systems in mammals. Adapted from (Hu and Shilatifard, 2016). (A) Development of haematopoietic activity from embryonic tissues to bone marrow of mice. Aorta–gonad–mesonephros (AGM); Days post coitum (dpc) (B) Schematic overview of haematopoietic cascade from haematopoietic stem cells (HSCs) with capability of self-renewal and multipotent potential to progenitors and terminal mature immune cells in PB and secondary immune organs.

1.1.1. Myeloid neoplasms

Myeloid neoplasms refer to all haematologic neoplasms with features of myeloid lineages, including granulocytic, monocytic/macrophage, erythroid, and megakaryocytic lineages, and cover a range of heterogenous malignancies from mild myelodysplastic disorders such as myelodysplastic syndromes (MDS) to myeloproliferative neoplasms (MPN) and acute myeloid leukaemia (AML) (Vardiman et al., 2009). Morphological, cytochemical, and immunophenotypic features in initial diagnostic peripheral blood (PB) and BM specimens are crucial for identification of the lineages of neoplastic cells and assessment for their maturation. Meanwhile, the percentage of blasts are still the practical indicator for categorizing the malignancies and disease progression. By definition, a myeloid neoplasm with ≥20 % blasts in PB or BM is regarded as AML either from de-novo evolution or secondary transformation. While cytogenetic abnormalities involving recurrent gene rearrangements resulting in chimera fusions such as PML-RARα (t(15:17)), AML1-ETO (t(8:21)), MLL fusions (11q23) and CBFP-MYH11 (inv(16)) could be the major event for leukaemogenesis of de-novo AML, which usually leads to assembly of gigantic transcriptional complexes and re-writes the transcriptional profiling (Figure 1.2) (Zeisig et al., 2012), accumulation of gene mutations involved in signalling pathways (e.g. *CBL*, *FLT3*, *NRAS*, *JAK2*), transcriptional factors (e.g. *CEBPA*, *RUNX1*, *ETV6*, *TP53*), epigenetic regulators (e.g. *DNMT3A*, *TET2*, *IDH1*, *IDH2*, *ASXL1*, *EZH2*), and spliceosome (e.g. *SF3B1*) with normal karyotype may also result in evolution from previously diagnosed myelodysplastic disorders such as MDS and MPN to secondary AML (Murati et al., 2012) (Mufti, 2004).

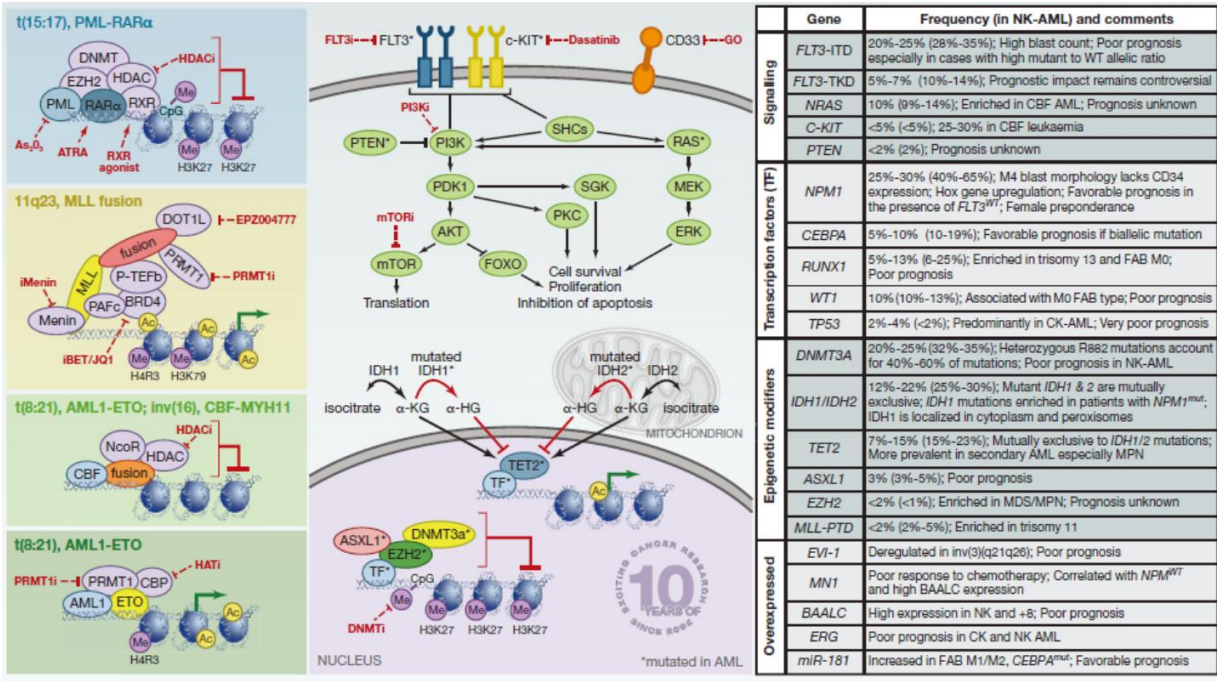

	Gene	Frequency (in NK-AML) and comments
Signalling	*FLT3*-ITD	20%-25% (28%-35%); High blast count; Poor prognosis especially in cases with high mutant to WT allelic ratio
	FLT3-TKD	5%-7% (10%-14%); Prognostic impact remains controversial
	NRAS	10% (9%-14%); Enriched in CBF AML; Prognosis unknown
	C-KIT	<5% (<5%); 25-30% in CBF leukaemia
	PTEN	<2% (2%); Prognosis unknown
Transcription factors (TF)	*NPM1*	25%-30% (40%-65%); M4 blast morphology lacks CD34 expression; Hox gene upregulation; Favorable prognosis in the presence of $FLT3^{WT}$; Female preponderance
	CEBPA	5%-10% (10-19%); Favorable prognosis if biallelic mutation
	RUNX1	5%-13% (6-25%); Enriched in trisomy 13 and FAB M0; Poor prognosis
	WT1	10% (10%-13%); Associated with M0 FAB type; Poor prognosis
	TP53	2%-4% (<2%); Predominantly in CK-AML; Very poor prognosis
Epigenetic modifiers	*DNMT3A*	20%-25% (32%-35%); Heterozygous R882 mutations account for 40%-60% of mutations; Poor prognosis in NK-AML
	IDH1/IDH2	12%-22% (25%-30%); Mutant *IDH1 & 2* are mutually exclusive; *IDH1* mutations enriched in patients with $NPM1^{mut}$; IDH1 is localized in cytoplasm and peroxisomes
	TET2	7%-15% (15%-23%); Mutually exclusive to *IDH1/2* mutations; More prevalent in secondary AML especially MPN
	ASXL1	3% (3%-5%); Poor prognosis
	EZH2	<2% (<1%); Enriched in MDS/MPN; Prognosis unknown
	MLL-PTD	<2% (2%-5%); Enriched in trisomy 11
Overexpressed	*EVI-1*	Deregulated in inv(3)(q21q26); Poor prognosis
	MN1	Poor response to chemotherapy; Correlated with NPM^{WT} and high BAALC expression
	BAALC	High expression in NK and +8; Poor prognosis
	ERG	Poor prognosis in CK and NK AML
	miR-181	Increased in FAB M1/M2, $CEBPA^{mut}$; Favorable prognosis

Figure 1.2. Molecular mechanism and recurrent mutations in AML. Adapted from (Zeisig et al., 2012). Left 4 panels show common chimeric proteins and transcriptional complexes that they assemble, usually resulting in epigenetic dysregulation and leading to leukaemogenesis of AML. The middle diagram illustrates the transcriptional factors, epigenetic modifiers and signalling pathways involved in leukaemogenesis, and their frequency of mutations found in AML with normal karyotype (right table).

MDS is a group of diversified BM disorders characterized with impaired and ineffective haematopoiesis in myeloid lineages (myelodysplasia), which subsequently leads to cytopenia such as anaemia (low levels of red blood cells (RBC)), neutropenia and thrombocytopenia due to failure of maturation of myeloid cells (Mufti, 2004), and in human, the minimal morphological criteria for the diagnosis of MDS is the presence of at least 10% dysplastic cells within one particular myeloid lineage (erythroid, granulocytic, megakaryocytic) (Bowen et al., 2003). Moreover, MDS can be further classified into several subtypes (e.g. refractory anaemia with ring sideroblasts (RARS), refractory cytopenia with multilineage dysplasia (RCMD)) according to cytological characters and blood findings (Vardiman et al., 2009). On the other hand, MPN is

characterized with indolent clonal proliferation of one or more myeloid lineages in BM, ultimately resulting in expansion of terminal mature myeloid cells in PB, and can be divided into two subtypes based on detection of Philadelphia chromosome (*BCR-ABL1* fusion gene). While chronic myeloid leukaemia (CML) is diagnosed by the appearance of *BCR-ABL1* in BM biopsies, the other *BCR-ABL1* negative MPN subtypes such as polycythemia vera (PV), essential thrombocythemia (ET) and primary myelofibrosis (PMF) can be determined according to clinical and laboratory features with histopathological examination. In addition to *BCR-ABL1* positive MPN, in *BCR-ABL1* negative MPN, mutations in protein tyrosine kinase such as *JAK2*V167F has been found in most of PV and half of PMF, suggesting the important roles of activating mutations of protein tyrosine kinase (PTK) in development of MPN (Jones et al., 2005; Tefferi et al., 2005).

The 2001 World Health Organization (WHO)-sponsored classification of haematopoietic tumour has, for the first time, defined a rare group of myeloid neoplasms termed myelodysplastic/myeloproliferative neoplasms (MDS/MPN), characterized with simultaneous presence of myelodysplastic and myeloproliferative features (Orazi and Germing, 2008). While MDS-like features like cytopenia and occurrence of dysplasia in myeloid lineages might be seen in the patients, features commonly associated with MPN such as leucocytosis, thrombocytosis and organomegaly are observed as well, and amongst this group, chronic myelomonocytic leukaemia (CMML), atypical chronic myeloid leukaemia (aCML), juvenile myelomonocytic leukaemia (JMML) and MDS/MPN with ring sideroblasts and thrombocytosis (RARS-T) are best-defined entities (Vardiman et al., 2009). CMML is unequivocally defined by its monocytosis in PB, and aCML shares similar features with *BCR-ABL1* positive CML, including splenomegaly due to leukaemic infiltration,

elevation of granulocytic cells in PB and moderate anaemia. However, aCML could be further distinguished from CML by its myelodysplasia in granulopoiesis (Oscier, 1997).

1.1.2. Lymphoid neoplasms

Lymphoid neoplasms are a group of blood cancers sharing features of lymphoid lineages, ranging from the most indolent to the most aggressive human malignancies, and may present as leukaemia, lymphoma or both (Campo et al., 2011). While leukaemia results from excessive production of abnormal white blood cells in bone marrow or blood forming organs, leading to circulation of leukaemic cells in blood, lymphoma is derived from transformation of lymphocytes residing in lymph nodes, and lymphoma can be further divided into two main types: Hodgkin's lymphoma, the first discovered haematological malignancy in 1832 with identification of Reed-Sternberg cells (Aisenberg, 2000), and non-Hodgkin's lymphoma (NHL), which contributes to more than half of lymphoid neoplasms. The majority of NHL is B cell lymphoma, comprising indolent NHL such as follicular lymphoma (FL), mantle cell lymphoma (MCL), marginal zone lymphoma to aggressive NHL like diffuse large B-cell lymphoma (DLBCL) and Burkitt's lymphoma. Nowadays, lymphoid neoplasms can be categorized into several subtypes of precursor B-cell/T-cell neoplasms (B-ALL or T-ALL) and mature B cell/T cell neoplasms (e.g. chronic lymphocytic leukaemia (CLL) and NHLs) based on morphologic, clinical, immunophenotypic, and genetic information. Clinical evaluation of lymphocytosis by internists and haematologists is usually the first line for diagnosis of mature B-cell neoplasms, and a general approach has been set up for the workup (Figure 1.3). A threshold of $\geq 5\times10^9$ /L absolute lymphocyte counts (ALC) is suggested for the further investigation (Strati and Shanafelt, 2015), and a complete history and physical examination is the step to rule

out the common causes resulting from reactive lymphocytosis, virus infection or autoimmune responses for examples. Furthermore, the clonality and neoplastic origins are evaluated through analysis of the ratio of kappa/lambda light chains and surface markers by means of flow cytometry, and B cell count is crucial criteria for distinguishing CLL from the precursor stage monoclonal B-cell lymphocytosis (MBL) (Marti et al., 2005).

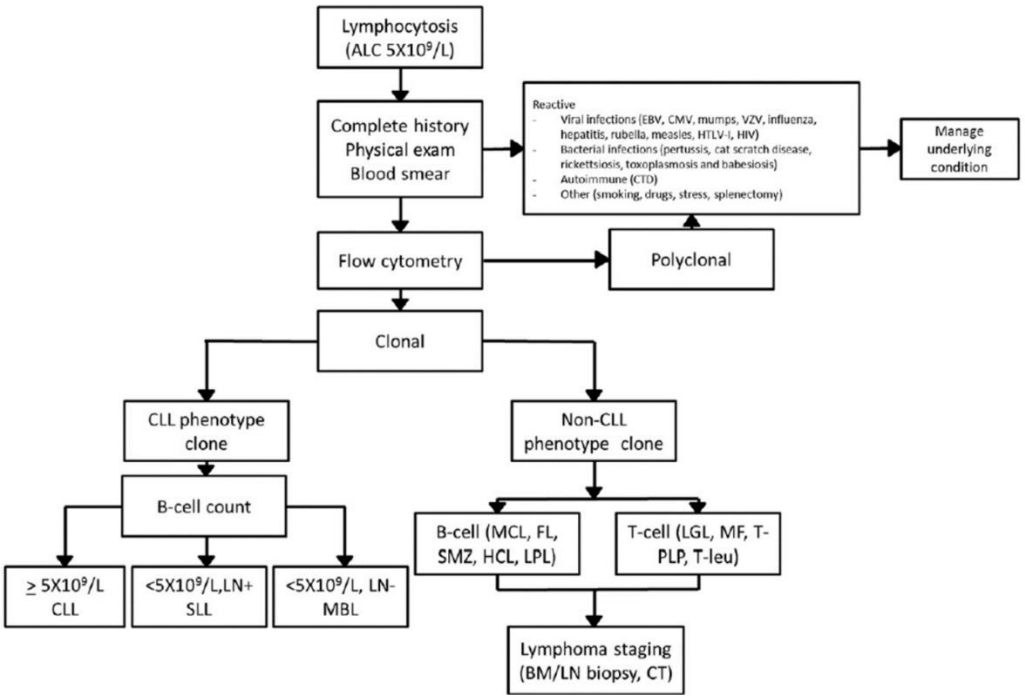

Figure 1.3. General approach to the workup of lymphocytosis. Adapted from (Strati and Shanafelt, 2015). Absolute lymphocyte number (ALC); Cytomegalovirus (CMV); Connective tissue disease (CTD); Epstein-Barr virus (EBV); Human T-lymphotropic virus (HTLV); varicella zoster virus (VZV); Follicular lymphoma (FL); Hairy cell leukaemia (HCL); Large-granular leukaemia (LGL); Lymph nodes (LN); Lymphoplasmacytic lymphoma (LPL); Mantle cell lymphoma (MCL); Splenic marginal zone lymphoma (SMZ); Mycosis fungoides (MF); T prolymphocytic leukaemia (T-PLP); T-cell leukaemia (T-leu).

1.1.3. Chronic lymphocytic leukaemia

Chronic lymphocytic leukaemia (CLL), the most common adult leukaemia in western countries, is characterized with accumulation of mono-clonal $CD5^+$ B cells in the PB, bone marrow, and secondary lymphoid organs such as spleens and lymph nodes, resulting in lymphocytosis, infiltration of neoplastic small lymphocytes into bone marrow, organomegaly and lymphadenopathy (Kipps et al., 2017). Nowadays, CLL has been divided into two main subsets based on the mutation status on the immunoglobulin heavy-chain variable regions (*IGHV*), reflecting the stage of B cell differentiation that they originate from, and by comparison with patients diagnosed with CLL bearing mutated *IGHV* (M-CLL), CLL patients with unmutated *IGHV* (U-CLL) exhibit worse prognostic outcome and drug resistance to conventional chemoimmunotherapy (Damle et al., 1999; Hamblin et al., 1999). In addition, several factors such as genetic alternations, signalling from surface immunoglobulins, known as B cell receptor (BCR) as well, and the tumour microenvironment, also take crucial part in the pathogenesis and clinical progression of CLL.

80% of CLL patients carry at least one of four common chromosomal alternations including deletion in chromosome 13q14.3 (del(13q)), 17p (del(17p) and 11q (del(11q)) and trisomy 12 (Dohner et al., 2000). Del (13q) is the most common cytogenetic mutation in CLL patients, accounting for over 50% CLL patients, and it has been demonstrated that loss of DLEU2–mir15a/16-1 cluster, which is encoded in the 13q14.3 region, leads to upregulation of mir15a/16-1 targeting genes involved in cell cycle checkpoints and anti-apoptosis, ultimately resulting in development of CLL (Klein et al., 2010). On the other hand, del(17p) is associated with *TP53* mutations in approximately 7% CLL patients who are difficult to treat (Zenz et al., 2010), and

del(11q) causes loss of *ATM*, encoding a protein crucial for initiating DNA damage response. Both of cases are correlated with adverse clinical outcome (Dohner et al., 2000). In addition to chromosomal alternations, recurrent somatic mutations have also been uncovered in a wide range of genes involved in Notch and WNT signalling, DNA damage response (*ATM* and *TP53*), RNA splicing (*SF3B1*), and histone modifiers (*CHD2*, *ASXL1* and *ZMYM3*), all of which contribute to the high degree of genetic heterogeneity in CLL (Fabbri et al., 2011; Pleasance et al., 2010; Puente et al., 2015; Wang et al., 2011).

BCR signalosome is assembled by recruitments of protein kinases like LYN, spleen tyrosine kinase (SYK), Bruton's tyrosine kinase (BTK), phosphoinositide 3-kinase (PI3K) and B cell-linker protein (BLNK) to the surface transmembrane immunoglobulins (mainly sIgM and sIgD in CLL) with CD79A and CD79B heterodimers to trigger a signalling cascade including MEK/ERK, NFκB, RAC1/RHOA and mTOR pathways, and functional BCR signalling is essential for the survival and proliferation of mature B cells as well as malignant mature B cells, especially U-CLL, which is more responsive to BCR-cross linking with robust intracellular signalling (Lam et al., 1997; Lanham et al., 2003). Moreover, expression of quasi-identical (stereotyped) BCR among different patients suggests antigen binding and activation of BCR with common antigens or autoantigens are required for CLL pathogenesis. Meanwhile, the breakthrough of U-CLL therapy by blocking BCR signalling via targeting tyrosine kinases such as BTK and PI3K also underscores the importance of BCR signalosome, and shed light on tackling relapsed CLL with BCR inhibitors (Awan and Byrd, 2014).

The survival of CLL cells has been relying on the interaction with tumour microenvironment, in which non-neoplastic cells like bone marrow stromal cells (BMSC), monocyte derived nurse-like cells (NLSC) and T cells play important roles in protecting and activating CLL cells within the tissues (Kipps et al., 2017; ten Hacken and Burger, 2014). In the proliferation centre, NLSCs released crucial TNF family factors such as BAFF and APRIL (TNFSF13) to activate NFκB signalling for the survival of CLL cells (Endo et al., 2007), and activated T cells provide proliferation signalling by secreting IL2, IL4 and IL10 and CD40L/CD40 interaction (Aguilar-Hernandez et al., 2016; Scielzo et al., 2011). CXCL12, which is secreted by BMSCs, is required for the bone marrow homing through CXCL12/CXCR4 chemotaxis, and high level of expression of CXCR4 is also associated with abundant lymphoid organ infiltration (Burger et al., 1999; Calissano et al., 2009). Recently, in addition to CXCL12, the importance of CXCL13, secreted by NLSCs and follicular dendritic cells, in lymphoid organ migration and CLL pathogenesis has been clarified as well in a *Cxcr5* mutant *Eμ-TCL1* CLL mouse model (Heinig et al., 2014). Genetic depletion of CXCR5 or blocking CXCL13/CXCR5 axis with anti-CXCL13 antibodies significantly reduced CLL burden and leukaemic infiltration into spleens and lymph nodes, suggesting targeting CLL homing could be also a promising therapeutic strategy for CLL treatment.

1.2. Polycomb repressor complex 2 (PRC2)

In eukaryotic cells, the genome is compacted into chromatin, where DNA is wrapped around histone octamers as nucleosomes, which not only provides structural purposes to accommodate linear genome into the finite space of nucleus but also offers functional purposes to allow conformations of different areas to be condensed or open

in the genome through epigenetic modification for specific regulation of gene expression. The term epigenetics refers to alternations of gene expression that are inheritable after cell division without any changes in DNA sequence. In addition to DNA methylation, an increasing number of epigenetic modifications on histones, including acetylation, methylation and ubiquitination, have been identified in cancers, resulting in repression of tumour suppressor genes and/or activation of oncogenic pathways (Baylin and Jones, 2011). Amongst epigenetic histone modifiers, polycomb group proteins (PcGs) are one representative group dysregulated in haematological malignancies (Iwama, 2017; Laugesen et al., 2016).

Polycomb repressor complexes, large multimeric protein complexes, are assembled by a group of proteins (PcGs) originally identified in *Drosophila* as crucial transcriptional repressors to regulate a cohort of transcriptional factors such as *Hox* genes for fly development, whereas Trithorax (Trx) family proteins counteracts this to activate gene expression, and their orthologs have been subsequently discovered in a wide range of species from plants to mammals to modulate global gene expression patterns (Laugesen and Helin, 2014). Amongst these, polycomb repressor complex (PRC) 1 and 2 are the two best characterized epigenetic repressor complexes. PRC1, containing core members including RING1A or RING1B with the catalytic activity (E3 ligase) for monoubiquitination toward H2A119K (H2A119Kub1) and 1 of 6 polycomb repressor RING fingers (PCGF 1-6) can be further divided into canonical PRC1 (CBX and PHC) and non-canonical PRC1 (RYBP/YAF2) with different additional subunits (Di Croce and Helin, 2013; Gao et al., 2012). On the other hand, mammal PRC2 consists of at least 4 subunits with a core complex necessary for catalytic function (Ezh2, Suz12 and EED) and at least one of several accessory factors like RBBP4/7, JARID, AEBP2, PCL1-3, C17orf96, and C10orf12 as well as non-coding RNA to repress target genes

through the methyltransferase activity of Ezh2 toward lysine 27 on histone 3 (H3K27) via its SET domain (Cao et al., 2002; Kuzmichev et al., 2002; Pasini et al., 2004). In general, different composition of subunits are thought to affect the catalytic activity and recruitments of PRC on the target genes, but no subunit is solely responsible for the recruitments although some of them bear DNA or histone binding activities (Di Croce and Helin, 2013).

Unlike *Drosophila*, where polycomb response elements (PRE) have been identified and thought to be binding DNA elements for PcGs, the recruitments of PRCs in mammalian cells are still elusive as lacking distinct PRE (Orsi et al., 2014). It has been reported PRC2 is preferentially enriched at CpG rich contexts, and its enrichment matched well with the H3K27me3 positive regions (Ku et al., 2008; Peters et al., 2003; Tanay et al., 2007), suggesting PRC2 might bind to CpG islands to exert its repressive function. Moreover, the WD40 domain of EED displays affinity to H3K27 trimethylation, which may assist PRC2 in spreading H3K27 methylation over the genome (Hansen et al., 2008; Montgomery et al., 2005). Previous studies reveal that the binding patterns of PRC1 and PRC2 overlap in human and murine embryonic cells (Boyer et al., 2006; Bracken et al., 2006), and the recruitment of PRC1 is dependent on PRC2 along with the finding that one of canonical PRC1 subunits CBX shows affinity to H3K27me3 as well (Cao et al., 2002; Fischle et al., 2003; Min et al., 2003), proposing a hierarchical recruitment model, in which PRC2 trimethylated H3K27 on target genes, subsequently recruiting PRC1 to add H2A119Kub1 to provide chromatin compaction and cooperate in transcriptional repression (Cao et al., 2002; Rastelli et al., 1993; Wang et al., 2004). Indeed, while H3K27 methylation is essential for gene repression and early development, H2A119Kub1 is not required for global H3K27 methylation in *Drosophila* (Illingworth et al., 2015; Pengelly et al., 2015). However, further detailed

studies in mouse embryonic stem cells show deletion of PRC2 components only had limited effects on the global levels of H2A119Kub1 and PRC1 binding to the target loci, and the non-canonical PRC1 with RYBP or YAF2, both of which lack H3K27me3 binding capacity, could be recruited to chromatin in PRC2-deficient mouse embryonic cells, suggesting an alternative H3K27me3 independent pathway for PRC1 recruitment as well (Blackledge et al., 2015; Tavares et al., 2012).

1.2.1. Structure & functions of Enhancer of Zeste Homolog 2 (EZH2)

Human *EZH2*, locating at chromosome 7q36.1, belongs to histone lysine methyltransferase family, and can be translated into a 764 amino acid enzyme with the catalytic domain SET domain (Su(var)3–9 enhancer of zeste trithorax) in the C-terminus and numerous functional domains including a WDB domain in the N-terminus, Domain1/2, two SANT domains and a CXC domain (cysteine-rich domain) in the C-terminal (Margueron and Reinberg, 2011). Although Ezh2 is the catalytic subunit of PRC2, it is not able to exert its full enzymatic function without assistance of the other two noncatalytic core partners. When complexing with suppressor of zeste 12 (Suz12) and embryonic ectoderm development (EED) through Domain 2 and the WDB domain respectively, Ezh2 gains robust H3K27 methyltransferase activity, and Suz12 and EED are also crucial for maintaining the integrity of PRC2 and the stability of Ezh2 (Montgomery et al., 2005; Montgomery et al., 2007; Pengelly et al., 2013). Notably, in mammals, there is another Ez homolog named Ezh1, involved in PRC2 repressive machinery (Margueron et al., 2008). Although Ezh1 was cloned and identified first in mammals, its functions and biological roles are not well characterized as its mammalian homolog Ezh2 and the original ortholog Ez. By comparison with Ezh2, the H3K27 methyltransferase activity of Ezh1 is relatively low, and the expression of Ezh1 is

ubiquitous, whereas Ezh2 is preferably expressed in proliferating tissues. However, even if the global levels of di- and tri-methylation drastically dropped after genetic depletion of Ezh2 in ESCs, H3K27me3 remains in certain developmental genes, and it has also been reported that Ezh1 controls an overlapping set of PRC2 in human cell lines, suggesting Ezh1 may function as a backup to prevent de-repression of all Ezh2 target genes (Margueron et al., 2008; Shen et al., 2008).

Methylation of H3K27 by the SET domain of Ezh2 has been reported a processive monomethylation from un-, mono- (H3K27me1) and di-methylated form (H3K27me2) to H3K27 trimethylation, and different states of H3K27 methylation are found in different genomic contexts (Zee et al., 2010). The levels of H3K27me1 and H3K27me2 are re-established in newly incorporated histones very fast after DNA replication in each cell cycle (Alabert et al., 2015; Zee et al., 2010), and in embryonic stem cells (ESCs), while 5 to 10 % of histones carry H3K27me1, which is mainly distributed in gene bodies of transcriptionally active genes, H3K27me2 has been found in the majority of histones (approximately 50-70%) and proposed to prevent inappropriate transcription and enhancer activity, suggesting no specific DNA sequences and composition is required for the immediate mono-and di-methylation (Ferrari et al., 2014; Jung et al., 2010; Jung et al., 2013). Moreover, the appearance of H3K27me1 is more likely due to indirect demethylation by UTX or JMJD3, the H3K27 demethylase during gene activation, rather than regulatory recruitment of PRC2 to active transcriptional machinery (Swigut and Wysocka, 2007). On the contrary, only 5 to 10% of histones are modified with H3K27me3, and the reestablishment of H3K27me3 is relatively slow during cell cycles. However, the distribution of H3K27me3 overlapped well with the binding patterns of PRC2, and in vitro activity results of PRC2 showed the slower conversion to H3K27 trimethylation (Ferrari et al., 2014; Jung et al., 2010; Jung et al., 2013; Peters et al., 2003;

Sneeringer et al., 2010), suggesting that more stable and specific binding of PRC2 might be required for further H3K27 trimethylation in gene regulation.

1.2.2. Structure & functions of Additional Sex Combs-Like 1 (ASXL1)

Additional sex combs-like 1 (*ASXL1*), locating at chromosome 20q11.21, has been identified in 2003 with other homologs (*ASXL2* and *ASXL3*) as an ortholog of *Additional sex combs* (*Asx*), which was originally discovered based on a mutagenesis screen in *Drosophila*, whereby mutations of *Asx* enhanced the phenotypes resulting from TrxG mutations and PcGs mutations, suggesting Asx is involved in the repression as well as activation of *Hox* genes in *Drosophila* (Fisher et al., 2003; Muller et al., 2002; Sinclair et al., 1998). Hence, Asxl1 is categorized into enhancer of trithorax and polycomb group (ETP), and shares sequence similarity of conserved functional domains (approximately 70%) with Asxl2 and Asxl3, including ASXN in the N-terminus, ASXH (ASX homolog), ASXM1/M2 and the cysteine cluster plant homeodomain (PHD) in its C-terminus (Fisher et al., 2006). However, the expression of Asxl3 is restricted to certain tissues such as brains and eyes, whereas Asxl1 and Asxl2 are widely expressed in mammalian tissues including haematopoietic cells.

Getting insights into the functional domains, while ASXN, which is predicted to be a DNA binding domain, does not exist in *Drosophila*, revealing a divergence between Asx and mammalian Asxl (Sanchez-Pulido et al., 2012), ASXH is highly homologous to the DEUBAD domain (deubiqutinase adaptor) of Asx, which has been found bound to Calypso (the ortholog of BAP-1 in *Drosophila*), a PcG with histone deubiquitinase activity toward H2A119ub1 to counteract the repressive function of PRC1 (Scheuermann et al., 2010), and ASXM1 and ASXM2 have been reported to associate

with hormone receptors such as androgen receptor and estrogen receptor (Grasso et al., 2012), further supporting the involvement of Asxl1 in epigenetic and transcriptional regulation. Furthermore, the mammalian homolog of Asx Asxl1 has been proved to bind BAP-1 (BRCA1 associated protein 1) and co-exist with BAP-1 in a complex termed polycomb repressor deubiquitinase complex (PR-DUB) (Figure 1.4). Asxl1 functions as a cofactor for BAP-1 to help deubiquitinating H2A119ub1, in agreement with *Drosophila*, where loss of Asx and Calypso lead to a global increase in H2A119ub1 (Sahtoe et al., 2016; Scheuermann et al., 2010). However, the BAP-1 binding domains (ASXH) of three Asxl proteins shared 60% of homolog, and all can bind to BAP-1 to facilitate H2A119 monoubiqutination (Sahtoe et al., 2016). Therefore, how much redundancy between ASXL family is still unclear. In addition to PR-DUB, it has also been demonstrated that Asxl1 is associated with PRC2, and loss of Asxl1 resulted in global H3K27 demethylation and upregulation of *HOXAs* in human leukaemic cell lines and mouse hematopoietic stem/progenitor cells (HSPCs) (Abdel-Wahab et al., 2012), indicating its dual function on both PRC1 and PRC2 in mammalian cells as well.

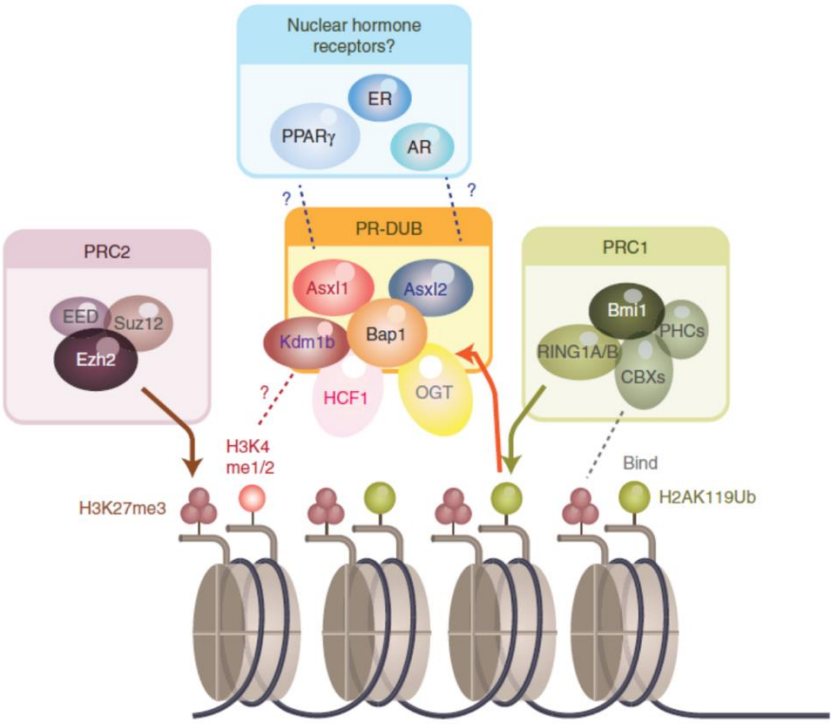

Figure 1.4. Proposed epigenetic functions of Asxl1 involved in PRCs. Adapted from (Micol and Abdel-Wahab, 2016). Asxl1 and Asxl2 co-exist with BAP1 in a complex termed Polycomb repressive deubiquitinase (PR-DUB) to catalyse deubiquitination toward H2AK119ub and counteract the repressive activity of PRC1, and the complex also associates with KDM1B, HCF1 and OGT. However, whether the association with KDM1B influences H3K4 methylation is still unclear. In addition, Asxl1 is also found associated with PRC2 and crucial for global H3K27 trimethylation in AML leukaemic cells. Finally, it has been proposed Asxl1 and Asxl2 physically bind to certain nuclear hormone receptors (NHR) such as androgen receptors (AR), estrogen receptors (ER) and PPARγ receptors.

1.3. Roles of PRC2 in leukaemogenesis

1.3.1. Genetic aberrations of PRC2 in haematopoietic malignancies

Loss-of-function mutations of PRC2 are frequently identified in haematopoietic malignancies such as MDS, MDS/MPN overlap and T-cell lymphoblastic leukaemia (T-ALL) through genetic aberrations of *EZH2* from cytogenetic insertion and deletion of chromosome to point mutations leading to homozygous amino-acid frame shifts,

most of which are believed to abolish the activity of PRC2 and correlated with poor prognosis (Bejar et al., 2011; Ernst et al., 2010; Nikoloski et al., 2010; Ntziachristos et al., 2012). In addition to amino-acid frame shifts and nonsense mutations, which lead to complete loss of Ezh2, missense mutations are also observed in EZH2, and while the majority of them are found in the catalytic domain (SET domain), significant clusters of mutations also appear in first SANT domain and the CXC domain, both of which have been proved important for the PRC2 assembly and DNA binding, suggesting missense mutations in EZH2 may result in loss of function of PRC2 as well through disruption of the complex (Figure 1.5).

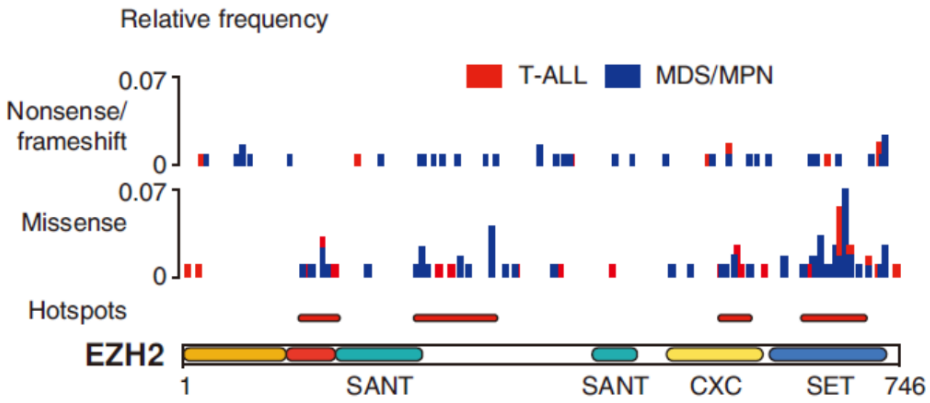

Figure 1.5. Histogram of Ezh2 mutations in myelodysplastic/myeloproliferative neoplasm (MDS/MPN) and T-cell acute lymphoblastic leukaemia (T-ALL). Taken from (Laugesen et al., 2016). Unlike nonsense and frameshift mutations, which equally occur across the full length of *EZH2*, missense mutations mainly cluster on functional domains crucial for the activity of H3K27 methylation such as the SET domain, CXC domain and two ends of SANT domain, hence leading to loss-of-function mutations.

While the other core PRC2 members such as Suz12 and EED are rarely mutated in haematological malignancies such as MDS/MPN and T-ALL (less than 2 %), mutations of *ASXL1*, the PRC2 associated factors, are commonly seen as amino-acid frame shifts and nonsense mutations on exon 12 in MDS (15-20%) (Bejar et al., 2011; Bejar et al., 2012; Thol et al., 2011), MDS/MPN (40-60%) (Gelsi-Boyer et al., 2009; Thol et al., 2011), and AML (2-25%) patients (Boultwood et al., 2010; Rocquain et al., 2010), resulting in loss of Asxl1 and expression of c-terminal truncated Asxl1 (Abdel-Wahab et al., 2012; Inoue et al., 2013), which further suggests loss of Ezh2 and Asxl1 are tolerated in haematopoietic cells and might be beneficial for leukaemogenesis (Figure 1.6).

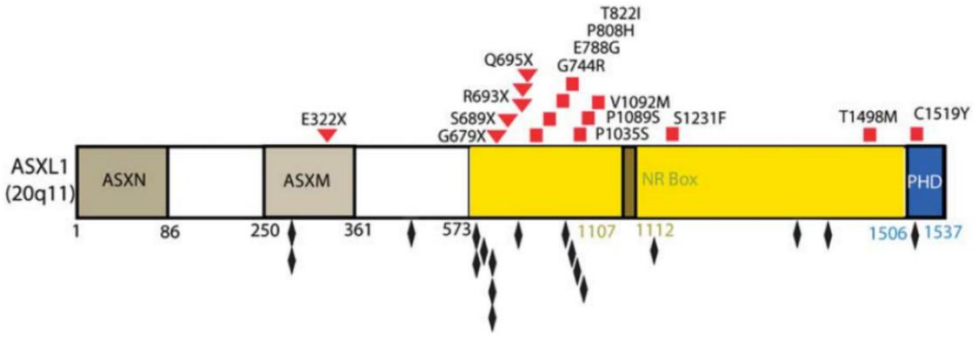

Figure 1.6. Gene diagram of somatic mutations throughout the coding region of Asxl1 in myeloid neoplasms. Exon 12 is outlined in yellow as a hot spot with cluster missense mutations (squares), nonsense mutations (triangle) and amino-acid frameshift (diamond). Adapted from (Abdel-Wahab et al., 2011)

Moreover, cluster mutations of *ASXL1* and *EZH2* have been reported in myeloid neoplasms, and growing evidence indicates somatic mutations of *ASXL1* tend to co-occur with *EZH2* mutations in CMML and PMF patients (Rinke et al., 2017; Triviai et al., 2019). Clinically, concomitant mutations of *ASXL1* and *EZH2* resulted in a prognostic detrimental outcome in CMML patients. The overall survival of chronic

myeloid monocytic leukaemia (CMML) patients was reduced to 16 months (median) in comparison to 20 months for *ASXL1mt*/*EZH2wt* and 33 months for *ASXL1*/*EZH2* wild type patients ($p<0.001$) (Abdel-Wahab et al., 2011; Patnaik et al., 2018), suggesting double inactivation of Asxl1 and Ezh2 may further impact on the repressive function of PRC2 and facilitate the disease progress of myeloid malignancies.

Recurrent somatic point mutations have been identified in the SET domain of Ezh2 as gain-of-function mutations in B lymphoid neoplasms, especially follicular lymphoma (FL) and diffuse large B-cell lymphoma (DLBCL) (Morin et al., 2010; Morin et al., 2011), providing Ezh2 with hyperactivating catalytic activity and then conferring greater levels of H3K27 trimethylation (Sneeringer et al., 2010; Yap et al., 2011). The hyperactivating mutations mainly results from substitution of a tyrosine at Y646 on the SET domain (Y646 F/N/S/H/C) although they were not regarded as gain-of-function mutations at the original reports showing its inefficiency at H3K27 mono- or di-methylation (Bodor et al., 2013; Morin et al., 2010). Nonetheless, subsequent studies have demonstrated its hyperactive catalytic activity at H3K27 trimethylation, and the presence of wild type Ezh2 is essential to provide the H3K27me2 as substrates for the activating mutant, which further explains why the gain-of-function mutation is always heterozygous in these B-cell lymphomas (Sneeringer et al., 2010; Swalm et al., 2014).

Loss-of-function mutations could also exist in B-cell lymphoid neoplasms although the frequency is relatively low. A previous cytogenetic study revealed 9 of 747 (1.2%) patients with chronic lymphoid malignancies including 3 CLL patients, had deletions of 7q36, which literally covered the gene locus of *EZH2* (7q36.1) (Table 1.1) (Oscier et al., 1996). In addition, somatic point mutations of *ASXL1* were also identified in 5

out of 506 CLL patients (approximately 1 %) in a comprehensive genomic analysis based on whole genomic sequencing (WGS) (Puente et al., 2015; Quesada et al., 2011), which included 3 nonsense mutations and 1 amino-acid frame-shift mutation. Although it remains to see if ASXL1 mutation and the 7q36 deletion also coexist in CLL patients, these findings suggest the possible involvement of PRC2 and ASXL1 in CLL pathogenesis.

Table 1.1 Cytogenetic abnormality of chromosome 7q in B-LPD.

Case No.	Age	Sex	Diag	Tissue	Karotype
1	77	M	CLL	LN	46,XY,add(6)(p?),del(7)(q11.2q36),−8,add(12)(q?),+mar[3]/46,XY[10]
2	77	F	PLL	B	46,XX,t(?11;17)(p13;p11.2),t(19;19)(q13.1q13.3)[20]/46,idem,del(6)(q23),del(7)(q22q36)[5]
3	71	F	NHL	B	47,XX,+X,der(7)del(7)(q22.3q34)t(1;7)(q21;q34)/47,idem,del(6)(q21q25)[4]/ 47,idem,t(14;18)(q32;q21)[2]/47,idem,del(6)(q21q25),add(9p)[1]/46,XX[20]
4	77	M	SLVL	B	46,XY,del(11)(q13.5q21),dup(21)(qter→q21.2::p11→qter)[17]/46,idem, del(7)(q22q32)[11]/46,XY[2]
5	65	F	CLL	B	47,XX,+12[2]/47,XX,t(6;14)(q21q31),der(7)del(7)(q22q32)t(7;10)(q22q25),+12[13]/46,XX[1]
6	75	F	FCCL	B	46,XX,del(1)(q21),dup(1)(q?22q?32),t(3;12)(q?26;q?22),del(7)(q22q32),del(13)(q?14),der(14)t(14;?) (q32;?)[12]/46,XX[1]
7	80	F	SLVL	B	46,XX,del(7)(q22q?32)[12]/46,XX[6]
8	77	M	HCLV	B	43/44,XY,del(1)(q?32),del(6)(q?15q?25),del(7)(q34q36),del(7)(q22q36),add(8)(p23),del(10)(p13), add(12)(p13),add(15)(p11),add(18)(q23),dic(3;19)(p21p13),del(14)(q24),add(22)(q13)inc[10]
9	73	F	SLVL	B	46,XX,del(7)(q31.2q36)[7]/46,XX,?del(7)(q32.1q32.3)[7]/46,XX[25]
10	64	M	DLCL	LN	47,XY,−1,der(1)t(1;7)(p36.11;q21.2),del(7)(q31q34),+del(7)(q31q34), add(14)(q?),del(18)(q21.3)[12]/46,XY[2]
11	63	F	MZL	S	45,X,del(X)(q12),t(1;14)(q21;q32),?del(2)(q?13q21),del(7)(q32q36),−18[cp4]/46,XX[14]
12	84	F	SLVL	B	46,XX,del(7)(q32q34)[1]/47,idem,+3[19]/45,X,−X[3]/46,XX[37]
13	71	F	MCL	S	46,XX,add(1)(q?),del(3)(q?),del(4)(q24q31),del(7)(q32q34),t(8;12)(q11.1;p11.21), −inv(9)(p11q13)c,−10,−17+der(10)t(10;17)(q26;q11),+2mar[14]/46,XX,inv(9)(p11q13)[27]
14	61	M	NHL	LN	46,XY,del(7)(q?34q?36)[4]/46,XY[26]
15	—	F	CLL	B	46,XX,add(1)?dup(1)(q23q24),del(7)(q34q36),?8p[1]/46,idem,add(3)(p26)[8]/ 46,idem,add(21)(q?13)[3]
16	85	F	NHL	B	45,XX,del(1)(q?34p36),inv(2)(?p23q13),−6,del(7)(q34q36),der(9)t(9;17)(p24;q12),t(12;?)(p13;?), +12,del(14)(q4?),?t(14;19)(q32;q13),−17,?t(17;18)(q21;q21)[10]
17	70	F	CLL	B	46,XX,del(7)(q34q36)[5]/46,XX[23]
18	76	F	SLVL	B	46,XX,t(2;7)(p11.23;q22.1),del(7)(q34q36.1),der(8)t(8;12)(p21;q11.1)[23]/46,XX[46]
19	57	M	CLL	B	46,XY,inv(7)(p22q32),del(13)(q12q14)[15]/46,XY[9]
20	91	F	SLVL	B	46,XX,del(7)(q34q36),?t(9;9),−20,+der(20)t(12;20)(q13;p13)[5]
21	87	F	MCL	B	48,XX,r(7)(?p11q36),+12,del(14)(q22q32),+18[18]/46,XX[2]
22	81	F	CLL	B	46,XX,t(7;15)(q11.23;q15.3),del(13)(q12q14)[7]/47,XX[17]
23	—	F	DLCL	LN	46,XX,?t(1;9;12)(q21;q21;p12),del(2)(p?10),del(3)(p?),add(4)(q?),−5,inv(7)(q22q36),del(10)(p11), t(19;?),add(21)(q?)[cp7]
24	46	M	CLL	B	46,XY,t(2;7)(p11;q21.2)[8]/46,XY[22]
25	63	M	HCLV	B	44,XY,−7,−10,der(17)t(7;10;17)(17qter→17p13::10q11→10q24::7q21.2→7qter),t(2;8)(p12;q24)[22]/ 46,XY[24]
26	71	M	DLCL	LN	46,XY,del(2)(q33),ins(7;?)(q22;?),t(12;20)(q13;q?12),?t(14;14)(q32;q24)[22]/46,XY[6]
27	54	M	SLVL	B	46,XY,t(2;7)(p11;q22)[28]/46,XY[1]
28	70	F	MCL	BMS	45,XX,t(7;21)(q22;q22),t(9;17)(p11;q11),der(9)t(9;17)(p11;q11),−17[24]/46,XX[13]
29	89	F	SLVL	B	46,X,t(X;7)(q22;q36)[10]

CLL, chronic lymphocytic leukemia; DLCL, diffuse large cell lymphoma; FCCL, follicular center cell lymphoma; HCLV, hairy cell leukemia variant; MCL, mantle cell lymphoma; MZL, marginal zone lymphoma; NHL, non Hodgkin's lymphoma; PLL, prolymphocytic leukemia; SLVL, splenic lymphoma with villous lymphocytes.

1.3.2. Loss of Ezh2 in development of haematologic malignancies

The impact of loss of Ezh2 in development of haematologic malignancies has been discussed for the past decade in several mouse studies using conditional knockout (cKO) mouse models to address the role of Ezh2 in leukaemogenesis pathologically and molecularly. Tissue-specific depletion of Ezh2 in BM cells and foetal liver cells developed myelodysplastic disorders, such as MDS and MDS/MPN, characterized with myelodysplasia and myeloproliferative features like monocytosis in PB, splenomegaly and extramedullary haemotopoiesis (EMH) in recipient mice after primary transplantation, which further progressed into heterogenous diseases including lymphoid neoplasms such as T-ALL/lymphoma and B-LPD upon secondary transplantation, suggesting the profound influence of PRC2 on a wild range of leukaemogenesis (Mochizuki-Kashio et al., 2015). Molecularly, loss of Ezh2 reprogramed transcriptional profiling and the landscape of H3K27 methylation in HSPCs, in which Ezh1 was required to restore the levels of H3K27me3 in a part of genes to compensate the loss of Ezh2 and maintain haematopoiesis (Mochizuki-Kashio et al., 2015).

Furthermore, as clusters of mutations in genes involved in epigenetic modification and signalling pathways are identified in myeloid malignancies, a variety of compound mutant mice have been generated to study the disease progression of Ezh2-deficient mouse models. While double knockout of *Ezh2* with *Tet2*, a methylcytosine dioxygenase involved in DNA demethylation, enhanced the lethality of the MDS/MPN-like phenotype, and significantly shortened the disease latency (Muto et al., 2013), *Ezh2* cKO mice with constructive expression of activating mutants of NRAS (G12D) and JAK2 (V617F), both of which have been identified in MPN patients, developed PMF,

a more progressive myeloid malignancies, with short latency (2 to 5 months) with organomegaly and reticular fibres in spleen and livers (Gu et al., 2019; Sashida et al., 2016). Getting insight into the molecular aspects, PRC2 targets and JAK2-STAT downstream genes were upregulated in HSPCs from *JAK2V617F/Ezh2* cKO mice, resulting in active JAK/STAT signalling and specific oncogene expression such as *Hmga2*, which markedly promoted cell growth of HSPCs and expanded abnormal megakaryocytes. Likewise, loss of Ezh2 also promoted NRASQ61K-driven leukaemogenesis of T-ALL through derepressing IL6rα and activating JAK/STAT signalling, suggesting the tumour supporting role of JAK/STAT signalling in both myeloid and lymphoid malignancies (Danis et al., 2016). On the other hand, in the *NRasG12D/Ezh2* cKO mice, loss of Ezh2 derepressed branched aminotransferase isozyme 1 (BCAT1) in HSPCs, subsequently leading to increase in branched amino acids (BCAA) pools (leucine, isoleucine, and valine) in corporation with NRASG12D, which increased intracellular glutamate (Glu) pools, the substrate of BCAT1, through glutaminase-mediated glutamine (Gln) to Glu conversion, and promoting mTOR signalling pathways (Gu et al., 2019). Genetic and pharmacological inhibition of BCAT1 and mTOR prolonged the disease latency and reduced splenomegaly, intriguingly correlating BCAA metabolism with cancer progression.

1.3.3. Loss of Asxl1 in development of haematologic malignancies

Unlike the heterogeneity of loss of Ezh2 in leukaemogenesis, loss of Asxl1 resulted in relative myeloid-restricted haematopoietic malignancies. Although the disease phenotype was mild, loss of Asxl1 in BM cells also led to development of MDS-like phenotypes, with cytopenia and observation of dysplastic cells in BM and PB, and the disease could be further progressed to lethal myelodysplastic disorders, with

splenomegaly and EMH after serial transplantation (Abdel-Wahab et al., 2013). Likewise, several compound mutant mice were also established to study the pathogenic roles of loss of Asxl1 in myeloid malignancies. Concurrent knockout of *Asxl1* with *Tet2* resulted in a lethal MDS/MPN phenotype and accelerated the disease latency of myelodysplastic disorders, and loss of Asxl1 globally reduced the levels of H3K27me3, and enriched gene sets involved in apoptosis, cell cycle and MLL-rearranged leukaemogenesis (Abdel-Wahab et al., 2013). Similarly, loss of Asxl1 together with transgenic expression of JAK2V617F in haematopoietic cells contributed to a progressive PMF phenotype in recipient mice, whereas the single mutants only resulted in mild myeloid malignancies (Guo et al., 2019).

Molecularly, Asxl1 is associated with PRC2 and crucial for its repressive function. Either silencing Asxl1 or overexpression of c-terminal truncated Asxl1, considered a dominant negative form, induced expression of *HOXAs,* known to contribute myeloid transformation, in myeloid leukaemic cell lines through diminishing H3K27 methylation (Abdel-Wahab et al., 2012; Inoue et al., 2013), further supporting the tumour supporting roles of loss of PRC2 activity in myeloid leukaemogenesis (Figure 1.7). In addition to PRC2, Asxl1 also co-exists with BAP-1 in PR-DUB, whose tumour repressor role is getting clear due to clinical relevance and several functional studies on BAP-1 (Carbone et al., 2013). BAP-1 is located on 3q21.1, a locus frequently deleted in cancers, and loss-of-function somatic mutations of BAP-1 has also increasingly found in a variety of malignancies. Conditional knockout of BAP-1 in haematopoietic cells led to a disease phenotype resembling human MDS in mice (Dey et al., 2012). However, unlike *Drosophila*, loss of Asxl1 in human leukaemic cells is not clearly linked to the change of H2A119ub1 likely due to the redundancy of other Asxl proteins with BAP-1 binding activity in mammalian cells (Abdel-Wahab et al., 2012; Sahtoe et

al., 2016), suggesting that loss of Asxl1-driven leukaemogenesis might be independent of H2A119 deubiqutination.

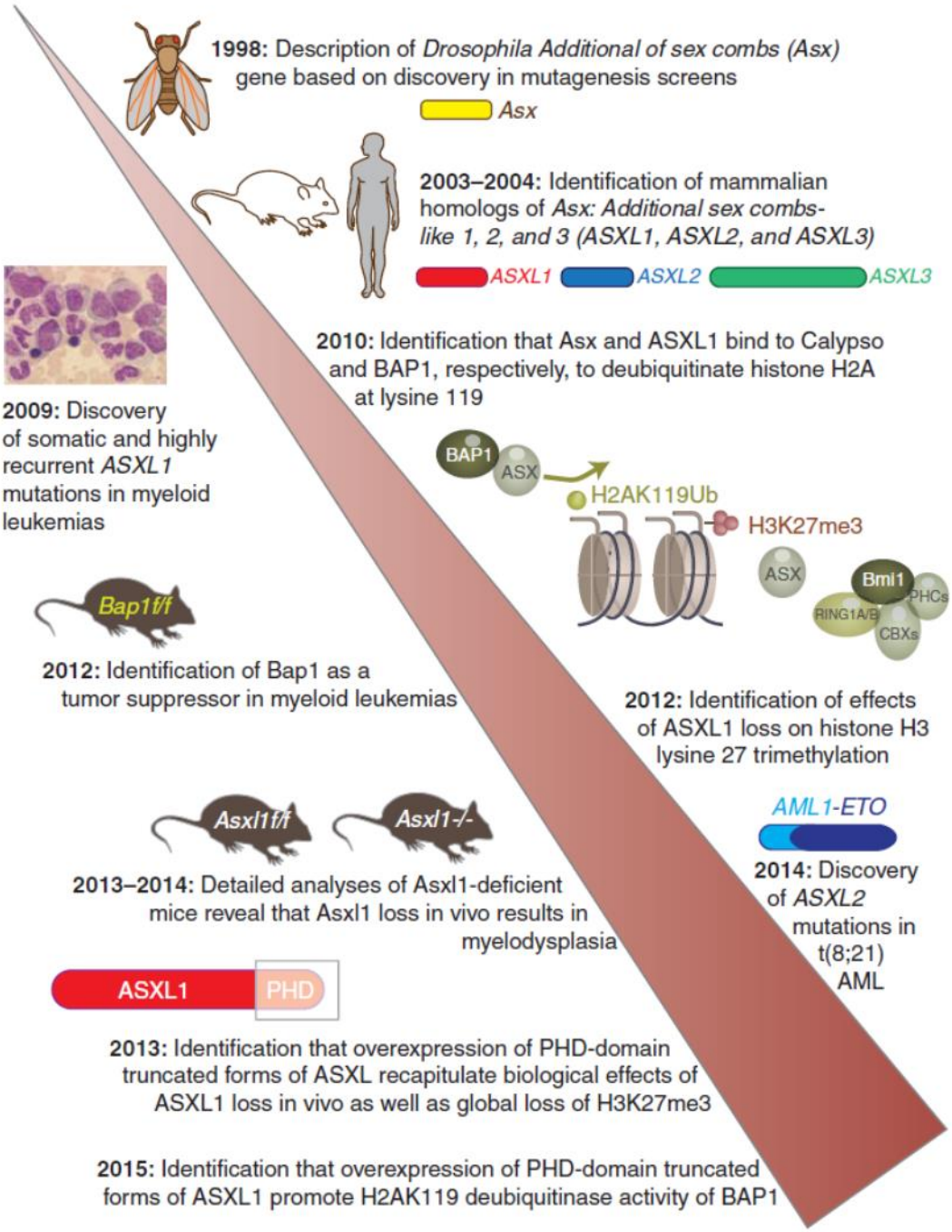

Figure 1.7. Timeline of discovery of Asxl1 and functional characterization in epigenome and leukaemia. Adapted from (Micol and Abdel-Wahab, 2016).

Charter 2: Project Aims

Recurring mutations affecting Asxl1 and Ezh2 have been reported in myeloid neoplasms, and Ezh2 mutations tend to co-occur with Asxl1 mutations in MDS/MPN and MPN. While genetic inactivation of Asxl1, the PRC2 associating factor crucial for the function of H3K27 methylation, leads to mild myelodysplastic disorders through reforming transcriptional patterns potentially via modulating H3K27 methylation mediated by PRC2. Depletion of Ezh2, the catalytic subunit of PRC2, in haematopoietic cells, results in heterogenous haematologic malignancies ranging from myelodysplastic disorders to lymphoid neoplasms including T-ALL as well as B-LPD in mouse models, consistently suggesting the critical roles of PRC2 in maintaining the equilibrium of cell proliferation and haematopoietic differentiation. In this study, we aim to further investigate the impact of incremental losses of PRC2 in haematopoiesis and leukaemogenesis using single and compound conditional knockout mouse model of *Asxl1* and *Ezh2*. The specific aims are listed as follows:

(1) To address the pathological roles of single vs concurrent loss of Asxl1 and Ezh2 in the early haemotopoiesis and development of haematologic malignancies.
(2) To investigate the underlying molecular mechanism for the leukaemogenesis of PRC2-defecient haematological malignancies.
(3) To establish a novel leukaemic model for pre-clinical research and identify potential targets for therapies of leukaemia.

Charter 3: Materials and Methods

3.1. Mouse work

3.1.1. Mice

Compound *Asx1*$^{fl/fl}$*Ezh2*$^{fl/fl}$ Rosa26-CreER mice were generated by back crossing *Ezh2*^{tm1Tara} (MGI2661097) (Su et al., 2003) Rosa26-CreER (MGI: 3699244) with *Asxl1*$^{tm1a(EUCOMM)Wtsi}$ (MGI4431878) in C57BL/6 (CD45.2) background, in which critical exons (exon 16 to 19 in *Ezh2* and exon 3 in *Asxl1*) are flanked with loxp sites (Figure 3.1), and knockout of the critical exons will eventually result in loss of Ezh2 and Asxl1 in mouse cells (Majumder et al., 2018; Moon et al., 2018; Yang et al., 2016). The genotyping of Asxl1 and Ezh2 were determined by PCR using primers targeting the floxed sites (Figure 3.1). Furthermore, C57BL/6 mice congenic for the Ly5 locus (CD45.1) (SJL) were used as recipient mice. All mice were held and kept in Biological Services Unit (BSU) at King's College London, and experiments were performed according to the protocols in the project licence (P8B15B1E1) under the Animals (Scientific Procedures) Act 1986.

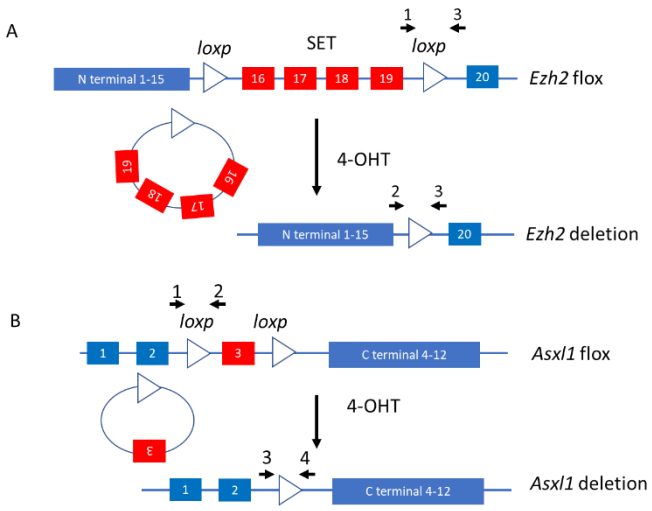

Figure 3.1. Floxed exons and PCR primer targeting sites in the alleles of *Asxl1* and *Ezh2*. Exons (16 to 19) encoding the SET domain of *Ezh2* (A) and exon 3 of *Asxl1* (B) were flanked with loxP, and 4-Hydroxytamoxifen (4-OHT) treatment activates Rosa-Cre to knockout the floxed exons (Red). Black arrows indicating PCR primers and the targeting sites for amplifying the flox, wt, and deletion bands (Table 3.2).

3.1.2. BM transplantation

2×10^6 BM cells collected from CD45.2$^+$ donor mutant mice were intravenously (i.v.) transplanted into CD45.1$^+$ recipient mice with lethal irradiation (13.5 Gy) together with 0.2 million rescue BM cells from recipient mice via tail veins in primary experiments, and subsequently, transplanted mice were injected with 120 µl tamoxifen (10 mg/ml) intraperitoneally (i.p.) one month after transplantation for 5 consecutive days to activate Rosa26-CreER for knocking out *Asxl1* and *Ezh2* (Figure 3.2). For following serial transfers, instead of lethal irradiation, 1×10^5 BM cells from leukaemic mice were transplanted into sublethally (11 Gy) irradiated CD45.1$^+$ recipient mice. The chimera of donor-derived haematopoietic cells was monitored through staining of CD45.1 and CD45.2, and the ratios of donor cells were evaluated by dividing CD45.2$^+$ cells into the sum of total CD45$^+$ cells.

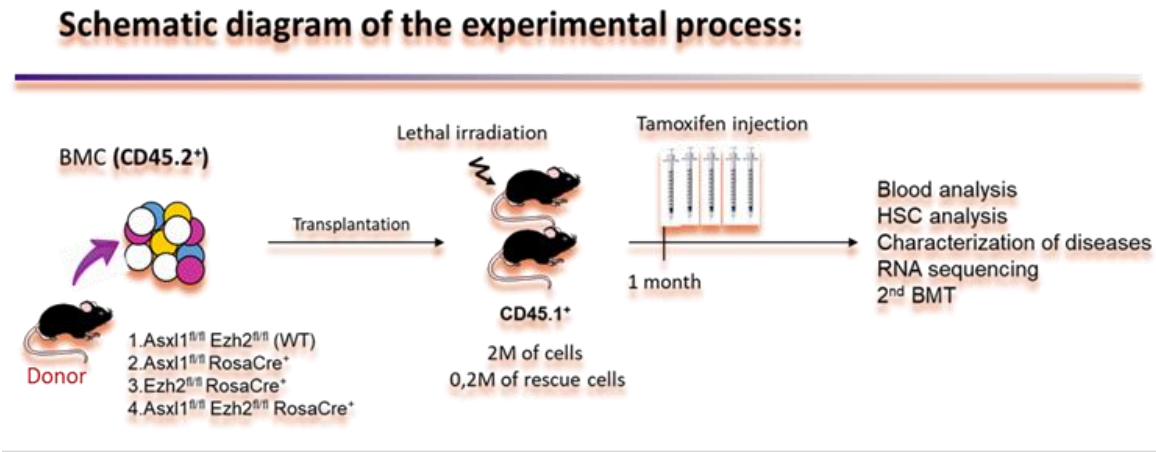

Figure 3.2. Illustration of the experimental process in primary transplantation. BM cells collected from indicated gene modified mice were injected into irradiated mice with rescue cells, and the mice were treated with TAM one month later to knock out *Asxl1* or/and *Ezh2*. Afterwards, several analyses were performed to study the effect of loss of PRC2 components on haematopoiesis and leukaemogenesis.

3.1.3. Sample collection and analysis

BM, spleens and livers were collected and analysed when mice came down. BM was flushed out from two hind limbs using PBS with 0.2% FBS (SM buffer), and $1x10^5$ BM cells were subjected to cytospin at 300 rpm for 5mins before lysis of red blood cells for MG/Giemsa staining and morphological examination. Furthermore, BM cells were incubated with red blood cell lysis buffer for 10 mins to remove red blood cells from BM. Spleens and livers were weighted before processed, and parts of samples were fixed by 10% formalin for H&E staining. The rest of spleens were grinded, and splenocytes were flushed and filtered out into SM buffer, followed by red blood cell lysis as well. Eventually, BM cells and splenocytes after red blood cell lysis were spun down and resuspended in 10 ml SM buffer. The cell numbers of BM cells were counted to examine BM cellularity, and 200 µl of BM cells and splenocytes were subjected to follow cytometry using a general staining cocktail to analyse proportions of myeloid populations, lymphoid populations, and expansion of B cells and T cells in more details. PB was taken from mouse hearts and maintained in Eppendorf's with ETDA, followed by analysis of blood parameters using Mythic 18 Vet Haematology Analyser (Woodley). 5 µl PB was further spread on a slide to make blood smear for MG/Giemsa staining.

3.1.3.1. Flow cytometry

BM cells, splenocytes and PB cells suspended in PBS with 0.2% FBS (SM buffer) after 10 min red blood cell lysis were stained with a general staining cocktail comprised of antibodies binding CD45.1, CD45.2, Mac1 (CD11b), Gr-1, B220, CD4, CD8 and c-Kit to divide myeloid populations ($Mac1^+$ or/and $Gr1^+$), total lymphoid populations ($Mac1^-Gr1^-$), normal B cells (B220) and T cells (CD4/8) and the CLL staining cocktail

comprised of antibodies targeting CD45.2, CD19, CD5, B220, CD43 and IgM at 1 in 400 dilution for 30 mins. Cell populations were analysed by FACS-LSR II (BD, USA). All antibodies for FACS were purchased from BioLegend® (Table 3.1).

3.1.3.2. HSC staining

4×10^6 BM cells after lysis of red blood cells were resuspended in 200 µl SM buffer, and subjected to incubation of unconjugated rate IgG ((7 Ab: Ter119, Mac1, Gr1, CD3ε, CD4, CD8, B220) in 40X dilution for 30 mins at 4°C, followed by incubation of Lin Ab Texas-Red (45X dilution) for another 30 mins at 4°c in the dark after wash and centrifuge at 1500 rpm for 8 mins. Furthermore, BM cells were subjected into HSC Ab staining for 30 mins at 4°c in the dark with indicated antibody dilution (Table 4.1), and specific cell types of HSPCs were gating based on the cell markers (Doulatov et al., 2012; Pietras et al., 2015). Lin-Sca1+c-Kit+ cells (LSK) were further divided into MPP3/4, MPP2, ST-HSC and LT-HSC by CD150 and CD48 staining. Lin-Sca1-c-Kit+ (MP) were divided into GMP, MEP and CMP by CD34 and CD16/32.

3.1.3.3. May-Gruenwald (MG) /Giemsa staining

Cytospin of 1×10^5 BM cells and PB smears were stained with May-Gruenwald (Sigma Aldrich) for 5 mins, followed by Giemsa stating at 10X dilution for 15 mins, and staining slides were washed with water and dried on air at room temperature. Finally, staining samples were fixed and covered with mounting medium for microscopic observation. Cells amongst granulocytotic maturation and myeloid dysplastic cells were identified by cell morphology according to a previous cytologic studies (Zhou et al., 2015), and left-shift of granulopoiesis was determining based on proportions of immature granulocytes.

3.1.3.4. Identification of *IGHVDJ*

To address the clonality of BCR, RNA was extracted, and reverse transcribed into cDNA as described in qRT-PCR. 2 µl cDNA was further amplified using a published primer set targeting mouse *IGHV* (forward) and *IGHJ* (reverse) (12 pmol VHR2 and 24 pmol VHF1-8, Table 3.2) (White, 1998; Yan et al., 2006) with 1X reaction buffer, 0.2 mM dNTP, 1.5 mM MgSO4, 3 units of Dream Taq DNA pol (Thermo Scientific) in a 50 µl volume for 35 cycles, each of which consisting of 30 s denaturation at 94 °C, 30 s annealing at 50°C and 1 min elongation at 72°C, followed by 10 min extension at 72°C. 10 ng/µl PCR products extracted from 2 % agarose gel using QIAquick Gel Extraction kit (QIAGEN) was sent for Sanger sequencing (Source BioScience), and *IGHVDJ* and *HCDR3* were identified using IgBLAST, NCBI.

3.1.4. Characterization of myelodysplastic disorders

MDS is characterized with cytological dysplasia and PB cytopenia in at least one myeloid lineage, and myelodysplasia, which encompasses morphological abnormalities in the affected myeloid lineages, is the key distinguishing feature for clinical diagnosis of myelodysplastic disorders (Zhou et al., 2015) (Greenberg et al., 2011). Therefore, to correlate the mouse disease phenotype with MDS, dysplastic cells in the three myeloid lineages granulopoiesis (Pseudo-Pelger-Huët anomalies), megakaryopoiesis (multiple separated nuclei, micro-megakaryocytes and ballooning platelets), and erythropoiesis (karyorrhexis, ringed sideroblasts and anisopoikilocytosis) were examined, and the left shift in granulocytic maturation was also identified to point out the abnormality in myeloid lineages (Figure 3.3) . Moreover, basic blood parameters including white blood cells (WBC), red blood cells (RBC), Haemoglobin (Hgb) and platelets (Plt) were also considered for the characterization of MDS. In contrast with MDS, MDS/MPN is

further characterized with myeloproliferative features. MDS/MPN patients show excessive proliferation in one of myeloid lineages, usually thrombocytosis, with or without cytopenia in PB, accompanied with splenomegaly due to EMH or infiltration of monocytes, which was the key feature to distinguish MDS/MPN from MDS in our characterization (DiNardo et al., 2014).

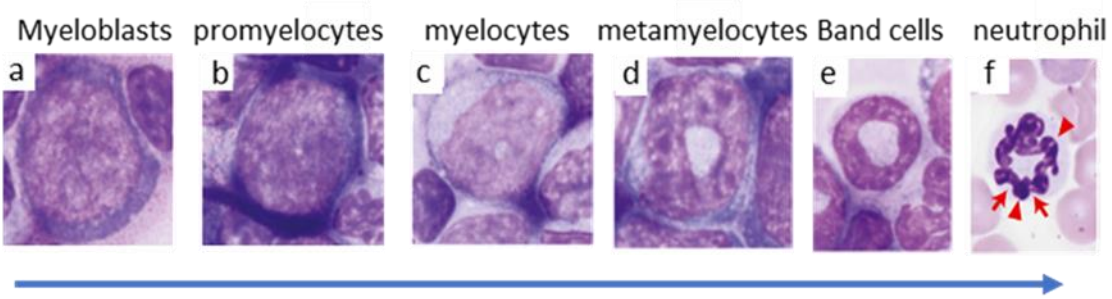

Figure 3.3 Morphological characteristics of granulocytic maturation in mice. Adapted from (Zhou et al., 2015). The blue arrow indicates the maturation from the precursor cells (a) myeloblasts and (b) promyelocytes to (f) mature neutrophils. Red arrows point out the filaments of chromatin separating nuclear segments.

3.1.5. In vivo treatments

1×10^5 BM cells from an *Asxl1*/*Ezh2* cKO CLL mouse in secondary experiments were i.v. injected into each sub-lethally irradiated (11 Gy) CD45.1$^+$ SJL recipient mouse via tail veins. Vehicles (10% HBC), 50 mg/kg olaparib and 15 mg/kg ibrutinib (PCI-32765, ABExBIO) were given to mice intraperitoneally (i.p.) one week after transplantation at 5 days per week for 4 weeks. Peripheral blood was collected from tail veins on day 35, and then blood counts and percentages of CD19$^+$CD5$^+$ donor cells were analysed, and spleen weights and engraftment of CD19$^+$CD5$^+$ donor cells in spleens were further examined after mice came down. Mice without engraftments (2 of

19) were taken out of the treatment experiment and not considered for the elucidation of the drug effects.

3.2. Cell culture and in vitro drug treatment

3.2.1. In vitro olaparib treatment

1×10^5/ml *Ezh2*$^{fl/fl}$ MLL-AF6 AML cells treated with 25 nM tamoxifen or 0.1% of ethanol as a control for 72 hrs for knocking out Ezh2 in the liquid culture condition, and then 1×10^5/ml *Ezh2* cKO MLL-AF6 AML cells or the wild type were treated with 0.1% DMSO or 1 to 10 μM olaparib (LC laboratories®) for 48 hrs, and the cells were subjected to MTT assay, Annexin V/PI staining, immunoblotting and immunofluorescence. For colony formation, 5000 *Ezh2* cKO MLL-AF6 AML cells seeded in 1 ml methylcellulose (MethoCult™ GF M3434, STEMCELL Technologies) with 1X 4 cytokines (IL3, IL6, SCF, GMCSF) were treated with 10 μM GSK126 (Biovison) and 1 μM olaparib, and the numbers of colonies were counted after 7-day treatment.

3.2.2. MTT assay and Annexin V/PI staining

50 μl of treated cells were transferred into a new 96 well plate, followed by adding 10 μl MTT (CellTiter96®AQueous, Promega) into each well for 1 hour incubation at 37°C, 5% CO2, and then the absorbance of 490 nm was measured according to the manufacturer's instructions using a plate reader (Bioteck). Looking into apoptosis, 300 μl of treated cells were stained with AnnexinV/PI (Annexin V Apoptosis Detection Kit, eBioscience) according to the manufacturer's instructions. Cells were stained with APC-conjugated Annexin V at 1 in 100 dilution for 15 mins, and suspended in 300 μl of Binding buffer containing PI (1 in 60 dilution) after wash steps. Ultimately, stained

cells were analysed by flow cytometry using a BD LSRII system (BD, USA), and distinguished into 4 group. Live (AnnexinV$^-$/PI$^-$), early-apoptotic (AnnexinV$^+$/PI$^-$), late apoptotic (AnnexinV$^+$/PI$^+$) and necrotic (AnnexinV$^-$/PI$^+$).

3.3. Molecular assays

3.3.1. qRT-PCR

RNA was extracted from splenocytes in primary experiments using RNEasy mini kit (QIAGEN), and 100ng RNA was subjected to reverse transcription under 20 µl reaction containing 1X First Strand Buffer, 200 units of Superscript III reverse transcriptase (Thermo Fisher Scientific), 0.5 mM dNTP, 100 pmol random hexamers (N6, NEB), 40 units of RNAse inhibitors and 5 mM DTT at 50°C for 1 hr. Subsequently, 1 µl cDNA was added into 20 µl reacting comprising of 0.5 µM forward and reverse primers (Table 3.2) and 1× PowerUp™ SYBR™ green master mix (Applied Biosystem) for qPCR.

3.3.2. RNA-seq library preparation and analysis

RNA was extracted from BM cells with over 90% engraftment in the wild type and mutant mice by RNeasy mini kits (QIAGEN), and the RNA integrity was measured before library preparation by running Agilent 2100 bioanalyzer (Eukaryote total RNA Nano assay, Agilent Technologies). 10 µl RNA from each BM sample was subjected to preparation of cDNA library using the TruSeq Stranded Total RNA LT Kit with RiboZero Gold according to manufacturer's protocol (Illumina, Inc). The quality of amplified cDNA libraries was verified by Agilent 2100 bioanalyzer (high sensitivity DNA assay, Agilent Technologies), and the concentration of cDNA was measured by Qubit dsDNA HS Assay Kit (Thermo Fisher Scientific). In the end, the libraries were

pooled equally with the final concentration of 5 nM and sent for sequencing. The quality of raw reads was checked using FASTQC v0.11.4, and adaptors and low-quality bases were trimmed with Trim Galore v0.4.0. Trimmed reads were map to GRCm38 (obtained from the Ensembl FTO server ftp://ftp.ensembl.org/pub/) using the short read mapper Tophat2 v2.2.0 (Kim et al., 2013), and read counts per gene were obtained using htseq-count v0.11 (Anders et al., 2015). Furthermore, downstream analysis was conducted in R using Biocondutor packages (R Core Team, 2015) (Huber et al., 2015), and differential expression analysis for BM cells from wild type and mutant mice was performed using EdgeR (Robinson et al., 2010). Genes expressed in more than 2 samples was filtered, and then the differential expression was accessed using a log ratio test (LRT).

3.3.3. Analysis of transcriptome of CLL mice

Differential gene lists showing the significantly upregulated and downregulated genes in BM cells of *Asxl*1 cKO mice (N=2), *Ezh2* cKO B-LPD mice (N=3) and *Asxl1*/*Ezh2* double cKO B-LPD mice (N=3) (< 0.05 adjusted p value) compared to the wild type were generated as described above. The upregulated genes and downregulated genes were compared and overlapped using Venny 2.1. To get further insights into the differential genes, KEGG pathways were analysed using DAVID Bioinformatics Resources 6.8, NIAID/NIH (Bordoli et al., 2009; Huang da et al., 2009), and the bar plots present the significant KEGG pathways (<0.05 FDR) ranked by FDR. Moreover, upregulation gene lists were subjected to ToppFun for analysis of correlated disease phenotypes and co-expression atlas, and 122 genes dysregulated in CLL were identified in double mutants based on DisGeNET. Transcriptional patterns of BCR

signalling pathway were presented by heatmaps using pheatmap v 0.2 with row normalized counts from each group to show greater contrast.

3.3.4. Immunoblotting

Cell pellets harvested from 48hr olaparib treatment were lysed with 1% SDS buffer (1% SDS, 10mM EDTA, 50mM Tris-HCl) for 10 mins, and sonicated in 0.65 ml Bioruptor® Microtube with 10 30s on-off cycles at 4°C by Bioruptor® Pico sonication device (Diagenode). Afterwards, the lysates were centrifuged at 4°C, and the supernatant were heated with 1×loading dye at 95°C for 10 mins. Furthermore, protein samples were subjected to 7.5% and 12% SDS polyacrylamide gel electrophoresis (PAGE) for approximately 2 hrs, and transferred to Amersham Hybond PVDF membranes. Eventually, membranes were incubated with blocking buffer (0.1% PBS-T containing 5% skimmed milk), followed by incubation primary and Horseradish Peroxidase (HRP)-conjugated secondary antibodies (Jackson ImmunoResearch) with proper dilution (Table 3.1).

3.3.5. Staining of γH2AX and Rad51 and foci counting

Slide preparation was done by cytospin of 1×10^5 cells at 300 rpm for 5 mins, and samples were subsequently fixed by 4% of paraformaldehyde (PFA) for 20 mins and washed with PBS three times before permeabilization, in which fixed cells were incubated with blocking buffer (10% FBS and 1% BSA in PBS) with 0.8% TritonX-100 for 15 mins at room temperature (RT). After washing, permeabilized cells were subjected to primary and secondary incubation. Incubation of anti-γH2AX mouse primary antibody (1:200) and anti-Rad51 rabbit primary antibody (1:100) was done at 4°C overnight, followed by incubation of Alexa488-conjugated anti-mouse goat secondary antibody and Cy3-conjugated ant-rabbit goat secondary antibody as well as

at RT for 1 hours (Table 3.1). Finally, stained cells were washed three times with PBST (PBS with 0.05% Tween20) and mounted with mounting medium (VECTASHIELD® Antifade Mounting Medium) for imaging. High throughput automatic foci counting of γH2AX and Rad51 was exerted and analysed using Focinator v2-31, in which multi-channel foci were evaluated and quantitated in nuclei marked as "Regions Of Interest" (ROIs) based on ImageJ bundled with Java, Bio-Formats Importer and the R script <Focinator v2-31.R> (Oeck et al., 2017; Oeck et al., 2015).

Table 3.1. List of antibodies

Antibody	Supplier	Catalog NO	Application	Dillution
Phospho-γH2AX (ser139)	Upstate	05-636	Immunofluorescence	1 in 200
Phospho-γH2AX (ser139)	Upstate	05-636	Immunoblotting	1 in 2000
Rad51 (H-92)	Scbt	Sc-8349	Immunofluorescence	1 in 100
Ezh2	BD	612666	Immunoblotting	1 in 1000
Atm	Sigma Aldrich	A1106	Immunoblotting	1 in 500
H3K27me3	Upstate	07-499	Immunoblotting	1 in 2000
Histone3 (H3)	Abcam	ab1791	Immunoblotting	1 in 50000
APC-CD45.2	Biolegend	109814	FACS (General staining)	1 in 400
FITC-CD45.1	Biolegend	110706	FACS (General staining)	1 in 400
PerCP-Cy5.5-Gr1	Biolegend	108428	FACS (General staining)	1 in 400
PE-Cy7-Mac1	Biolegend	101216	FACS (General staining)	1 in 400
Pacific Blue-B220	Biolegend	103227	FACS (General staining)	1 in 400
Alexa700-CD4	Biolegend	100430	FACS (General staining)	1 in 400
APC-Cy7-CD8α	Biolegend	100714	FACS (General staining)	1 in 400
PE-c-kit	Biolegend	105808	FACS (General staining)	1 in 400
APC-Cy7-CD19	Biolegend	115519	FACS (CLL staining)	1 in 400
Alexa700-CD5	Biolegend	100635	FACS (CLL staining)	1 in 400
FITC-CD43	Biolegend	553270	FACS (CLL staining)	1 in 400
PerCP-Cy5-IgM	Biolegend	406512	FACS (CLL staining)	1 in 400
FITC-kappa	Biolegend	40959	FACS (CLL staining)	1 in 400
PE-Lambda	Biolegend	407307	FACS (CLL staining)	1 in 400
PE-c-kit	Biolegend	105808	FACS (HSC staining)	1 in 100
PE-Cy7-Sca-1	Biolegend	108114	FACS (HSC staining)	1 in 50
BV421-CD150	Biolegend	115926	FACS (HSC staining)	1 in 25
Alexa 700-CD48	Biolegend	103426	FACS (HSC staining)	1 in 50
BV510-CD45.2	Biolegend	109837	FACS (HSC staining)	1 in 50

Table 3.2. List of primers

Primer	Sequence 5'>3'	Application
Asxl1 fl/wt F (1)	CCAATATGGCCTGGAACTGAC	genotyping
Asxl1 fl/wt R (2)	TAGAGACCAGGTGTGGTGGC	genotyping
Asxl1 del F (3)	AGCACACCAGGCTAAGATGCT	genotyping
Asxl1 del R (4)	ACAGACAAGCAAAGCTGAACAGA	genotyping
Ezh2 fl/wt/del 1	TTATTCATAGAGCCACCTGG	genotyping
Ezh2 fl/wt/del 2	ACGAAACAGCTCCAGATTCAGGG	genotyping
Ezh2 fl/wt/del 3	AGGGCATCAGCCTGGCTGTA	genotyping
VHF1	AGGTCCAGCTGCAGGAGTCTGG	clonality
VHF2	AGGTCCAGCTGCAGGAGTCAGG	clonality
VHF3	AGGTCCAGCTTCAGGAGTCTGG	clonality
VHF4	AGGTCCAGCTTCAGGAGTCAGG	clonality
VHF5	AGGTCCAACTGCAGGAGTCTGG	clonality
VHF6	AGGTCCAACTGCAGGAGTCAGG	clonality
VHF7	AGGTCCAACTTCAGGAGTCTGG	clonality
VHF8	AGGTCCAACTTCAGGAGTCAGG	clonality
VHR2	TGAGGAGACGGTGACCGTGGTCCCTTGGCCCC	clonality
AICDA F	AAAATGTCCGCTGGGCTAAG	qRT-PCR
AICDA R	AGGTCCCAGTCCGAGATGTAG	qRT-PCR
BCL-2 F	TGGGATGCCTTTGTGGAACT	qRT-PCR
BCL-2 R	ACAGCCAGGAGAAATCAAAC	qRT-PCR
CXCR5 F	TGGCCTTCTACAGTAACAGCA	qRT-PCR
CXCR5 R	GCATGAATACCGCCTTAAAGGAC	qRT-PCR
Myc F	AGCCCCTAGTGCTGC ATGA	qRT-PCR
Myc R	GCCTCTTCTCCACAGACACC	qRT-PCR
PARP1 F	GCTTTATCGAGTGGAGTACGC	qRT-PCR
PARP1 R	GGAGGGAGTCCTTGGGAATAC	qRT-PCR
Atm R	GGAGGAACATGCAGTGGGG	qRT-PCR
Atm F	TGAAAAGACTGGCATATCGGAGA	qRT-PCR
Atr F	TGGCCAGTGCTACTCCAGAA	qRT-PCR
Atr R	CATCACAGAGGTCGGCTGAG	qRT-PCR
Rad51 F	AAGTTTTGGTCCACAGCCTATTT	qRT-PCR
Rad51 R	CGGTGCATAAGCAACAGCC	qRT-PCR
Brca1 F	AAGAGACAGTAACTAAGCCAGGT	qRT-PCR
Brca1 R	GGGGCGGTCTGTAACAATTCC	qRT-PCR
Brca2 F	ATGCCCGTTGAATACAAAAGGA	qRT-PCR
Brca2 R	ACCGTGGGGCTTATACTCAGA	qRT-PCR
Ubc F	GATCTTTGCAGGCAAGCAG	qRT-PCR
Ubc R	AAAGATCTGCATCCCACCTC	qRT-PCR

Charter 4: Genetic co-inactivation of Asxl1 and Ezh2 led to multiple haematopoietic malignancies

4.1. Introduction

The roles of loss-of function mutation of Asxl1 or Ezh2 in the pathogenesis of haematopoietic diseases have been established few years ago via mouse models with tissue-specific genetic inhibition of Asxl1 or Ezh2 alone or concomitant deletion with Tet2, one of epigenetic regulators with high frequencies of mutations in myeloid malignancies, in haematopoietic cells (Abdel-Wahab et al., 2013; Abdel-Wahab et al., 2011; Mochizuki-Kashio et al., 2015). Although the reconstitution of donor-derived bone marrow showed inefficient production of lymphocytes, loss of Ezh2 promoted myeloid-biased repopulation and haematopoietic stem/progenitor cells in early haematopoiesis (Abdel-Wahab et al., 2011). Furthermore, conditional knockout of Ezh2 in BM cells led to development of mild haematopoietic diseases resembling human myelodysplastic disorders such as MDS and MDS/MPN. While no significant difference was observed in the survival of *Ezh2* conditional knockout (cKO) mice, co-inactivation of Ezh2 with Tet2 significantly shorted the disease latency and caused most of mice died by 10 months after transplantation (Abdel-Wahab et al., 2011; Mochizuki-Kashio et al., 2015), demonstrating cooperation of loss of epigenetic modifiers in pathogenesis of myelodysplastic disorders.

While both MDS and MDS/MPN-like phenotypes featured with leukopenia (low white blood cell counts), anaemia (low levels of Hgb) and appearance of dysplastic cells including pseudo-pelger Huet cells, hypersegmented neutrophils, giant platelets and red blood cells with Howell Jolly bodies, myeloproliferative features such as

splenomegaly, extramedullary haematopoiesis (EMH), and monocytosis or thrombocytosis in PB were identified in the MDS/MPN mice. Furthermore, more heterogenous disease phenotypes including MDS (34%), T-ALL/Lymphoma (33%), and B-LPD (25%), were developed in secondary transfer of BM cells from *Ezh2* cKO mice with myelodysplastic disorders. T-ALL was found in 4 of 12 mice with prominent expansion of $CD8^{+}Tcr\alpha b1^{+}$ T cells in thymus and PB. Intriguingly, expansion of $CD19^{+}B220^{low}CD5^{+}$ cells was detected in PB, and it was possible that some of them were clonal based on genomic PCR result of D-J rearrangement, suggesting that loss of Ezh2 may also have an impact on leukaemogenesis of CLL (Mochizuki-Kashio et al., 2015).

By comparison with Ezh2, loss of Asxl1 displayed relatively marginal disease phenotype in primary transplantation. Conditional knockout of *Asxl1* in BM cells only resulted in myelodysplasia in a long observation period with no lethality, which was featured with low BM cellularity, leukopenia, anaemia, and appearance of dysplastic cells such as pseudo-pelger Huet cells, and concomitant deletion of Tet2 did not significantly improve the disease lethality (Abdel-Wahab et al., 2013). However, the phenotype could be further progressed to MDS/MPN-like lethal phenotype with splenomegaly and EMH in spleens after serial transfer, and all mice came down in 45 weeks after tertiary transplantation. Meanwhile, in molecular aspects, genes involved in leukaemogenesis of AML such as *Hoxas* and their associated transcription factors like *Hes5* and *Gdf11* were upregulated in *Asxl1* cKO LSK and myeloid progenitors. This is consistent with an in vitro study showing the involvement of Asxl1 in the repressive function of PRC2, further suggesting the possibility that concurrent deletion of Ezh2 with Asxl1 may transform the mild myeloid haematopoietic disease to acute leukaemia (Abdel-Wahab et al., 2012). To investigate the pathogenesis of concurrent

deletion of Asxl1 and Ezh2 in haematological malignancies, their impacts on early and malignant haematopoiesis were characterized in the compound cKO mouse model.

4.2. Results

4.2.1. Loss of Asxl1 and Ezh2 perturbed haemotopoiesis toward myeloid-biased repopulation in early engraftments

With a view to investigating the impact of loss of PRC2 on haematopoiesis, BM cells from single and compound *Asxl1*$^{fl/fl}$*Ezh2*$^{fl/fl}$ mice driven by Rosa26-CreER and *Asxl1*$^{fl/fl}$*Ezh2*$^{fl/fl}$ mice without Rosa26-CreER as a control (*Wt*) in pure C57BL/6 background (CD45.2 positive) were transplanted into lethally irradiated recipient SJL mice (CD45.1 positive), and the early engraftments and haemotopoiesis were analysed after tamoxifen treatment (Figure 3.2). While the percentage of CD45.2^{+} donor cells in peripheral blood (PB) reduced after knocking out *Asxl1* or/and *Ezh2* in a month, the engraftments reconstituted gradually after 3 months together with the significant increase of myeloid components in *Ezh2* single cKO and *Asxl1*/*Ezh*2 cKO mice, whereas the proportion of lymphoid populations continued decreasing, showing myeloid-biased repopulation in early haematopoiesis as previous *Ezh2* knockout mouse studies (Muto et al., 2013) (Figure 4.1A). Meanwhile, the knockout efficiency was confirmed by PCR of genomic DNA from PB (Figure 4.1B). The absolute blood cell counts in PB further revealed that the bias was mainly resulting from the drastic reduction of lymphoid cells, especially B cells, from 1 month to 3 months after knockout of *Ezh2* (Figure 4.1C, right). On the other hand, loss of Ezh2 can be relatively tolerated in myeloid lineages, and the recovery of absolute numbers of myeloid populations were significantly improved when genetically co-inactivating Asxl1 with Ezh2 (Figure 4.1C, left). In addition, looking into the reproduction of terminal blood

cells, while mild anaemia (decrease in RBC and Hgb) were detected in *Asxl1*/*Ezh2* double cKO mice, the platelets were significantly increased one month after loss of Ezh2 and Asxl1, showing the improvement of megakaryopoiesis in the early stage (Figure 4.1D).

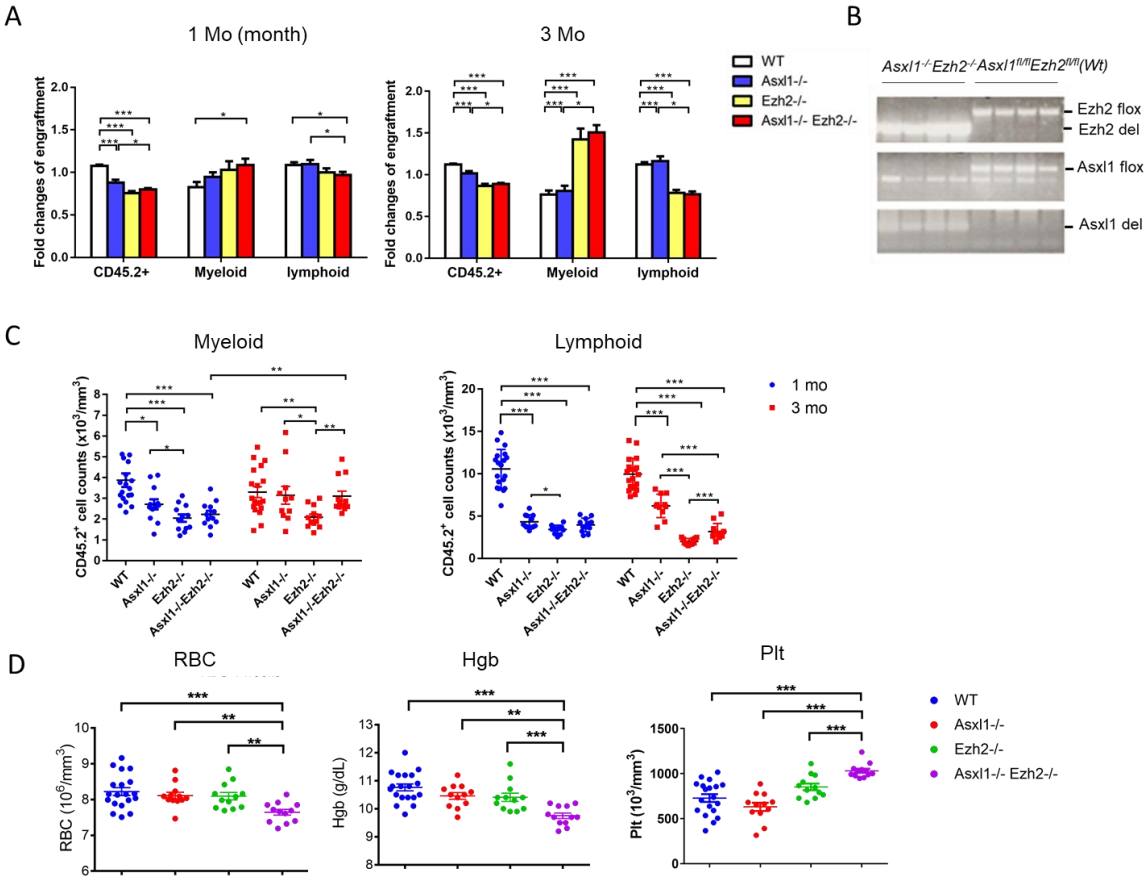

Figure 4.1. The effect of depletion of Asxl1 or/and Ezh2 on early repopulation of haematopoietic cells. BM cells form *Asxl1*$^{fl/fl}$*Ezh2*$^{fl/fl}$ (*Wt*), *Asxl1*$^{fl/fl}$-Rosa-Cre (*Asxl1*$^{-/-}$), *Ezh2*$^{fl/fl}$-Rosa-Cre (*Ezh2*$^{-/-}$), and *Asxl1*$^{fl/fl}$*Ezh2*$^{fl/fl}$-Rosa-Cre (*Asxl1*$^{-/-}$*Ezh2*$^{-/-}$) were transplanted into irradiated CD45.1^{+} recipient mice, and (A) the fold changes of engraftments (CD45.2^{+}), myeloid proportion (Mac1^{+} or/and Gir1^{+}) and lymphoid proportion (B220^{+}, CD4^{+} or CD8^{+}) in donor cells, (B) knockout efficiency and (C)) their absolute cell counts in PB were analysed at indicated months (mo) after TAM treatment. (D) blood counts in PB were analysed at 1 month after TAM treatment. Red blood cells (RBC); Haemoglobin (Hgb); Platelets (Plt). Bar graphs show mean+S.E.M. (*P<0.05, **P<0.01 and ***P<0.001, unpaired t-test).

Furthermore, analysis of repopulating capacity of HSPCs uncovered that concurrent deletion of *Asxl1* and *Ezh2* enhanced establishment of Lineage$^-$Sca1$^+$c-Kit$^+$ (LSK) cells and myeloid progenitors (Lineage$^-$c-Kit$^+$Sca1$^-$) in BM, in which the percentages of MPPs, GMPs and CMPs significantly increased while no change were found in LT-HSCs and ST-HSCs (Figure 4.2A), and Ki67 staining of LSK cells further demonstrated genetic co-inactivation of Asxl1 and Ezh2 accelerated cell cycle progression, in which the proportion of LSK cells in S-G2-M phases increased in the double mutants, partially accounting for the remarkable recovery of myeloid differentiation at 3 months in the compound mice (Figure 4.2B).

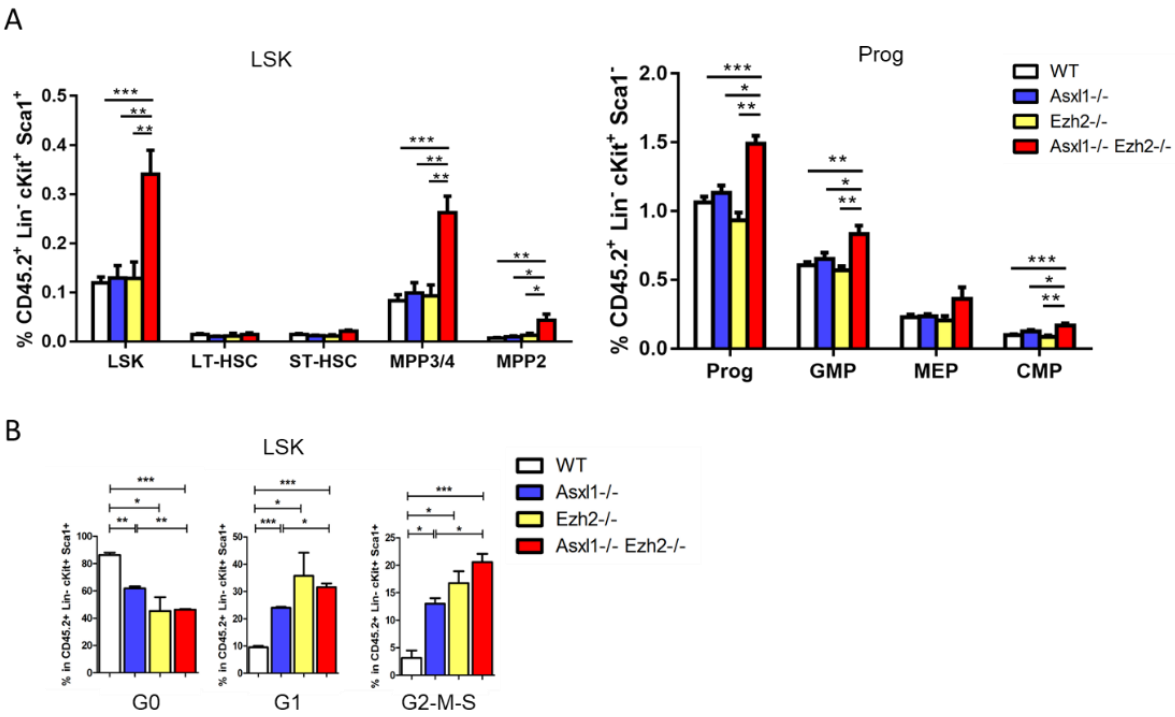

Figure 4.2. Establishments of LSKs and progenitors after *Asxl1* or/and *Ezh2* cKO. (A) Percentages of LSK (Lin$^-$c-Kit$^+$Sca1$^+$), myeloid progenitors (Lin$^-$c-Kit$^+$Sca1$^-$), and their subpopulations: long-term (LT) HSCs (CD48$^-$CD150$^+$), short-term (ST) HSCs (CD48$^-$CD150$^-$), multipotent progenitor (MPP) 3/4 (CD48$^+$CD150$^-$), MPP2 (CD48$^+$CD150$^+$), GMP (CD16/32$^+$CD34$^+$), CMP (CD16/32$^-$CD34$^+$) and MEP (CD16/32$^-$CD34$^-$) in BM from indicated mutant mice 4 weeks after TAM treatment. (B) Percentages of LSK in G0 (Ki67$^-$DAPI^{low}), G1 (Ki67$^+$DAPI^{low}) and G2-M-S (Ki67$^+$DAPI^{high}) phases in LSK cells based on Ki67 staining. Bar graphs show mean+S.E.M. (*P<0.05, **P<0.01 and ***P<0.001, unpaired t-test).

4.2.2. Knockout of *Asxl1* and *Ezh2* led to development of multiple haematopoietic malignancies

It has been established that genetic inhibition of Asxl1 or Ezh2 may result in mild myeloid disorders such as MDS and MDS/MPN overlap and lymphoid diseases in mouse models (Abdel-Wahab et al., 2013; Mochizuki-Kashio et al., 2015). In an attempt to identify the heterogenous phenotypes, BM, spleens and PB collected from sick mice were analysed, and comprehensive characterization was based on cytological staining, histopathological examination and follow cytometry of haematopoietic cells. While no *Wt* and *Asxl1* single cKO mice developed haematological malignancies, *Asxl1*/*Ezh2* double cKO mice started coming down with haematopoietic diseases after a long latency (60 weeks after primary transplantation) with a very high lethality rate (12 out of 14 mice). On the other hand, only a couple of Ezh2 single mutants become symptomatic and visually ill before the end of experiments (Figure 4.3A).

Knockout of *Asxl1* and *Ezh2* in haematopoietic cells were verified by PCR using primers targeting critical exons flanked with *loxp* sites (*flox*) and RNA-seq (Figure 4.4). While *Ezh2* genotyping only exhibited *flox* bands in the wild type mice ($Asxl1^{fl/fl}Ezh2^{fl/fl}$), Ezh2 deletion bands were detected in *Ezh2* single cKO ($Ezh2^{-/-}$) and double cKO mice ($Asxl1^{-/-/}Ezh2^{-/-}$). On the other hand, Asxl1 was deleted in *Asxl1* single cKO ($Asxl1^{-/-}$) and double cKO mice ($Asxl1^{-/-/}Ezh2^{-/-}$) (Figure 4.4A). The expression of floxed exons were further examined and analysed in RNA-seq results, showing efficient knockout of exon 3 in *Asxl1* and exon 16 to 19 in *Ezh2* in BM cells from mutant mice (Figure 4.4B)

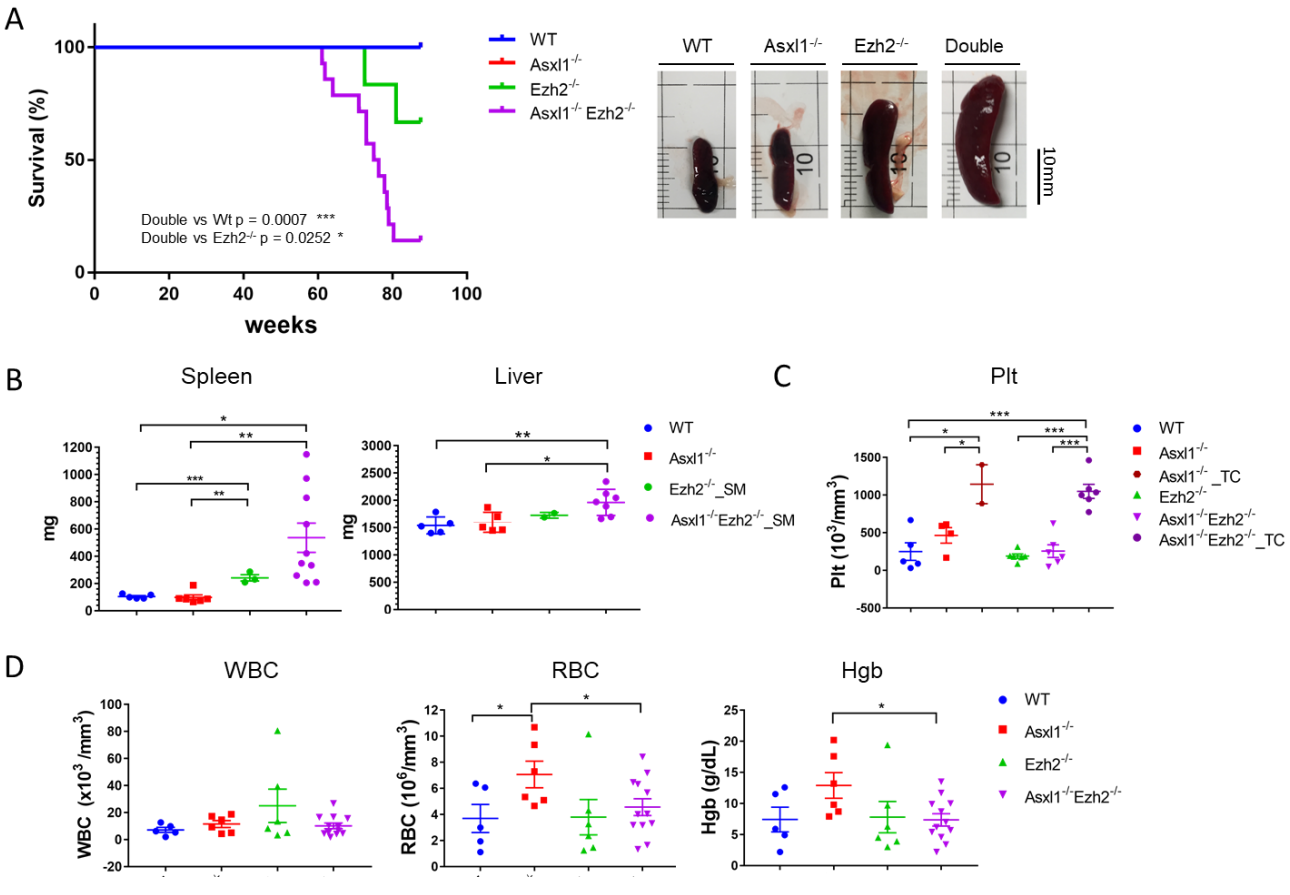

Figure 4.3. Disease latencies and penetrance of *Asxl1* or/and *Ezh2* cKO mice. (A) Survival curves of *Wt* (n=7), *Asxl1*$^{-/-}$ (N=6), *Ezh2*$^{-/-}$ (N=6) and *Asxl1*$^{-/-}$*Ezh2*$^{-/-}$ (N=14) mice in primary transplantation (left), and representative images of spleens (right). (B) Weights of spleen and livers from *Wt*, *Asxl1*$^{-/-}$, *Ezh2*$^{-/-}$ and *Asxl1*$^{-/-}$*Ezh2*$^{-/-}$ mice with splenomegaly (SM). (C) Platelets (Plt) and (D) blood counts in PB. White blood cells (WBC); Haemoglobin (Hgb); Thrombocytosis (TC). Scale bar, 1cm. Dot graphs show mean+S.E.M. (*P<0.05, **P<0.01 and ***P<0.001, unpaired t-test).

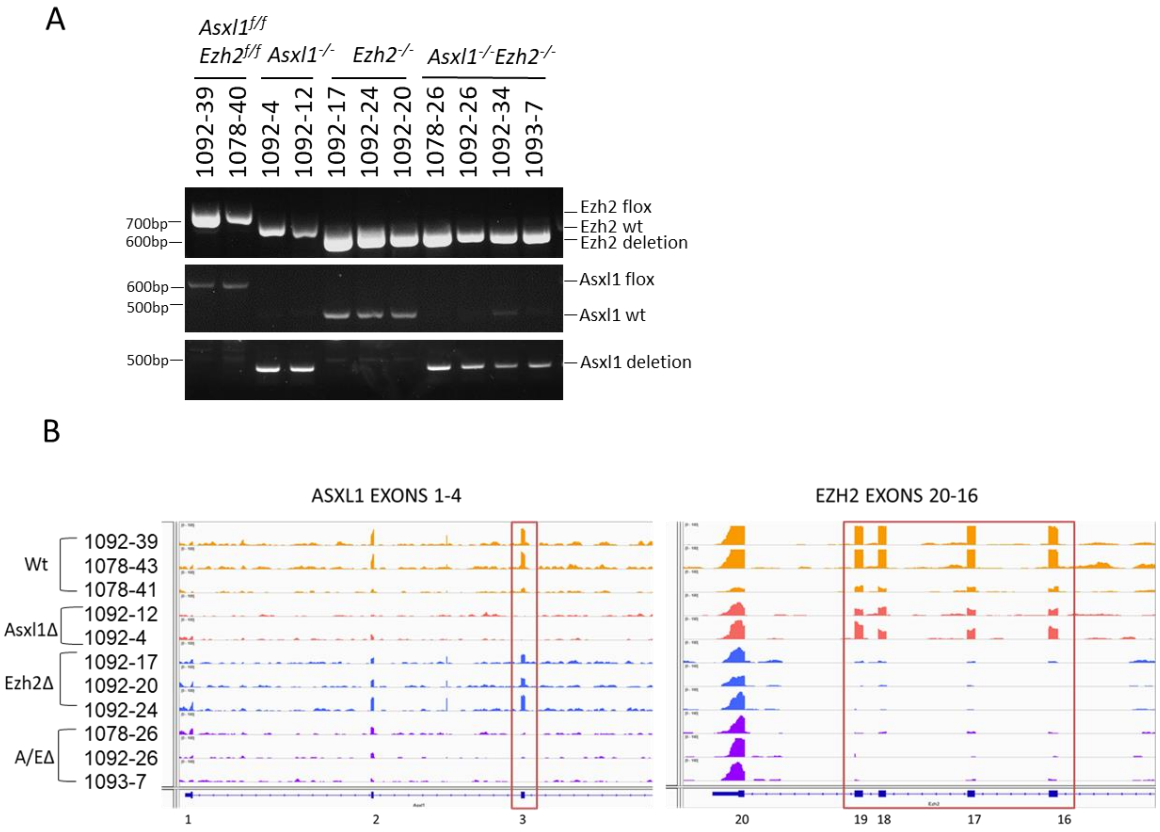

Figure. 4.4. Genotypes of mutant mice in primary experiments. (A) PCR results confirming the genotypes of *Asxl1* and *Ezh2* in splenocytes from *Asxl1*$^{f/f}$*Ezh2*$^{f/f}$ (*Wt*) and *Asxl1* cKO (*Asxl1*$^{-/-}$), *Ezh2* cKO (*Ezh2*$^{-/-}$) and double mutant (*Asxl1*$^{-/-}$*Ezh2*$^{-/-}$) mice. (B) RNA-seq showing the exon deletions of *Asxl1* (exon 3) and *Ezh2 (*exon 16-19) in BM cells from *Wt* (1092-39, 1078-43, 1078-41), *Asxl1* (1092-12, 1092-4), *Ezh2* (1092-17, 1092-20, 1092-24) and *Asxl1*/*Ezh2* cKO mice (1078-26, 1092-26, 1093-7).

Organomegaly, especially splenomegaly, where lymphoid follicles of spleens were effaced and disrupted, were found in *Asxl1*/*Ezh2* double cKO mice (Figure 4.3B). In addition, blood counts showed thrombocytosis (increase in platelets) in double mutants while no significant cytopenia were as observed (Figure 4.3C-D), and the existence of abnormal megakaryocytes in H&E staining of spleens further suggests extramedullary haematopoiesis (EMH) occurred in *Asxl1*/*Ezh*2 double mutant mice (Figure 4.5)

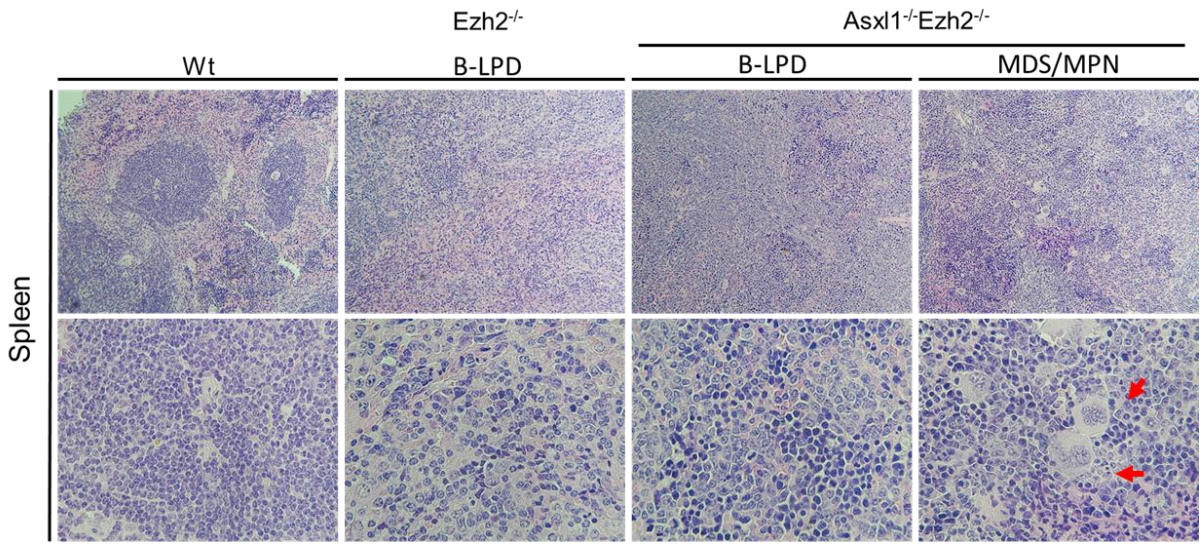

Figure 4.5. H&E staining of spleen sections from sick mice. H&E staining of spleen sections from *Wt*, *Ezh2* cKO mice with B-LPD phenotypes (1092-17) and *Asxl1*/*Ezh2* cKO mice with MDS/MPN (8749) or B-LPD phenotypes (1078-26). Megakaryocytes were pointed out with red arrows in MDS/MPN mice. Microscopic magnification: 10× (upper panels) or 40× (bottom panels).

Looking into myeloid lineages, granulopoiesis was left-shifted in BM from *Ezh2* single mutants and *Asxl1*/*Ezh2* double mutants especially, in which the percentage of myeloblasts and promyelocytes were significantly augmented, whereas proportions of band cells decreased (Figure 4.6A). In addition, MG/Giemsa staining revealed myeloid dysplastic cells such as abnormal megakaryocytes (monolobated, binucleated) and pseudo-pelger-Huet anomalies, were found in BM of *Ezh2* single cKO and *Asxl1*/*Ezh2* double cKO mice, indicating cytologic dysplasia in megakryopoiesis and granulopoiesis (Figure 4.6B).

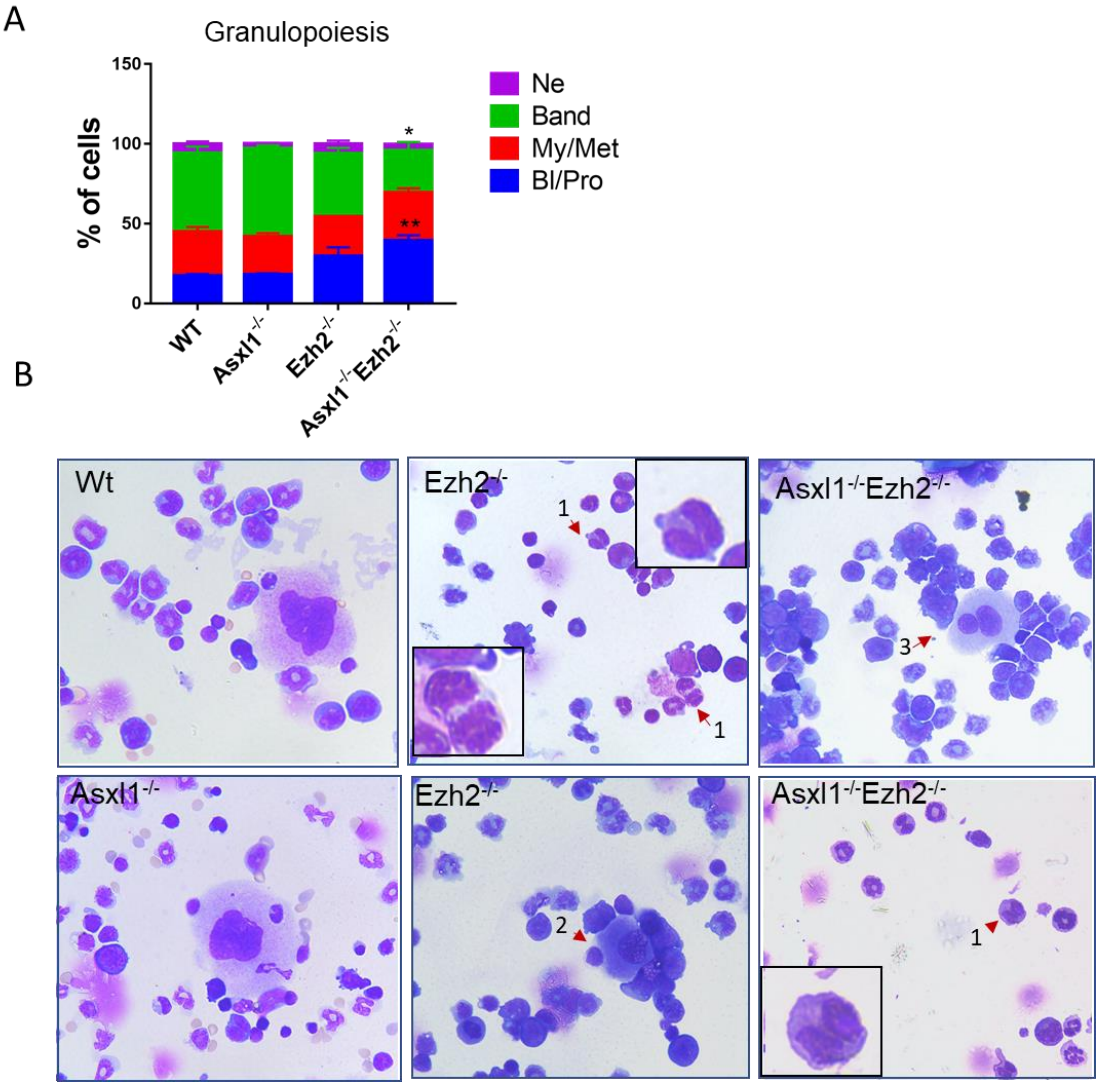

Figure 4.6. Myelodysplasia in *Ezh2* and *Asxl1*/*Ezh2* cKO mice. (A) Percentages of haematopoietic cells blasts/promyelocytes (Bl/Pro), myelocytes/metamyelocytes (My/Met), band cells and Neutrophils (Ne) in granulopoiesis from *Wt* and cKO mice with MDS phenotypes. Bar graphs show mean+S.E.M. (*P<0.05, **P<0.01 and ***P<0.001, unpaired t-test). (B) Representative images of MG-Giemsa staining of BM from *Wt*, *Asxl1*$^{-/-}$, *Ezh2*$^{-/-}$ and *Asxl1*$^{-/-}$*Ezh2*$^{-/-}$ mice. Myeloid dysplastic cells such as pseudo-Pelger-Huët anomalies (1), monolobated (2) and binucleated (3) megakaryocytes were found in the BM of MDS mice.

While EMH was observed in spleens from three *Asxl1*/*Ezh2* cKO MDS mice, showing MDS/MPN-like phenotype, small lymphocytes were found diffused in spleens from Ezh2 single mutants and the other Asxl1/Ezh2 double mutants, leading to splenomegaly (Figure 4.5), and lymphoid populations were highly expanded in BM from two *Asxl1*/*Ezh2* MDS cKO mice, revealing the possibility of co-existence of lymphoproliferations in the MDS mice (Figure 4.7A). $B220^{-/low}$ $CD4^{-}CD8^{-}$ lymphoid cells, which was thought to be B1α cells according to previous mouse studies (Klein et al., 2010; Mochizuki-Kashio et al., 2015; Planelles et al., 2004), became the dominant lymphoid population in the spleens of B-cell lymphoproliferative disorder (B-LPD) mice, especially *Asxl1*/*Ezh2* cKO B-LPD mice with high lymphoid infiltration in BM ($B\text{-}LPD^{high}$) (Figure 4.7B-C). Intriguingly, RNA-seq profiling revealed gene enrichment in spleen B1α cells-preferentially expressed genes in BM of B-LPD mice, further supporting the phenotype of B-LPD and suggesting B1α cells may infiltrate from the spleens into BM in the B-LPD mice (Figure 4.7D). Morphologically, typical CLL cells, with clumpy nuclei and a rim of visible cytoplasm, were identified in the BM of B-LPD mice (Figure 4.7E)

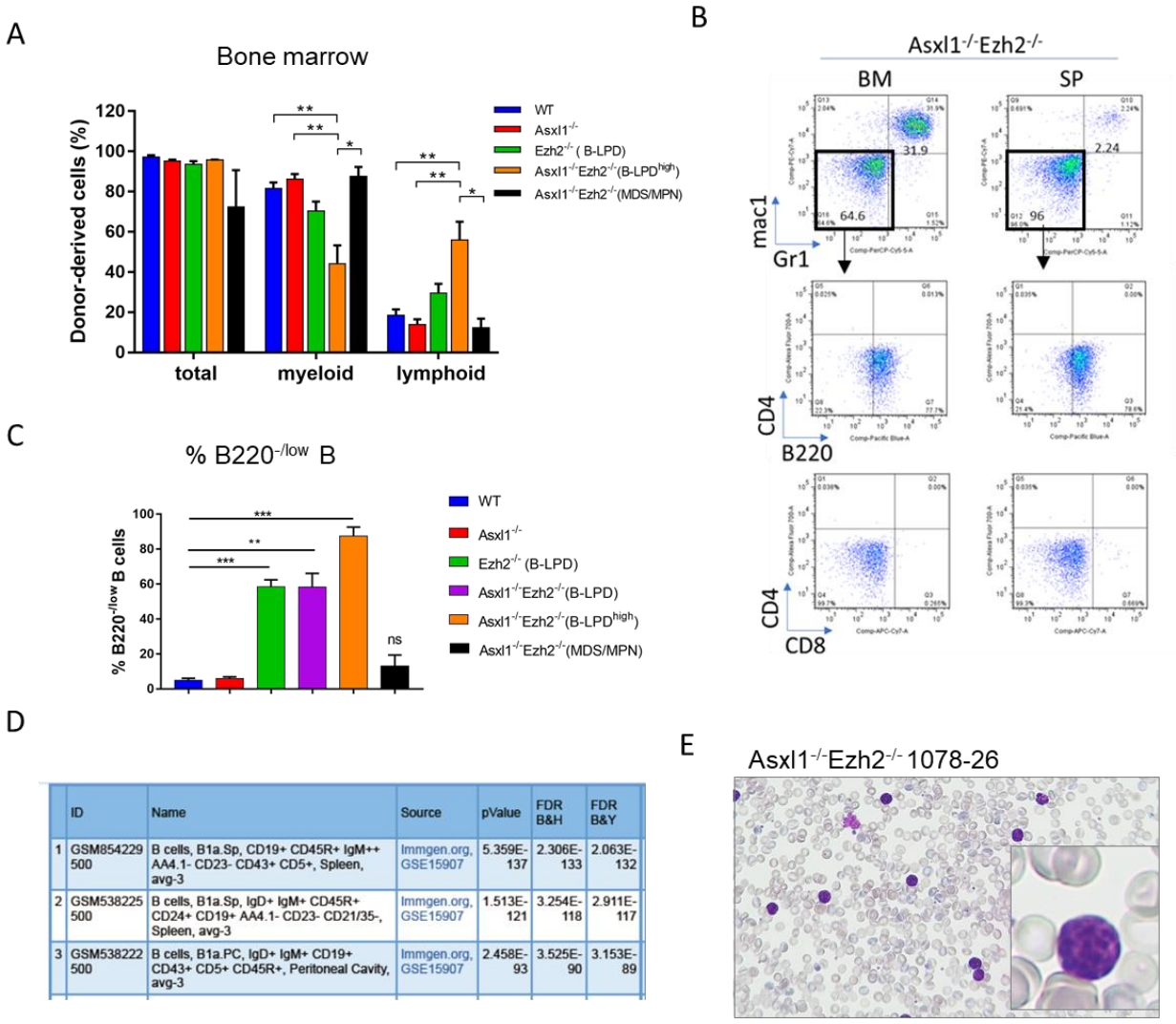

	ID	Name	Source	pValue	FDR B&H	FDR B&Y
1	GSM854229500	B cells, B1a.Sp, CD19+ CD45R+ IgM++ AA4.1- CD23- CD43+ CD5+, Spleen, avg-3	Immgen.org, GSE15907	5.359E-137	2.306E-133	2.063E-132
2	GSM538225500	B cells, B1a.Sp, IgD+ IgM+ CD45R+ CD24+ CD19+ AA4.1- CD23- CD21/35-, Spleen, avg-3	Immgen.org, GSE15907	1.513E-121	3.254E-118	2.911E-117
3	GSM538222500	B cells, B1a.PC, IgD+ IgM+ CD19+ CD43+ CD5+ CD45R+, Peritoneal Cavity, avg-3	Immgen.org, GSE15907	2.458E-93	3.525E-90	3.153E-89

Figure 4.7. Population of B220$^{-/low}$ B cells in *Ezh2* single and *Asxl1*/*Ezh2* double cKO LPD mice. (A) Engraftments of donor cells (CD45.2+) and their proportions of myeloid and lymphoid populations in BM from indicated mutant mice. *Wt* (N=5), *Asxl1*$^{-/-}$ (N=5), *Ezh2*$^{-/-}$ (MDS, B-LPD) (N=3), *Asxl1*$^{-/-}$*Ezh2*$^{-/-}$ (MDS/MPN) (N=3) and *Asxl1*$^{-/-}$*Ezh2*$^{-/-}$ (MDS, B-LPD^{high}) (N=2). (B) Representative flow cytometry profiling of donor cells in bone marrow and spleens from *Asxl1*$^{-/-}$*Ezh2*$^{-/-}$ B-LPD mice. (C) Bar charts showing % of B220$^{-/low}$ B cells in spleens from indicated mutant mice. LPD mice with high level of lymphoid expansion (> 50%) in BM was marked as B-LPD^{high}. Bar graphs show mean+S.E.M. (*P<0.05, **P<0.01 and ***P<0.001, unpaired t-test). (D) Co-expression atlas showing expansion of B1α cells in BM from *Ezh2* single and *Asxl1*/*Ezh2* double cKO mice based on UP differential gene lists from RNA-seq. (E) Representative images of MG-Giemsa staining of CLL cells in PB of an Asxl1$^{-/-}$*Ezh2*$^{-/-}$ B-LPD mouse (1078-26).

In summary, all sick mice exhibited characteristics of myelodysplasia such as left-shift in granulopoiesis and appearance of dysplastic cells in at least one myeloid lineage in double mutants, and 50% of *Asxl1*/*Ezh2* double cKO mice further displayed myeloproliferative features, including splenomegaly with infiltration of myeloid precursor cells in spleens or/and thrombocytosis. In addition, B-LPD were found in 42% of *Asxl1*/*Ezh2* double cKO mice, and all shows the $B220^{-/low}$ $CD4^{-}CD8^{-}$ immunophenotype, suggesting the possibility of development of CLL. Meanwhile, lymphoproliferation of B cells were also detected in 3 out of 6 Ezh2 cKO mice together with myelodysplasia phenotypes although one of them may not be expansion of B1α ($B220^{-/low}$). As a result, loss of Asxl1 and Ezh2 led to highly lethal diversified disease phenotypes including MDS (8.3%), MDS/MPN (25%), MDS/MPN_TC (25%), characterized with increase in platelet numbers but without severe myeloproliferative features in spleens (Mochizuki-Kashio et al., 2015), and myelodysplastic disorder overlapped with B-LPD (42%, CLL-like), whereas depletion of Ezh2 only contributed to the single phenotype MDS overlapped with B-LPD (50%, CLL-like 33%) (Figure 4.8).

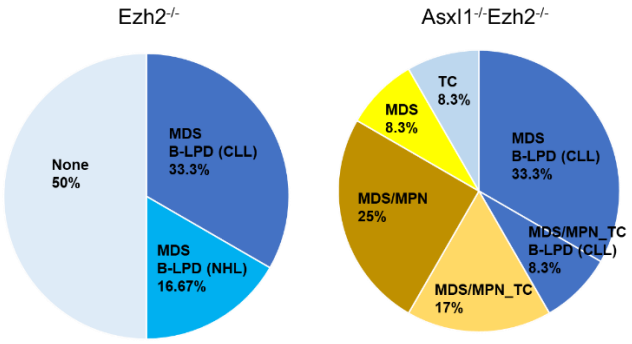

Figure 4.8. Summary of disease phenotypes in primary experiments. Pie charts showing the development of heterogenous haematologic malignancies and ratios in *Ezh2* single cKO mice and *Asxl1*/*Ezh2* double cKO mice. Thrombocytosis (TC); non-Hodgkin's lymphoma (NHL).

4.3. Discussion

The effect of loss of Ezh2 in early haematopoietic repopulation has been reported in a mouse study in which recipient mice transplanted with total BM cells or LSK cells with knockout of *Ezh2* displayed myeloid-biased differentiation (Muto et al., 2013). By comparison with the mice transplanted with *Wt* BM cells or *Wt* LSK cells, the engraftment of donor cells reduced in the PB from mice transplanted with *Ezh2* knockout haematopoietic cells from the primary transplantation in the first two months, showing the reconstitution capacity of haematopoietic cells might be attenuated after loss of Ezh2. However, the engraftment of *Ezh2*$^{-/-}$ donor cells recovered after 3 months, and while the lymphoid population was barely detected, the proportion of myeloid populations, LSK and myeloid progenitors (GMP, CMP and MEP) drastically increased, further revealing loss of Ezh2 could be tolerated in primary haematopoietic cells and may promote myeloproliferation (Mochizuki-Kashio et al., 2015; Muto et al., 2013). Similarly, the engraftments were attenuated soon after knockout of *Asxl1* and *Ezh2* in our primary transplantation, but gradually recovered with significant elevation of the percentage of myeloid populations in PB of *Ezh2* single cKO and *Asxl*/*Ezh2* double cKO chimeric mice (Figure 4.1A), showing myeloid biased repopulation as well, and looking into absolute cell counts further revealed loss of the PRC2 components was more tolerated in myeloid differentiation, thus leading to the biased repopulation (Figure 4.1C). Furthermore, genetic co-inactivation of Asxl1 with Ezh2 promoted the recovery of myeloid cell counts from 1 month to 3 months after knockout probably owing to enhancement of establishment of LSK cells and myeloid progenitors in early engraftments (Figure 4.1C-D), suggesting loss of Asxl1 and Ezh2 may augment the myeloproliferation in the early haematopoiesis and then accelerate myeloid disease progression.

Indeed, loss of Asxl1 and Ezh2 ultimately resulted in higher penetrance (92%) of lethal myelodysplastic disorders including MDS/MPN phenotypes (50%), whereas only 3 of 6 Ezh2 cKO mice displayed myelodysplasia, demonstrating the pathological impact of cluster mutations on PRC2 for development of myeloid neoplasms (Figure 4.1-4.3 and Table 4.1). In Asxl1 single mutants, although no visual illness and myelodysplastic cells was observed, increase in platelet numbers were also detected in two of Asxl1 single mutants (Figure 4.3C), suggesting loss of Asxl1 may contribute the phenotype of thrombocytosis to double mutants.

According to the previous mouse studies of Ezh2, only phenotypes of mild myelodysplastic disorders were displayed in the primary transplantation although more diversified phenotypes of haematological malignancies such as T-ALL/lymphoma and B-LPD developed in the secondary transplantation (Mochizuki-Kashio et al., 2015). While our *Ezh2* knockout also resulted in development of myelodysplasia in the granulocytic lineage and megakaryocytic lineage (Figure 4.3-4.6), no T-ALL phenotype and expansion of CD4/8 T cells was identified in our *Ezh2* single cKO mice as in the previous studies. Half of Ezh2 mutant mice developed B-LPD in the primary transplantation, indicating a longer latency was probably required for the development of lymphoproliferation in the primary host. 2 out of 3 B-LPD exhibited expansion of B1α ($B220^{-/low}$) in BM and spleens with mild splenomegaly, revealing a novel tumour suppressor role of Ezh2 in CLL leukaemogenesis (Figure 4.8 and Table 4.1).

By comparison with the *Ezh2* single cKO mice, concurrent deletion of *Asxl1* with *Ezh2* provided myeloproliferative features to the mice with myelodysplasia, in which the precursor cells in the megakaryocytic lineage infiltrated into spleens, leading to splenomegaly (Figure 4.5), and the terminal blood cells platelets were significantly

increased in PB, resulting in thrombocytosis (Figure 4.3), showing the megakaryocytic lineage prone leukaemogenesis in the *Asxl1*/*Ezh2* double cKO mouse model. On the other hand, loss of Asx1 and Ezh2 also enhanced the lymphoproliferative phenotype. *Asxl1*/*Ezh2* cKO B-LPD mice were characterized with more severe splenomegaly, and two of them exhibited exceptionally high BM infiltration, suggesting loss of Asxl1 and Ezh2, two key components of PRC2, may also cooperate in leukaemogenesis of CLL. Therefore, to further characterize the CLL phenotype of our mouse models, the clonality of immunoglobulins, immunophenotypes of B1α cells, underlying mechanism and potential factors critical for the CLL leukaemogenesis mediated by Ezh2 single mutants and Asxl1/Ezh2 double mutants will be studied in more details in the following chapter.

Table 4.1. Characterization of haematopoietic malignancies.

Genotypes	Code	Myeloid blast	Granulopoiesis	Megakaryocyte	Spleno-megaly	TC	Myeloid infiltration of spleen	B1α proliferation	Clonality	Diseases
Asxl1$^{-/-}$Ezh2$^{-/-}$	1078-26	16%	left-shift, Pseudo-Pelger Huet	mnolobatedand binuclea	big		none	yes (high)	Mono (U)	MDS, B-LPD (CLL)
Asxl1$^{-/-}$Ezh2$^{-/-}$	1078-27	18.30%	left-shift	mnolobated and multinuclea	none	yes	none	unknown		MDS/MPN_TC
Asxl1$^{-/-}$Ezh2$^{-/-}$	1092-26	15.30%	left-shift	mnolobated	big		none	yes (high)	Mono (U)	MDS, B-LPD (CLL)
Asxl1$^{-/-}$Ezh2$^{-/-}$	1092-27	10.10%	left-shift	mnolobated	big	yes	yes (EMH)	none		MDS/MPN
Asxl1$^{-/-}$Ezh2$^{-/-}$	1093-7	11.90%	left-shift, Pseudo-Pelger Huet	mnolobated and binuclea	yes	yes	none	yes	Mono (U)	MDS/MPN_TC, B-LPD (CLL)
Asxl1$^{-/-}$Ezh2$^{-/-}$	1092-34	13.40%	left-shift	mnolobated	big		none	yes		MDS, B- LPD (CLL)
Asxl1$^{-/-}$Ezh2$^{-/-}$	1092-35		None	normal shape	None	yes	none	none		TC
Asxl1$^{-/-}$Ezh2$^{-/-}$	1092-36	8.50%	left-shift, Pseudo-Pelger Huet	bi and multinuclea	yes		none	yes		MDS, B-LPD (CLL)
Asxl1$^{-/-}$Ezh2$^{-/-}$	8748	17.70%	left-shift, Pseudo-Pelger Huet	mnolobated, and binuclea	big		yes (EMH)	none		MDS/MPN
Asxl1$^{-/-}$Ezh2$^{-/-}$	8749	11.50%	left-shift, Pseudo-Pelger Huet	microform and bionuclea	big	yes	yes (EMH)	none		MDS/MPN
Asxl1$^{-/-}$Ezh2$^{-/-}$	8745		left-shift	mnolobated	None	yes	none	none		MDS/MPN_TC
Asxl1$^{-/-}$Ezh2$^{-/-}$	8746	13.90%	left-shift, Pseudo-Pelger Huet	mnolobated	None		none	none		MDS
Ezh2$^{-/-}$	1092-17	12.20%	left-shift, Pseudo-Pelger Huet	mnolobated	yes		none	yes	Mono (U)	MDS, B-LPD (CLL)
Ezh2$^{-/-}$	1092-20		left-shift, Pseudo-Pelger Huet	bi and multinuclea	yes		none	yes	Mono (U)	MDS, B-LPD (CLL)
Ezh2$^{-/-}$	1092-24	17.80%	left-shift	mnolobated	yes		none	none	Bi ? (M)	MDS, B-LPD (NHL)
Ezh2$^{-/-}$	1078-19		None	normal shape	None		none	none		None
Ezh2$^{-/-}$	1092-15		None	normal shape	None		none	none		None
Ezh2$^{-/-}$	1092-19		None	normal shape	None		none	none		None
Asxl1$^{-/-}$	1092-4		None	normal shape	None		none	none		None
Asxl1$^{-/-}$	1092-12		None	normal shape	None		none	none		None
Asxl1$^{-/-}$	1078-1		None	normal shape	None	yes	none	none		TC
Asxl1$^{-/-}$	1078-2		None	normal shape	None		none	none		None

EMH (extramedullary haematopoiesis), Mono (Mono-clone), U (unmutated IGHV), M (mutated IGHV), TC (thrombocytosis)

Charter 5: Modelling of *Asxl1*/*Ezh2* double knockout CLL mouse models

5.1. Introduction

Genetically engineered CLL mouse models have been being established for in vivo pathological studies of critical mutations with clinical relevance and in the hope of providing useful pre-clinical models for elucidation of efficacy and mechanism of novel therapies (Simonetti et al., 2014). In general, to model mouse CLL, the disease phenotype is characterized with clonal expansion of B1α cells in PB, spleens and BM, in which the CD5 positive immunophenotype and clonality of BCR were used to define human CLL. *Eμ-TCL1* transgenic mice, the first transgenic CLL model, is well characterized and widely used for study of CLL pathogenesis as its high penetrance (Bichi et al., 2002).

T cell leukaemia-1 (TCL-1) is commonly activated in T cell leukaemia due to translocation to T cell receptor locus (Narducci et al., 1997; Virgilio et al., 1994), and ectopic expression of TCL1 driven by *Lck* promoter in T cell components led to development of mature T cell leukaemia (Virgilio et al., 1998). Tissue specific overexpression of TCL1 in B cells by *IGH* promoter (*Eμ*) driven transgenic system successfully developed a disease resembling human CLL, featured with clonal expansion of B1α cells (IgM^+CD5^+) at 6 months of age in BM, spleen and peritoneal cavity. The CLL mice became visually ill and came down around the age of 13 to 18 months with organomegaly, lymphadenopathy and lymphocytosis. Moreover, cytological and histopathological staining showed infiltration of lymphocytes with clumped nuclear chromatin in lymph nodes, BM and livers. Furthermore, clonality

studies correlated the *Eμ-TCL1* transgenic model with treatment-resistant CLL patients with unmutated *IGHV* and high HCDR3 similarity, and its sensitivity to BTK inhibitors further displayed clinical relevance to *IGHV*-unmutated (U) CLL patients (Ponader et al., 2012; Yan et al., 2006). In addition to TCL-1, genes found dysregulated in CLL were also overexpressed (APRIL and BCL-2 x traf2dn) or genetically inactivated (mir-15a/16-1) to build novel CLL mouse models. APRIL, a TNF-like secreted ligand crucial for the survival of mature B cells, was found overexpressed in around 45% of CLL tumour samples. APRIL transgenic mice developed a CLL-like B1α neoplasm at 12 to 19 months of age, which was characterized with expansion of B1α ($CD19^{+}CD5^{+}CD43^{+}B220^{dim}IgM^{dim}$) in mouse lymph nodes, lymphadenopathy and infiltration of livers and kidneys, suggesting the tumour supporting role of APRIL/ TNFRSF13B ligand-receptor interaction in CLL (Planelles et al., 2004). Overexpression of the anti-apoptotic protein BCL-2 is a key feature of CLL cells, and expressing human BCL-2 in B lymphocyte also resulted in splenomegaly and clonal expansion of B1α in spleens and PB with around 80% penetrance in the cooperation with expression of TRAF2DN, a truncated form TRAF2 (Zapata et al., 2004). Although both models lacked well characterized clonality and *IGH* rearrangements, they successfully correlated the dysregulated molecules with the CLL pathogenesis, and further provided potential targets for CLL therapy.

On the other hand, loss of function genetic lesions found in CLL can also lead to development of CLL disease in mouse models. Deletion in chromosome 13q14.3 (del 13) is the most common abnormality in CLL, and DLEU2/miR15a/miR16-1 cluster is right inside the deletion region, which supressed expression of proteins involved in anti-apoptosis and cell cycle progression (Dohner et al., 2000). Conditional knockout of minimal deletion region (MDR) on the cluster in mice (chromosome 14qC3) and

miR15a/miR16-1 resulted in clonal B cell lymphoproliferations (42% of *MDR*$^{-/-}$ mice and 26% of *miR15a/miR16-1*$^{-/-}$ mice) including CLL (B220^{low}CD5^{+}) and non-Hodgkin lymphoma (NHL) (CD5 negative) phenotypes, in 15 to 18 month old mice, and sequencing *IGHV* revealed the unmutated and stereotypic *IGHV* in CLL with high similarity of HCDR3 (≥80%), whereas NHLs mostly bear somatic mutated *IGHV*. In molecular levels, while several cell cycle associated proteins that have roles in G0/G1-S phase transition were upregulated in mouse B cells with deletion of miR15a/miR16-1, induction of miR15a/miR16-1 impaired cell proliferation and downregulated CCND1/2, CCDE, CCK4/6 and CHK1 in human CLL cell line with del 13q14.3, further suggesting an initiating role of cell cycle progression in CLL pathogenesis (Klein et al., 2010). Given the known mutations affecting Asxl1 and Ezh2 in CLL patients, we further characterized the role of these PRC2 components in CLL pathogenesis.

5.2. Results

5.2.1. Monoclonal unmutated BCR in B-LPD mice

To correlate the lymphoproliferative disorders with leukaemia, the clonality of B cells in B-LPD mice was investigated through looking into RNA expression and sequencing of immunoglobulin heavy chains (*IGH*), known as segments of B cell receptors (BCR). Transcriptional profiling of *IGH* variable regions (*IGHV*) in BM from *Wt*, *Asxl1* single cKO, *Ezh2* single cKO B-LPD and *Asxl1*/*Ezh2* double cKO B-LPD mice was shown in a heatmap and bar plots showing with normalized counts of *IGHV* in RNA-seq data (Figure 5.1-2). As a result, the RNA levels of specific *IGH* variable regions (*IGHV*) surged in BM from B-LPD mice, especially in *Asxl1*/*Ezh2* cKO mice while diversified *IGHV* expressed in *Wt* mice and *Asxl1* single cKO mice, suggesting

mono-clonal B cells may proliferate and infiltrate into BM of B-LPD mice, where lymphoid population enormously expanded (Figure 4.7).

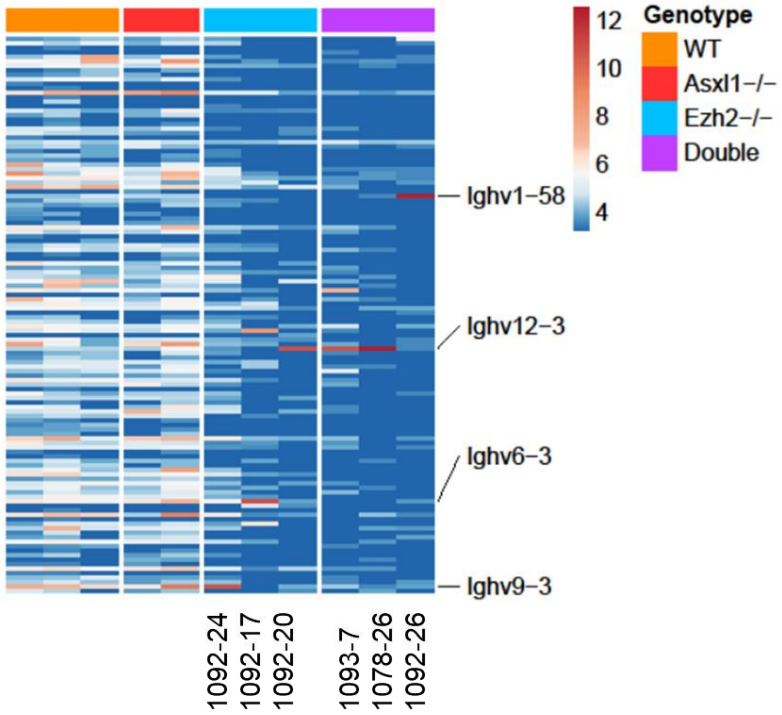

Figure 5.1. RNA-seq profiling of *IGHV* in BM. A heatmap displaying 124 vst normalized counts of mouse *IGHV* from indicated B-LPD mice, and 61 *IGHV* with zero counts was removed. The *IGHV* with substantial expression are pointed out in each B-LPD mouse.

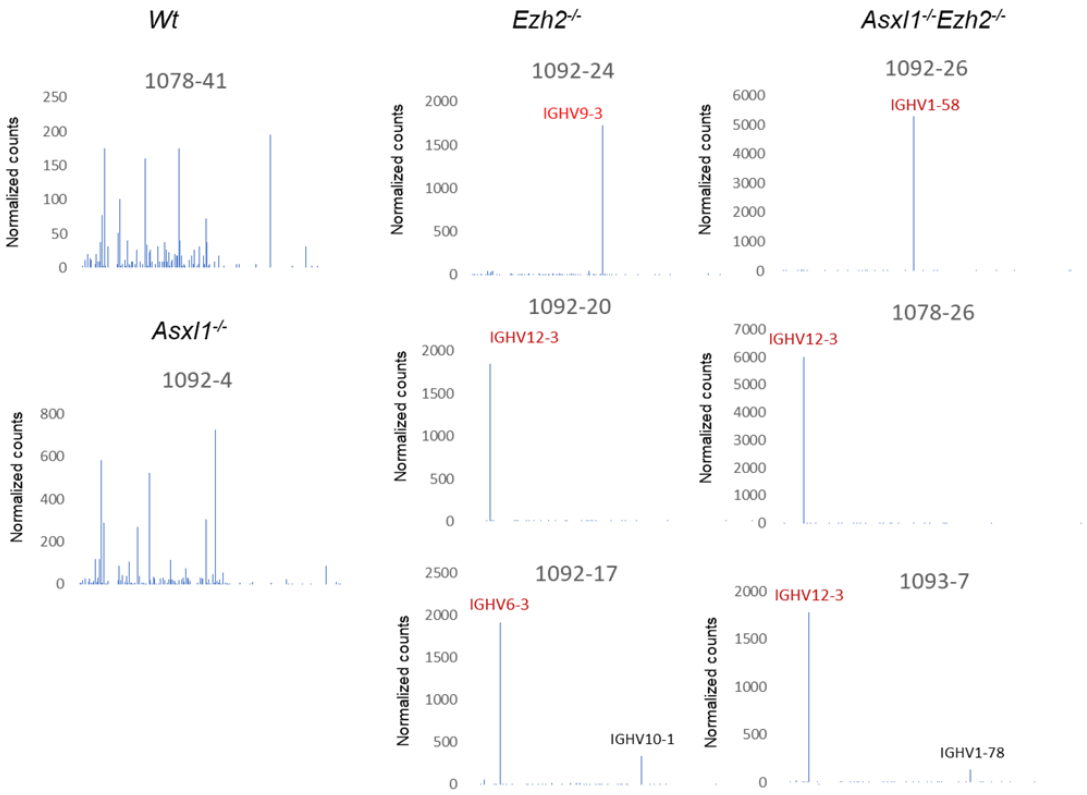

Figure 5.2. Normalized counts of IGHV in BM. Bar charts of normalized counts of *IGHV* in RNA-seq data of BM cells from normal (*Wt*, *Asxl*1 cKO) and B-LPD mice (*Ezh2* cKO and *Asxl1*/*Ezh2* cKO). The outstanding *IGHV* was marked with red colour, and indicated the monoclonal expansion of B cells in BM.

In CLL, structural features of BCR are highly correlated with disease progress and treatments. Patients with BCR comprised of unmutated *IGHV* follow aggressive course and worse prognostic outcomes (Damle et al., 1999; Hamblin et al., 1999). Remarkable structural similarity in heavy chain complementary determining regions (HCDR3) of BCR between patients revealed antigen selection and drive may be important factors for the development of CLL (Tobin et al., 2003; Tobin et al., 2002). Furthermore, to identify the VDJ recombination and sequences of BCR, a primer set targeting the 5' end of *IGHV* (forward) and the conserved region of *IGH* joining segments (*IGHJ*) (reverse) was utilized to amplify mouse V-D-J regions of *IGH* (Size: 339~393 bp)

(White, 1998; Yan et al., 2006), and sequences of *IGHVDJ* in splenocytes of B-LPD were identified by means of Sanger sequencing of the RT-PCR products (Figure 5.3A). Looking into the agarose gel electrophoresis result, PCR products of *IGHVDJ* were exactly located between 300 bp and 400 bp, and compared to *Wt* and *Asxl1* cKO mice, a clear and sharp major band was visualized in *Ezh2* cKO and *Asxl1*/*Ezh2* cKO B-LPD mice although the signals in two B-LPD mice 1092-20 and 1092-34 were relatively low (Figure 5.3B).

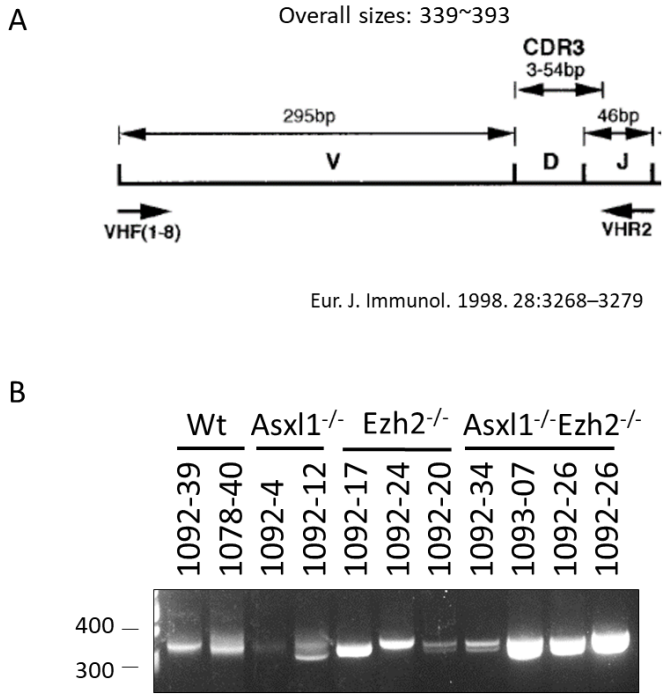

Figure 5.3. RT-PCR of mouse *IGHVDJ* in primary experiments. (A) Schematic diagrams of mouse *IGHVDJ* regions, sizes and primer target sites. Adapted from (White, 1998). (B) RNA extracted from splenocytes from normal (*Wt*, *Asxl*1 cKO) and B-LPD mice (*Ezh2* cKO and *Asxl1*/*Ezh2* cKO) were subjected to RT-PCR of *IGHVDJ* regions.

To further analyse the length and distribution of amplified V-D-J, PCR products were purified and an equal amount of purified DNA from each group was subjected to Agilent Bioanalyzer. As a result, while a peak of PCR products that covered the

predicted range of sizes was shown in *Wt* and *Asxl1* cKO mice, a taller needle-like peak can be detected in B-LPD mice although some of them were coupled with another small minor peak (Figure 5.4A). Clean sequencing chromatograms of purified PCR products from each group revealed mono-sequences of *IGHVDJ* in the B-LPD mice (Figure 5.4B). Furthermore, sequencing of the PCR products gel-extracted from these major sharp bands identified specific V-D-J sequences with unmutated variable region (≥98% identity to germline counterpart) in B-LPD mice, whereas sequencing minor bands only showed noisy signals, suggesting the clonality of B-LPD was monoclonal unmutated *IGHV* (Table 5.1), and 3 out of 6 B-LPD mice shared the same *VH* and *JH* families, and displayed high similarity on HCDR3 (>80%), indicating a common antigen or autoantigen for the clonal expansion of PRC2-defective CLL cells. Together the clonality and characteristics of BCR with the immunophenotypes of B1α, the mouse B-LPD phenotype could be chronic lymphocytic leukaemia (CLL), the most prevalent leukaemia in western countries (Table 4.1).

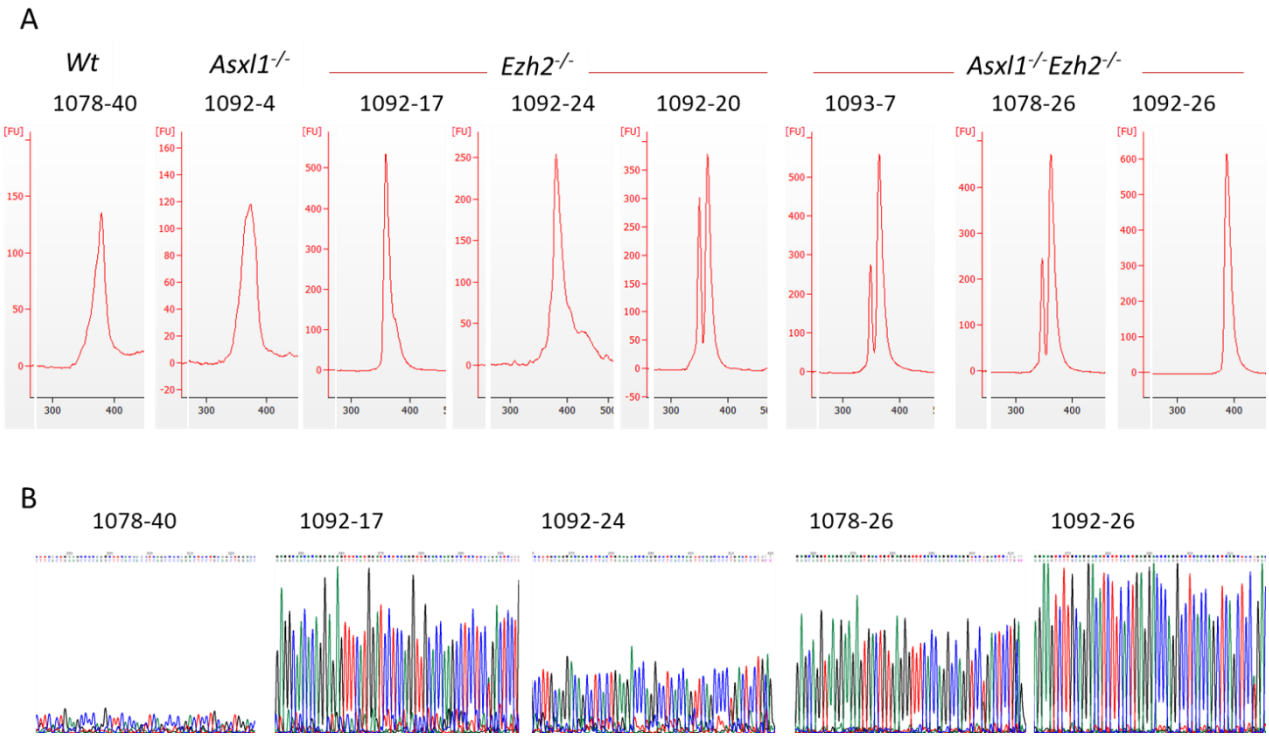

Figure 5.4. Identification of VDJ through sequencing PCR products of IGH. (A) Further analysis of RT-PCR products of *IGHVDJ* from normal (*Wt*, *Asxl*1 cKO) mice and B-LPD mice (*Ezh2* cKO and *Asxl1*/*Ezh2* cKO) through DNA high sensitivity chips of Agilent Bioanalyzer. X axis indicates sizes of base pairs. (B) chromatography of sequences of purified total RT-PCR products from indicated mice.

Table 5.1. Clonality in B-LPD mice.

Genotype	Animal No.	Clone	VH	D	JH	Mutation	HCDR3
Ezh2 KO	1092-17	Mono	V 6-3		JH3	(U)	T G G G S W F A Y (9)
Ezh2 KO	1092-24	Mono	V1-52	D2-1	JH4	(M)	T R G G Y S G H Y G A V D Y (14)
Ezh2 KO	1092-20	Mono	V 12-3	D4-1	JH1	(U)	A G D R T G Y W Y F D V (12)
A/E KO	1093-7	Mono	V 12-3	D1-1	JH1	(U)	A G D S Y G Y W Y F D V (12)
A/E KO	1078-26	Mono	V 12-3		JH1	(U)	A G D I G G Y W Y F D V (12)
A/E KO	1092-26	Mono	V 1-58	D2-5	JH4	(U)	A R S D Y S N Y V S Y Y Y A M D Y (16)

Analysis of *IGHVDJ from* splenocytes of B-LPD mice.
A/E KO (*Asxl1/Ezh2* cKO), Mono (Mono-clone), U (unmutated *IGHV*), M (mutated *IGHV*),
Heavy chain complementary determining regions (HCDR3)

5.2.2. High-risk *Asxl1*$^{-/-}$*Ezh2*$^{-/-}$ CLL developed in secondary transfer

To assess the leukaemic property, BM cells from B-LPD and MDS/MPN mice in primary transplantation were further transferred into sub-lethally irradiated SJL recipient mice. While no engraftments and sign of haematologic diseases were observed in mice transplanted with BM cells from *Asxl1* cKO, *Ezh2* cKO (MDS, B-LPD) and *Asxl1/Ezh2* cKO (MDS/MPN) mice (Figure 5.5A), an aggressive CLL phenotype were further developed with short latency (6 to 12 weeks) and 67 % penetrance (6 out of 9) in transplantation of BM cells from *Asxl1/Ezh2* cKO B-LPD mice with high BM infiltration (B-LPD^{high}) (Figure 5.6A). In addition, the CLL mice were symptomatic with severe organomegaly (splenomegaly and hepatomegaly), high bone marrow cellularity, leucocytosis and anaemia (reduction in RBC), referring to a high-risk stage III according to Rai staging system, in which CLL patients are divided into 5 groups from 0 to IV based on lymphocytosis, organomegaly, anaemia, and thrombopenia, and normally CLL patients should proceed to therapy immediately in the high-risk stage III and IV, (Kipps et al., 2017) (Figure 5.5B). Meanwhile, spleens were engrafted with nearly 100% lymphoid donor cells, and high levels of lymphoid infiltration can be detected in BM of *Asxl1*/*Ezh2* cKO CLL mice, whereas low engraftments with normal ratios of myeloid and lymphoid populations were detected in mice transplanted with BM from *Wt* primary mice (Figure 5.6A). Morphologically, typical CLL cells, with clumpy nuclei and a rim of visible cytoplasm, were identified in spleens, PB, and BM in the aggressive CLL mice, and the structure of spleens and livers were completely disrupted (Figure 5.6B).

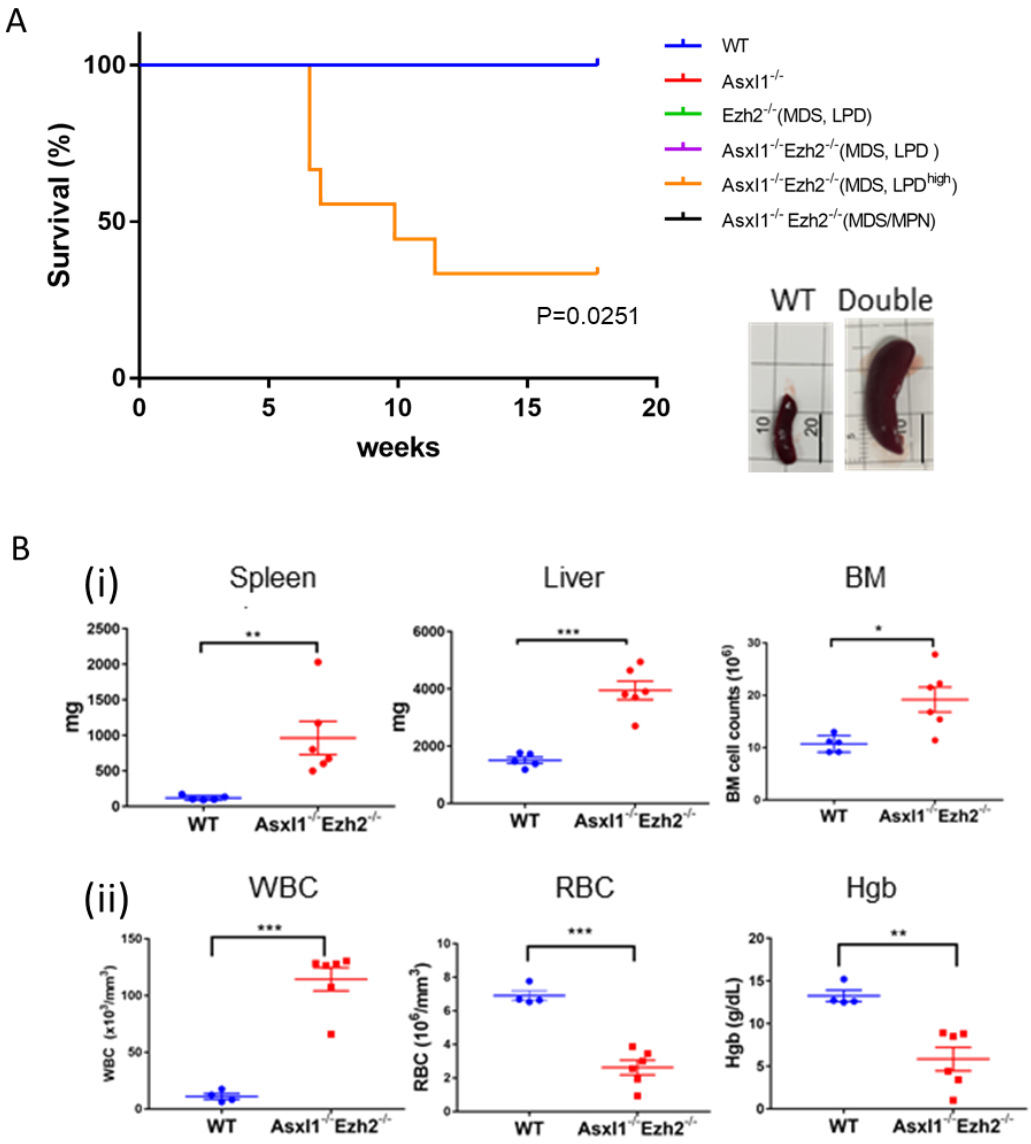

Figure 5.5. Development of aggressive CLL in secondary experiments. (A) Survival curves of mice transplanted with 1×10^5 BM cells form *Wt* (N=5), *Asxl1*$^{-/-}$ (N=5), *Ezh2*$^{-/-}$ (MDS, B-LPD) (N=10), *Asxl1*$^{-/-}$*Ezh2*$^{-/-}$ (MDS/MPN) (N=3), *Asxl1*$^{-/-}$*Ezh2*$^{-/-}$ (MDS, B-LPD) (N=4) and *Asxl1*$^{-/-}$ *Ezh2*$^{-/-}$ (MDS, B-LPD^{high}) (N=9) in primary experiments and representative images of spleens from *Wt* and *Asxl1*/*Ezh2* double cKO CLL mice. Scale bar, 1cm. (B) (i) Weights of spleen and livers and BM cellularity of *Wt* (N=5) and *Asxl1*/*Ezh2* double cKO CLL mice (N=6). (ii) WBC, RBC and Hgb counts in *Wt* (N=4) and *Asxl1*/*Ezh2* double cKO CLL mice (N=6). Dot graphs show mean+S.E.M. (*P<0.05, **P<0.01 and ***P<0.001, unpaired t-test).

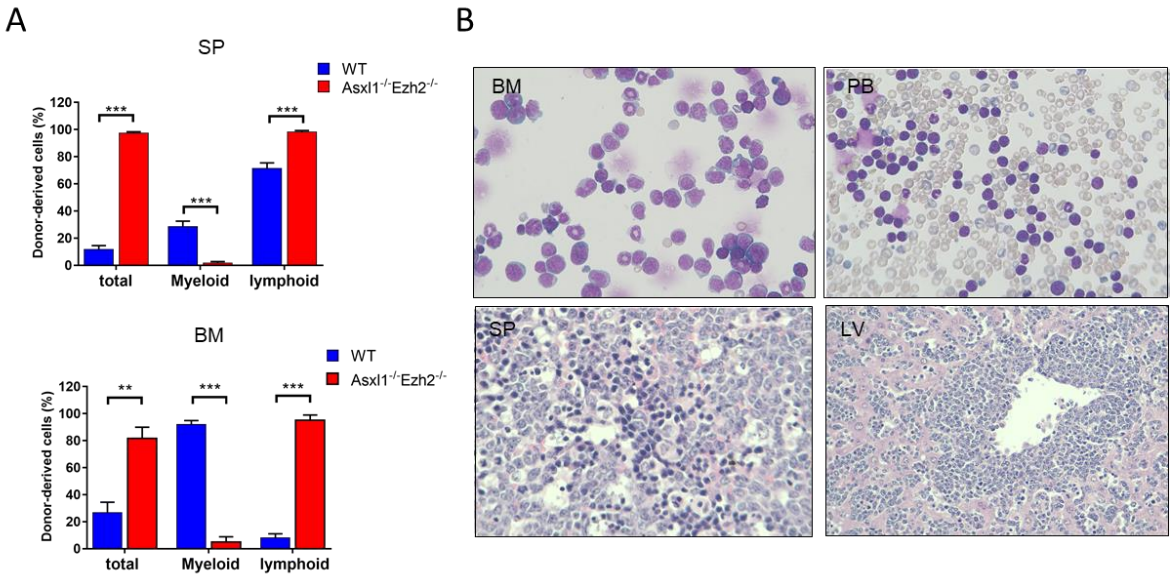

Figure 5.6. Engraftments and staining of CLL cells. (A) Engraftments of donor cells ($CD45.2^+$) and their ratios of myeloid and lymphoid populations in BM and spleen from *Wt* (N=5) and *Asxl1*/*Ezh2* double cKO CLL mice (N=6). Bar graphs show mean+S.E.M. (*P<0.05, **P<0.01 and ***P<0.001, unpaired t-test). (B) MG-Giemsa staining and H&E staining of BM cells, PB smears, spleen (SP) and livers (LV).

Moreover, the $CD19^+CD5^+IgM^+B220^{-/low}CD43^+$ CLL immunophenotype was characterized in BM cells and splenocytes by means of flow cytometry (Figure 5.7A). Almost all donor cells were CD19 positive, and over 70% $CD19^+$ donor cells were CD5 double positive (Figure 5.7A). $CD19^+CD5^+$ cells showed IgM and CD43 positive, whereas no $CD45.2^+$ B1α cells were detected in BM of *Wt* mice (Figure 5.7B). As analysis of the ratio of *kappa* (κ) and *lambda* (λ) light chains is the first step to examine the clonality in clinical workup of B cell lymphocytosis (Strati and Shanafelt, 2015), FACS analysis of κ/λ was performed to quickly check the clonality of $CD19^+$ donor B cells in the secondary transfer although mice mainly use *kappa* light chains (over 90 %) (Woloschak and Krco, 1987). As a result, although most of recipient B cells in spleens of *Wt* mice were *kappa* positive, a minority of $CD19^+$ population still showed the *lambda* positive

immunophenotype. In contrast, only a *kappa* positive population can be detected in *Asxl1*/*Ezh2* cKO CLL mice, showing clonal expansion of B1α cells in the secondary transfer. (Figure 5.8).

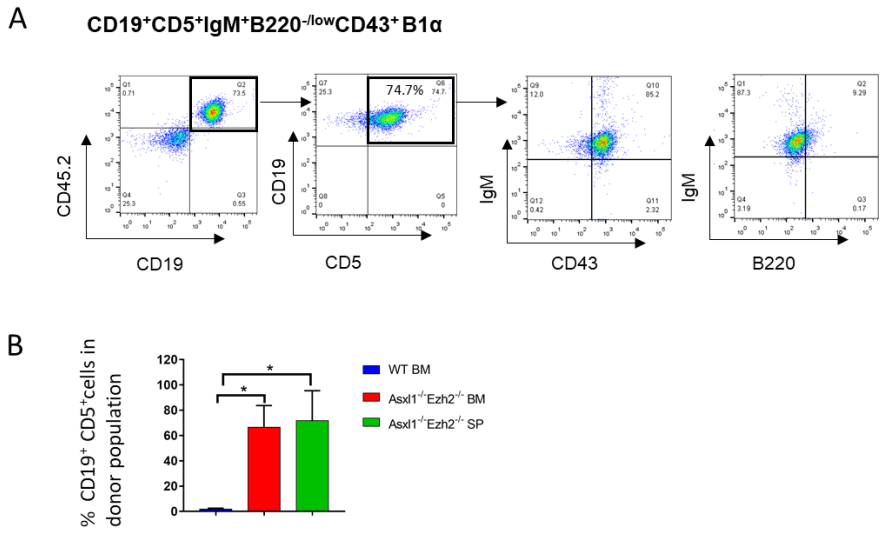

Figure 5.7. Immunophenotypes of BM cells and splenocytes in *Asxl1*/*Ezh2* cKO CLL mice. (A) Representative flow cytometry profiling of CD45.2^{+} B1α cells in BM from *Asxl1*/*Ezh2* double cKO CLL mice, and (B) the percentage of CD19^{+}CD5^{+} cells in donor cells from BM and spleens. Bar graphs show mean+S.E.M. (*P<0.05, **P<0.01 and ***P<0.001, unpaired t-test).

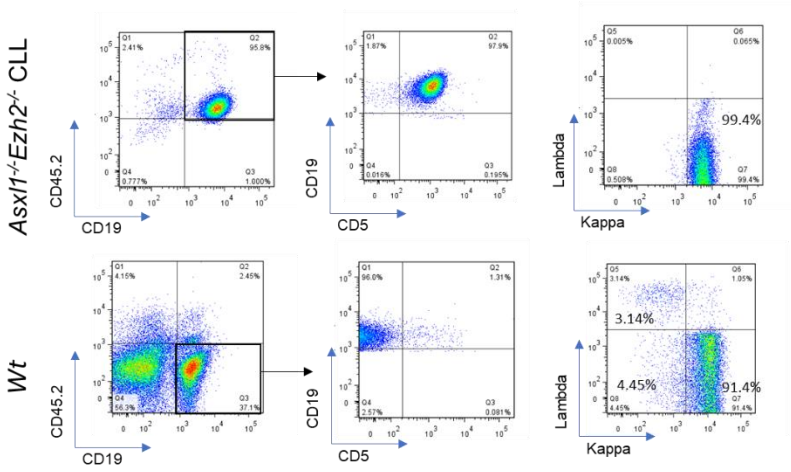

Figure 5.8. *kappa/lambda* of B cells in *Asxl1*/*Ezh2* cKO CLL mice. Proportions of kappa/lambda light chains in CD19^{+} donor splenocytes from *Asxl1*/*Ezh2* double cKO CLL mice and CD19^{+} recipient splenocytes from *Wt* mice.

To further characterize the *Asx1l*$^{-/-}$*Ezh2*$^{-/-}$ CLL mouse model for pre-clinical study, tertiary transplantation was performed with BM cells or splenocytes from *Asxl1*$^{-/-}$*Ezh2*$^{-/-}$ CLL mice and splenocytes from TCL1 mice as comparison. While TCL1 CLL showed relatively low lethality in a 4-month period, transferring splenocytes from secondary *Asx1l*$^{-/-}$*Ezh2*$^{-/-}$ CLL mice led to all mice coming down in 2 months, with mass organomegaly in spleens, livers and lymph nodes (Figure 5.9A-B). Although moderate splenomegaly could be observed in TCL1 CLL mice, no hepatomegaly and enlarged lymph nodes were founded (Figure 5.9B). Instead, the CD19/CD5 double positive cells were highly circulating in PB, showing less tissue invasion ability in TCL1 CLL mice (Figure 5.9B). Furthermore, in addition to lymphocytosis, anaemia and thrombocytopenia were also identified in *Asxl1*$^{-/-}$*Ezh2*$^{-/-}$ CLL mice (Figure 5.9D), and together with the organomegaly, the aggressive phenotype of *Asxl1*$^{-/-}$*Ezh2*$^{-/-}$ CLL could be defined as high-risk Rai stage IV in tertiary transplantation, whereas the TCL1 CLL phenotype was similar to patients with intermediate Rai stage II, without anaemia and thrombocytopenia. Moreover, while only typical morphology of CLL cells were observed in TCL1 CLL mice, large cleaved CLL cells were also identified in PB of *Asxl1*$^{-/-}$*Ezh2*$^{-/-}$ CLL mice , correlating the *Asxl1*$^{-/-}$*Ezh2*$^{-/-}$ CLL with atypical CLL morphology, which has also been regarded as one of aggressive marker in the clinical behaviour of CLL (Criel et al., 1997; Marionneaux et al., 2014) (Figure 5.9E).

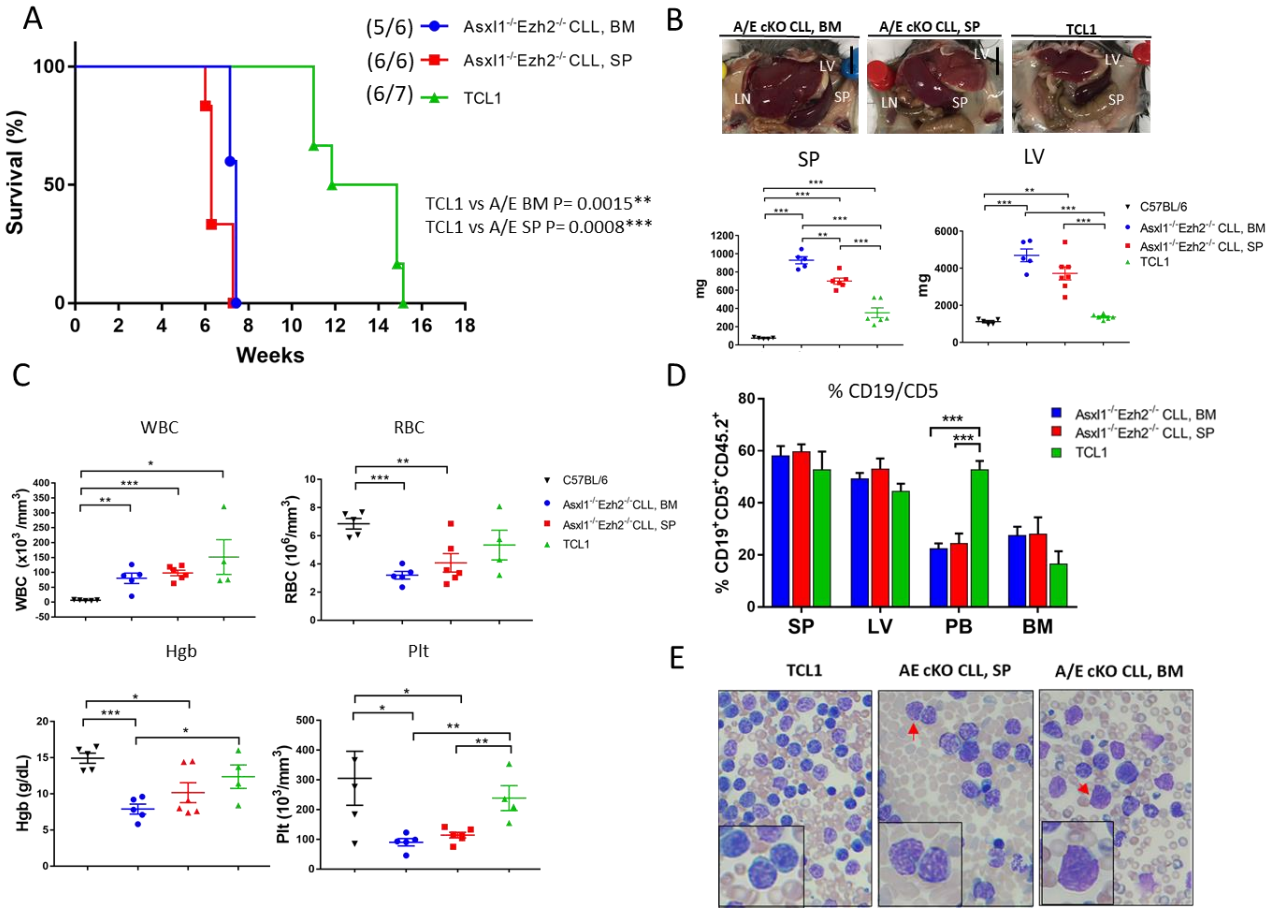

Figure 5.9. Disease modelling of the clinical high-risk *Asxl1*$^{-/-}$*Ezh2*$^{-/-}$ CLL mouse model in tertiary transplantation. (A) Survival curves of CLL mice by transplantation with BM cells and splenocytes from a secondary *Asxl1*$^{-/-}$*Ezh2*$^{-/-}$ CLL mouse or splenocytes from a secondary TCL1 CLL mouse. All mice transplanted with splenocytes from a secondary *Asxl1*$^{-/-}$*Ezh2*$^{-/-}$ CLL were engrafted and developed CLL (6/6). (B) Gross pathology of representative C57BL/6, TCL1 and *Asxl1*$^{-/-}$*Ezh2*$^{-/-}$ CLL mice (upper). Scale bar, 1cm. Spleens (SP), Liver (LV), Lymph nodes (LN). Weight of spleens and livers from indicated mice (bottom). (C) Blood counts in C57BL/6, TCL1 and *Asxl1*$^{-/-}$*Ezh2*$^{-/-}$ CLL mice. (D) The percentage of CD19/CD5 double positive donor cells in spleens (SP), livers (LV), PB and BM. (E) Representative images of MG-Giemsa staining of PB from TCL1 and *Asxl1*$^{-/-}$*Ezh2*$^{-/-}$ CLL mice. Large cleaved CLL cells were identified in *Asxl1*$^{-/-}$*Ezh2*$^{-/-}$ CLL mice (red arrow). Dot graphs and Bar graphs show mean+S.E.M. (*P<0.05, **P<0.01 and ***P<0.001, unpaired t-test).

5.2.3. Global RNA-seq profiling uncovered transcriptional landscape of CLL

It has been reported that depletion of Ezh2 or Asxl1 changed the pattern of H3K27 methylation and remodelled the transcriptional landscape of LSK cells, thus leading to perturbation of haematopoiesis and development of haematologic malignancies ultimately (Abdel-Wahab et al., 2012; Abdel-Wahab et al., 2013; Mochizuki-Kashio et al., 2015). In order to get insights into molecular impact of double inactivation of Ezh2 and Asxl1 in CLL leukaemogenesis, RNA-seq was employed to assess the transcriptional level and gene dysregulation in BM cells from B-LPD mice. Looking into the differential gene lists, knocking out *Ezh2* alone significantly dysregulated 939 genes, including 692 upregulated (UP) genes by comparison with the wild type, whereas loss of Asxl1 and Ezh2 further resulted in thousands of genes dysregulated, including 1452 upregulated genes and 1195 downregulated (DN) genes, literally covering the majority of genes discovered in single mutants (Figure 5.10). On the other hand, only a limited number of genes changed in *Asxl1* single cKO mice (57 genes UP and 5 genes DN), which is consistent with the mild phenotype in vivo.

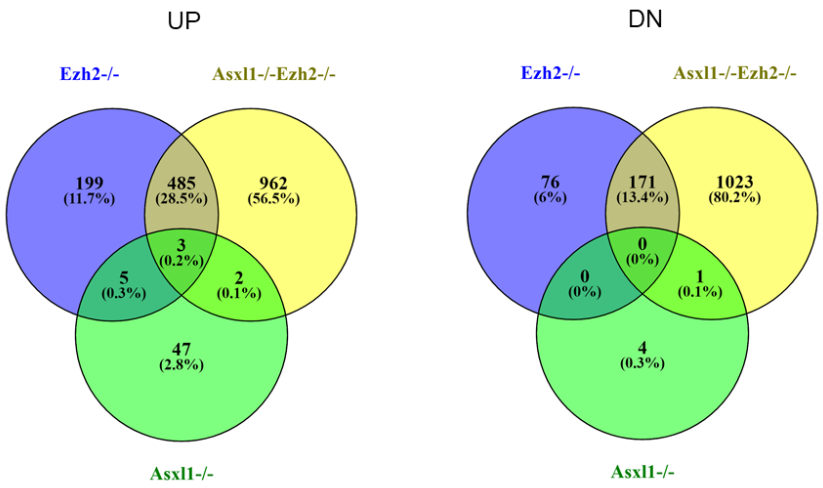

Figure 5.10. Venn diagrams of differential genes in BM cells from primary mutant mice. Overlapping maps of differential gene lists of (A) significantly upregulated (UP) genes and (B) downregulated (DN) genes (adjusted P values <0.05) in BM cells from primary *Asx11* cKO (1092-4 and 1092-12), *Ezh2* cKO B-LPD (1092-17, 1092-24 and 1092-20) and *Asxl1*/*Ezh2* cKO B-LPD (1093-7, 1078-26 and 1092-26) mice.

Furthermore, to figure out the pathways involved in the CLL leukaemogenesis, KEGG pathways were analysed based on commonly UP differential gene lists from *Ezh2* cKO and *Asxl1*/*Ezh2* double cKO B-LPD mice. While the genes involved in immune responses such as allograft rejection, antigen processing and presentation, and intestinal immune network for IgA production were upregulated in both *Ezh2* single and *Asxl1*/*Ezh2* double mutants probably due to infiltration of B cells into BM (Figure 5.1), a number of interesting pathways such as ribosome pathway, BCR signalling pathway and base excision repair (BER) were transcriptionally activated in *Asxl1*/*Ezh2* cKO B-LPD mice, which may eventually contribute to its leukaemogenesis of aggressive CLL phenotype in secondary transfer (Figure 5.11).

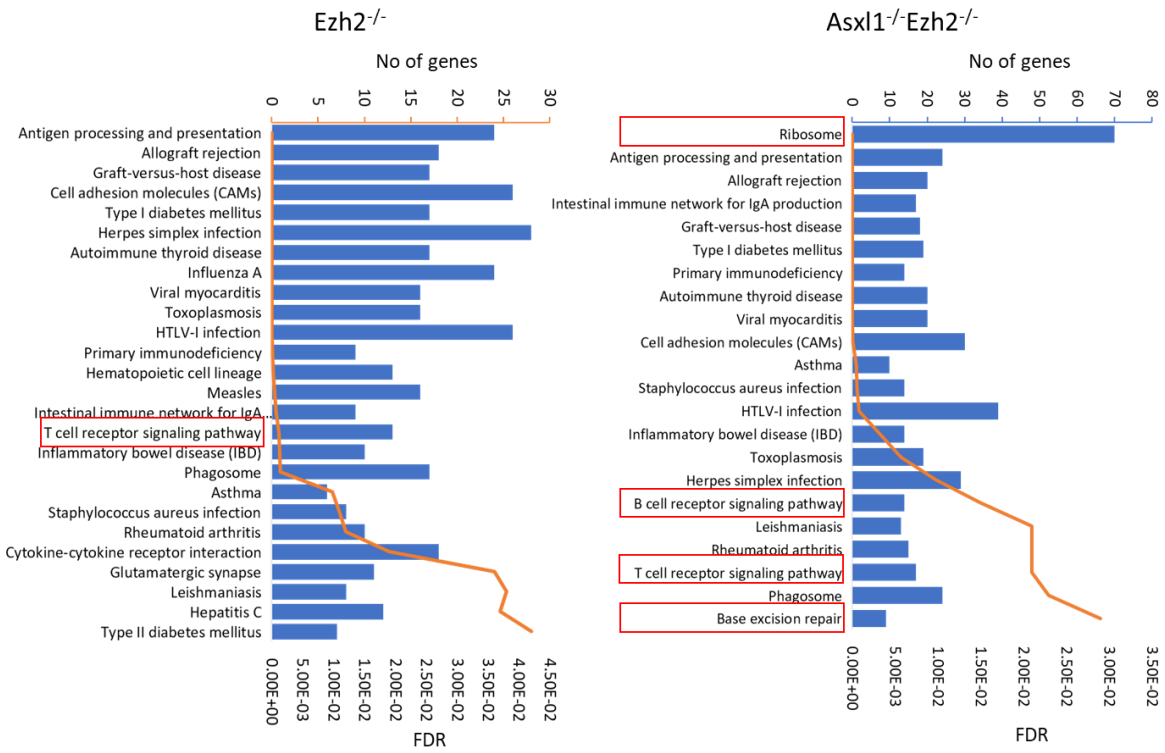

Figure 5.11. Analysis of KEGG pathways based on UP differential gene lists. Bar graphs showing KEGG pathways with significant gene enrichment (FDR <0.05) based on UP differential genes in BM cells from primary *Ezh2* cKO B-LPD (692 genes) and *Asxl1*/*Ezh2* cKO B-LPD mice (1452 genes).

Meanwhile, the BCR pathway in *Ezh2* cKO and *Asxl1*/*Ezh2* double cKO B-LPD mice showed transcriptional profiling as opposed to *Wt* and *Asxl1* cKO mice, in which the RNA levels of BCR signalosome such as *CD19, CD72, CD79a/b, Pi3k, Vav2 and Blnk* were highly expressed in the double mutants in particular, suggesting the sensitivity to inhibitors targeting BCR pathway like clinical CLL patients with unmutated *IGHV* (Kipps et al., 2017) (Figure 5.12). Furthermore, amongst the 1452 upregulated genes in *Asxl1*$^{-/-}$*Ezh2*$^{-/-}$ CLL mice, 122 genes were found highly relevant to CLL, whereas only 65 CLL related genes were identified in *Ezh2* cKO mice by analysis of functional enrichments using ToppFun (Figure 5.13A). Looking into the 122 CLL related genes, 55 genes were overlapped with Ezh2 single mutants, *Zap70* and *Ccnd2*

for example, and 67 genes only transcriptionally activated in the double mutants, including *Cxcr5*, *Myc*, *Bcl2* and *Parp1*, which were further verified using in qRT-PCR and significantly expressed in *Asxl1*$^{-/-}$*Ezh2*$^{-/-}$ B-LPD mice, accounting for its development of aggressive CLL phenotype in secondary transfer (Figure 5.13B and Table 5.2). Meanwhile, the total significant differential genes in *Asxl1*$^{-/-}$*Ezh2*$^{-/-}$ CLL mice were compared with a published differential gene list in primary human CLL cells collected from 98 CLL patients by comparison with normal B cells from healthy donors (Ferreira et al., 2014). 479 differential genes were overlapped with the human CLL cells (Figure 5.14A), and analysis of KEGG pathways revealed genes enriched in the ribosome pathway and NFκB signalling pathway, which also includes Zap70 and BCL2, further supporting that the two CLL genes may be crucial for the leukaemogenesis of *Asxl1*$^{-/-}$*Ezh2*$^{-/-}$ CLL (Figure 5.14B).

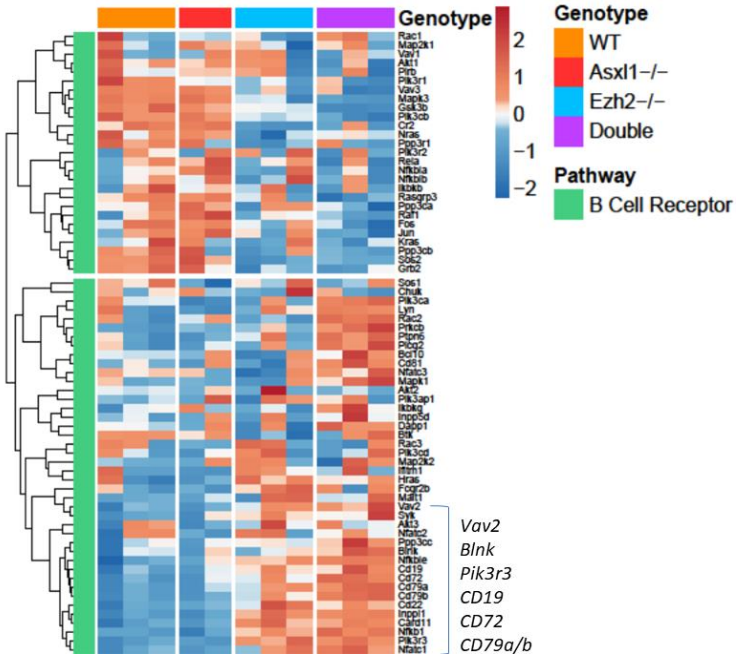

Figure 5.12. BCR signalling pathways in primary mutant mice. A cluster heatmap of genes involved in B cell receptor signalling pathways (BCR) in BM cells from normal (*Wt*, *Asxl1* cKO) mice and B-LPD mice (*Ezh2* cKO and *Asxl1*/*Ezh2* cKO).

A

1452 UP in Asxl1$^{-/-}$Ezh2$^{-/-}$

	ID	Name	Source	pValue	FDR B&H	FDR B&Y	Bonferroni	Genes from Input	Genes in Annotation
1	C0024141	Lupus Erythematosus, Systemic	DisGeNET Curated	6.706E-16	4.411E-12	4.133E-11	4.411E-12	122	941
2	C2931850	Aase Smith syndrome 2	DisGeNET Curated	1.668E-15	5.485E-12	5.139E-11	1.097E-11	15	19
3	C0023434	Chronic Lymphocytic Leukemia	DisGeNET Curated	5.758E-12	1.263E-8	1.183E-7	3.788E-8	122	1067
4	C0079744	Diffuse Large B-Cell Lymphoma	DisGeNET Curated	8.455E-10	1.390E-6	1.303E-5	5.561E-6	73	566
5	C1260899	Anemia, Diamond-Blackfan	DisGeNET Curated	1.161E-9	1.527E-6	1.431E-5	7.637E-6	20	66

692 UP in Ezh2$^{-/-}$

	ID	Name	Source	pValue	FDR B&H	FDR B&Y	Bonferroni	Genes from Input	Genes in Annotation
1	C0024141	Lupus Erythematosus, Systemic	DisGeNET Curated	2.696E-17	1.318E-13	1.196E-12	1.318E-13	77	941
2	C0004364	Autoimmune Diseases	DisGeNET Curated	1.920E-13	4.692E-10	4.257E-9	9.385E-10	73	1018
3	C0011854	Diabetes Mellitus, Insulin-Dependent	DisGeNET Curated	2.157E-10	3.516E-7	3.189E-6	1.055E-6	58	830
4	C0026769	Multiple Sclerosis	DisGeNET Curated	9.027E-10	1.103E-6	1.001E-5	4.413E-6	61	931
5	C0042769	Virus Diseases	DisGeNET Curated	1.406E-9	1.375E-6	1.247E-5	6.875E-6	58	872
6	C0019693	HIV Infections	DisGeNET Curated	2.118E-9	1.635E-6	1.483E-5	1.036E-5	54	790
7	C0023418	leukemia	DisGeNET Curated	2.341E-9	1.635E-6	1.483E-5	1.145E-5	96	1842
8	C0023434	Chronic Lymphocytic Leukemia	DisGeNET Curated	4.497E-9	2.748E-6	2.493E-5	2.199E-5	65	1067

B

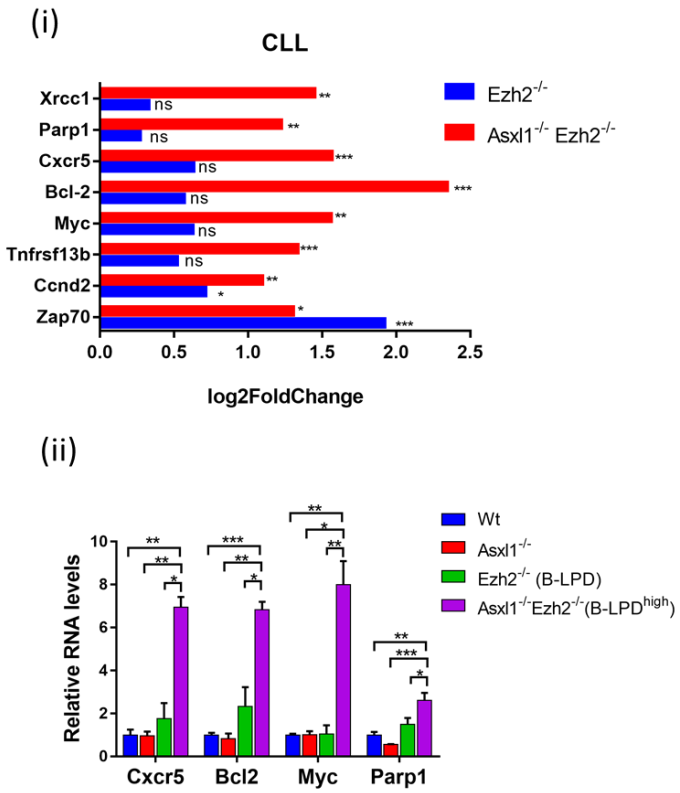

Figure 5.13. Upregulation of CLL genes in *Ezh2* single and *Asxl1*/*Ezh2* double mutants. (A) Analysis of disease phenotypes in Toppfun based on UP differential gene lists from *Ezh2* cKO and *Asxl1*/*Ezh2* cKO B-LPD mice. (B) (i) 8 representative CLL-related genes significantly upregulated in double mutants. (*padj<0.05, ** padj<0.01 and *** padj<0.001). (ii) qRT-PCR of CLL related genes. Bar graphs show mean+S.E.M. (*P<0.05, **P<0.01 and ***P<0.001, unpaired t-test).

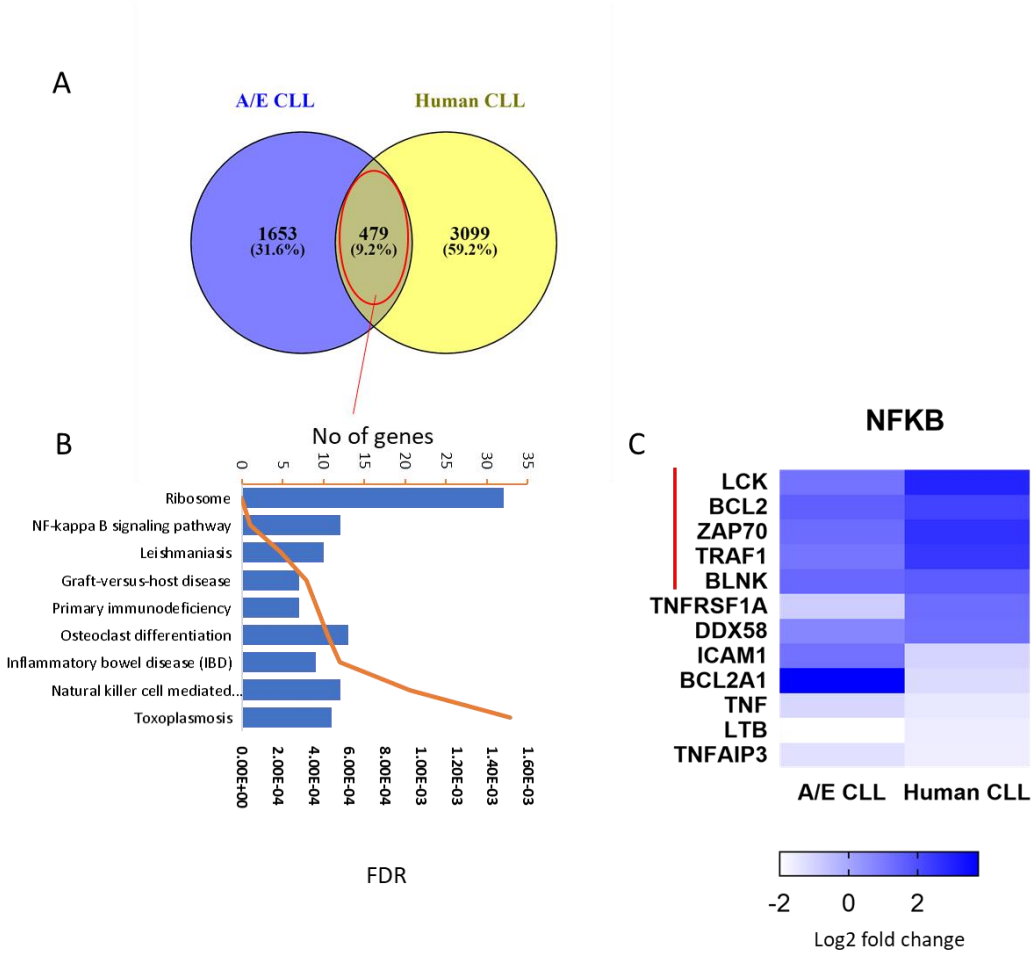

Figure 5.14. Differential genes overlapped with a gene list of RNA-seq from 98 CLL patients. (A) Venn diagrams showing 479 overlapped genes between the total differential genes from *Asxl1*/*Ezh2* cKO mice and a published differential gene list from 98 CLL patients (Ferreira et al., 2014). (B) 479 overlapped genes were subjected to analysis of KEGG pathways, and (C) overlapped genes involved in the NFκB signalling pathway were shown in a heatmap.

Table 5.2. 122 CLL-related genes in the double mutant.

1	19	ABCA1	ATP binding cassette subfamily A member 1	ENSMUSG00000015243
2	57379	AICDA	activation induced cytidine deaminase	ENSMUSG00000040627
3	51237	MZB1	marginal zone B and B1 cell specific protein	ENSMUSG00000024353
4	2099	ESR1	estrogen receptor 1	ENSMUSG00000019768
5	6209	RPS15	ribosomal protein S15	ENSMUSG00000063457
6	2113	ETS1	ETS proto-oncogene 1, transcription factor	ENSMUSG00000032035
7	2119	ETV5	ETS variant 5	ENSMUSG00000013089
8	8323	FZD6	frizzled class receptor 6	ENSMUSG00000022297
9	142	PARP1	poly(ADP-ribose) polymerase 1	ENSMUSG00000026496
10	2214	FCGR3A	Fc fragment of IgG receptor IIIa	ENSMUSG00000059089
11	10419	PRMT5	protein arginine methyltransferase 5	ENSMUSG00000023110
12	51384	WNT16	Wnt family member 16	ENSMUSG00000029671
13	4282	MIF	macrophage migration inhibitory factor	ENSMUSG00000033307
14	57569	ARHGAP20	Rho GTPase activating protein 20	ENSMUSG00000053199
15	4345	CD200	CD200 molecule	ENSMUSG00000022661
16	4350	MPG	N-methylpurine DNA glycosylase	ENSMUSG00000020287
17	22806	IKZF3	IKAROS family zinc finger 3	ENSMUSG00000018168
18	28951	TRIB2	tribbles pseudokinase 2	ENSMUSG00000020601
19	348	APOE	apolipoprotein E	ENSMUSG00000002985
20	350	APOH	apolipoprotein H	ENSMUSG00000000049
21	445	ASS1	argininosuccinate synthase 1	ENSMUSG00000076441
22	8651	SOCS1	suppressor of cytokine signaling 1	ENSMUSG00000038037
23	2547	XRCC6	X-ray repair cross complementing 6	ENSMUSG00000022471
24	4609	MYC	MYC proto-oncogene, bHLH transcription factor	ENSMUSG00000022346
25	567	B2M	beta-2-microglobulin	ENSMUSG00000060802
26	596	BCL2	BCL2 apoptosis regulator	ENSMUSG00000057329
27	597	BCL2A1	BCL2 related protein A1	ENSMUSG00000089929
28	6772	STAT1	signal transducer and activator of transcription 1	ENSMUSG00000026104
29	23158	TBC1D9	TBC1 domain family member 9	ENSMUSG00000031709
30	637	BID	BH3 interacting domain death agonist	ENSMUSG00000004446
31	639	PRDM1	PR/SET domain 1	ENSMUSG00000038151
32	640	BLK	BLK proto-oncogene, Src family tyrosine kinase	ENSMUSG00000014453
33	643	CXCR5	C-X-C motif chemokine receptor 5	ENSMUSG00000047880
34	654	BMP6	bone morphogenetic protein 6	ENSMUSG00000039004
35	4772	NFATC1	nuclear factor of activated T cells 1	ENSMUSG00000033016
36	10923	SUB1	SUB1 regulator of transcription	ENSMUSG00000022205
37	4794	NFKBIE	NFKB inhibitor epsilon	ENSMUSG00000023947
38	23239	PHLPP1	PH domain and leucine rich repeat protein phosphatase 1	ENSMUSG00000044340
39	2784	GNB3	G protein subunit beta 3	ENSMUSG00000023439
40	4842	NOS1	nitric oxide synthase 1	ENSMUSG00000029361
41	6895	TARBP2	TARBP2 subunit of RISC loading complex	ENSMUSG00000023051
42	4869	NPM1	nucleophosmin 1	ENSMUSG00000057113
43	2823	GPM6A	glycoprotein M6A	ENSMUSG00000031517
44	6929	TCF3	transcription factor 3	ENSMUSG00000020167
45	11040	PIM2	Pim-2 proto-oncogene, serine/threonine kinase	ENSMUSG00000031155
46	8995	TNFSF18	TNF superfamily member 18	ENSMUSG00000066755
47	23348	DOCK9	dedicator of cytokinesis 9	ENSMUSG00000025558
48	9026	HIP1R	huntingtin interacting protein 1 related	ENSMUSG00000000915
49	11093	ADAMTS13	ADAM metallopeptidase with thrombospondin type 1 motif 1	ENSMUSG00000014852
50	11126	CD160	CD160 molecule	ENSMUSG00000038304
51	894	CCND2	cyclin D2	ENSMUSG00000000184
52	64393	ZMAT3	zinc finger matrin-type 3	ENSMUSG00000027663
53	921	CD5	CD5 molecule	ENSMUSG00000024669
54	926	CD8B	CD8b molecule	ENSMUSG00000053044
55	11168	PSIP1	PC4 and SFRS1 interacting protein 1	ENSMUSG00000028484
56	930	CD19	CD19 molecule	ENSMUSG00000030724
57	931	MS4A1	membrane spanning 4-domains A1	ENSMUSG00000024673
58	933	CD22	CD22 molecule	ENSMUSG00000030577
59	942	CD86	CD86 molecule	ENSMUSG00000022901
60	951	CD37	CD37 molecule	ENSMUSG00000030798
61	958	CD40	CD40 molecule	ENSMUSG00000017652
62	115650	TNFRSF13C	TNF receptor superfamily member 13C	ENSMUSG00000068105

63	23495	TNFRSF13B	TNF receptor superfamily member 13B	ENSMUSG00000010142
64	972	CD74	CD74 molecule	ENSMUSG00000024610
65	973	CD79A	CD79a molecule	ENSMUSG00000003379
66	974	CD79B	CD79b molecule	ENSMUSG00000040592
67	5079	PAX5	paired box 5	ENSMUSG00000014030
68	9214	FCMR	Fc fragment of IgM receptor	ENSMUSG00000042474
69	1029	CDKN2A	cyclin dependent kinase inhibitor 2A	ENSMUSG00000044303
70	100532731	COMMD3-BMI1	COMMD3-BMI1 readthrough	ENSMUSG00000026739
71	5133	PDCD1	programmed cell death 1	ENSMUSG00000026285
72	7185	TRAF1	TNF receptor associated factor 1	ENSMUSG00000026875
73	5140	PDE3B	phosphodiesterase 3B	ENSMUSG00000030671
74	5150	PDE7A	phosphodiesterase 7A	ENSMUSG00000069094
75	3105	HLA-A	major histocompatibility complex, class I, A	ENSMUSG00000073409
76	3111	HLA-DOA	major histocompatibility complex, class II, DO alpha	ENSMUSG00000024334
77	9255	AIMP1	aminoacyl tRNA synthetase complex interacting multifunctior	ENSMUSG00000028029
78	3119	HLA-DQB1	major histocompatibility complex, class II, DQ beta 1	ENSMUSG00000073421
79	5175	PECAM1	platelet and endothelial cell adhesion molecule 1	ENSMUSG00000020717
80	5179	PENK	proenkephalin	ENSMUSG00000045573
81	3135	HLA-G	major histocompatibility complex, class I, G	ENSMUSG00000016206
82	3172	HNF4A	hepatocyte nuclear factor 4 alpha	ENSMUSG00000017950
83	5287	PIK3C2B	phosphatidylinositol-4-phosphate 3-kinase catalytic subunit t	ENSMUSG00000026447
84	9402	GRAP2	GRB2 related adaptor protein 2	ENSMUSG00000042351
85	5324	PLAG1	PLAG1 zinc finger	ENSMUSG00000003282
86	3315	HSPB1	heat shock protein family B (small) member 1	ENSMUSG00000004951
87	3339	HSPG2	heparan sulfate proteoglycan 2	ENSMUSG00000028763
88	3383	ICAM1	intercellular adhesion molecule 1	ENSMUSG00000037405
89	3399	ID3	inhibitor of DNA binding 3, HLH protein	ENSMUSG00000007872
90	5450	POU2AF1	POU class 2 homeobox associating factor 1	ENSMUSG00000032053
91	7515	XRCC1	X-ray repair cross complementing 1	ENSMUSG00000051768
92	7520	XRCC5	X-ray repair cross complementing 5	ENSMUSG00000026187
93	3428	IFI16	interferon gamma inducible protein 16	ENSMUSG00000073491
94	7535	ZAP70	zeta chain of T cell receptor associated protein kinase 70	ENSMUSG00000026117
95	50615	IL21R	interleukin 21 receptor	ENSMUSG00000030745
96	5578	PRKCA	protein kinase C alpha	ENSMUSG00000050965
97	5579	PRKCB	protein kinase C beta	ENSMUSG00000052889
98	83416	FCRL5	Fc receptor like 5	ENSMUSG00000048031
99	3560	IL2RB	interleukin 2 receptor subunit beta	ENSMUSG00000068227
100	3561	IL2RG	interleukin 2 receptor subunit gamma	ENSMUSG00000031304
101	3586	IL10	interleukin 10	ENSMUSG00000016529
102	9734	HDAC9	histone deacetylase 9	ENSMUSG00000004698
103	3604	TNFRSF9	TNF receptor superfamily member 9	ENSMUSG00000028965
104	83478	ARHGAP24	Rho GTPase activating protein 24	ENSMUSG00000057315
105	26191	PTPN22	protein tyrosine phosphatase non-receptor type 22	ENSMUSG00000027843
106	3663	IRF5	interferon regulatory factor 5	ENSMUSG00000029771
107	5747	PTK2	protein tyrosine kinase 2	ENSMUSG00000022607
108	50808	AK3	adenylate kinase 3	ENSMUSG00000024782
109	3708	ITPR1	inositol 1,4,5-trisphosphate receptor type 1	ENSMUSG00000030102
110	5775	PTPN4	protein tyrosine phosphatase non-receptor type 4	ENSMUSG00000026384
111	5777	PTPN6	protein tyrosine phosphatase non-receptor type 6	ENSMUSG00000004266
112	83666	PARP9	poly(ADP-ribose) polymerase family member 9	ENSMUSG00000022906
113	7965	AIMP2	aminoacyl tRNA synthetase complex interacting multifunctior	ENSMUSG00000029610
114	57120	GOPC	golgi associated PDZ and coiled-coil motif containing	ENSMUSG00000019861
115	1832	DSP	desmoplakin	ENSMUSG00000054889
116	3902	LAG3	lymphocyte activating 3	ENSMUSG00000030124
117	3932	LCK	LCK proto-oncogene, Src family tyrosine kinase	ENSMUSG00000000409
118	3981	LIG4	DNA ligase 4	ENSMUSG00000049717
119	55213	RCBTB1	RCC1 and BTB domain containing protein 1	ENSMUSG00000035469
120	4050	LTB	lymphotoxin beta	ENSMUSG00000024399
121	4064	CD180	CD180 molecule	ENSMUSG00000021624
122	6135	RPL11	ribosomal protein L11	ENSMUSG00000059291

5.3. Discussion

While knockout of *mir15a/16-1*, minimal deletion region *(MDR)* or common deletion region *(CDR)* on chromosome 13q14 resulted in unmutated CLL on aging mice with low penetrance (20 to 50%) (Klein et al., 2010), *Eμ-TCL1* transgenic mice, in which human *TCL1* is driven by *IGHV* promoter and enhancer (*Eμ*), developed 100 % unmutated CLL with a more consistent latency (Bichi et al., 2002; Johnson et al., 2006). Although no gain-of-function mutation of TCL1 has been identified in CLL patients to date, TCL1 CLL mouse model is still the major model utilized for in vivo CLL study, attributing to its high penetrance, resemblance of BCR to the treatment-resistant human CLL (Yan et al., 2006) and its oligo-clonality, in a way that also provides benefits for investigating disease progress through serial transfers (Chen et al., 2013). The long latency can be overcome through transferring the splenocytes or CLL cells to immunodeficient recipient mice such as SCID or NOD/SCID mice although 2 to 6 months are still required for mice to come down (Chen et al., 2013; Enzler et al., 2009; Simonetti et al., 2014; Woyach et al., 2014; Zanesi et al., 2006). Similar to the *Eμ-TCL1* transgenic mice, the clonality of *Asxl1*/*Ezh2* cKO CLL mice were also characterized as unmutated BCR with high similarity of HCDR3, and only monoclonal expansion of B cells was detected in the double mutant CLL mice (Table 5.1), showing similarity to CLL patients with resistance to chemotherapy (Kipps et al., 2017). Although the penetrance for developing CLL in primary *Asxl1*/*Ezh2* cKO mice was not as promising as *Eμ-TCL1* transgenic mice in primary transfer, the occurrence of disease gradually increased to 80 to 90% with injection of BM cells or 100% with injection of splenocytes in tertiary transplantation (Figure 5.15), in which *Asxl1*/*Ezh2* cKO CLL mice came down in two month with high-risk phenotypes including hepatomegaly, atypical morphology and Aicda expression, whereas indolent CLL, with low organ

invasion and lethality, was characterized in TCL mice, suggesting the *Asxl1*/*Ezh2* cKO CLL mouse model as an better model for study of CLL with worse clinical behaviours (Figure 5.9).

HCDR3s of human B-CLL cells show distinctive features in length, amino acid composition and charge. It has been reported that longer length and charged amino acid such as arginine (R), aspartate (D) and lysine (K) were often found in the HCDR3s of unmutated CLL (U-CLL) cells (Fais et al., 1998; Johnson et al., 1997; Widhopf and Kipps, 2001), and by comparison with normal B cells, some of leukaemic clones from individual CLL patients display HCDR3s with highly homologous sequences of amino acids, which is usually associated with stereotypic VDJ rearrangements, suggesting a role of common antigens or autoantigens in clonal expansion of CLL cells (Ghia et al., 2008). Therefore, to correlate CLL mouse models with human CLL, in addition to the status of mutation in variable regions of immunoglobulins, the amino acid sequences of HCDR3s were also identified and compared between different clones (Klein et al., 2010; Yan et al., 2006). Although only 6 clones have been identified, 5 clones showed the length of ≥ 12 amino acids in HCDR3s, and all of them bore charged amino acid such as arginine and aspartate, showing the similar HCDR3 features to treatment-resistant U-CLL (Table 5.1). Meanwhile, amongst the 6 clones, 3 clones were rearranged with the same VH region (V12-3) and JH region (JH1), thus creating the BCR with the quasi-identical antigen binding sides. However, to gain insights into the clonality and stereotypes of BCR, more leukaemic clones need to be included for a comprehensive analysis in the sequences of *IGHV*, VDJ rearrangement and HCDR3.

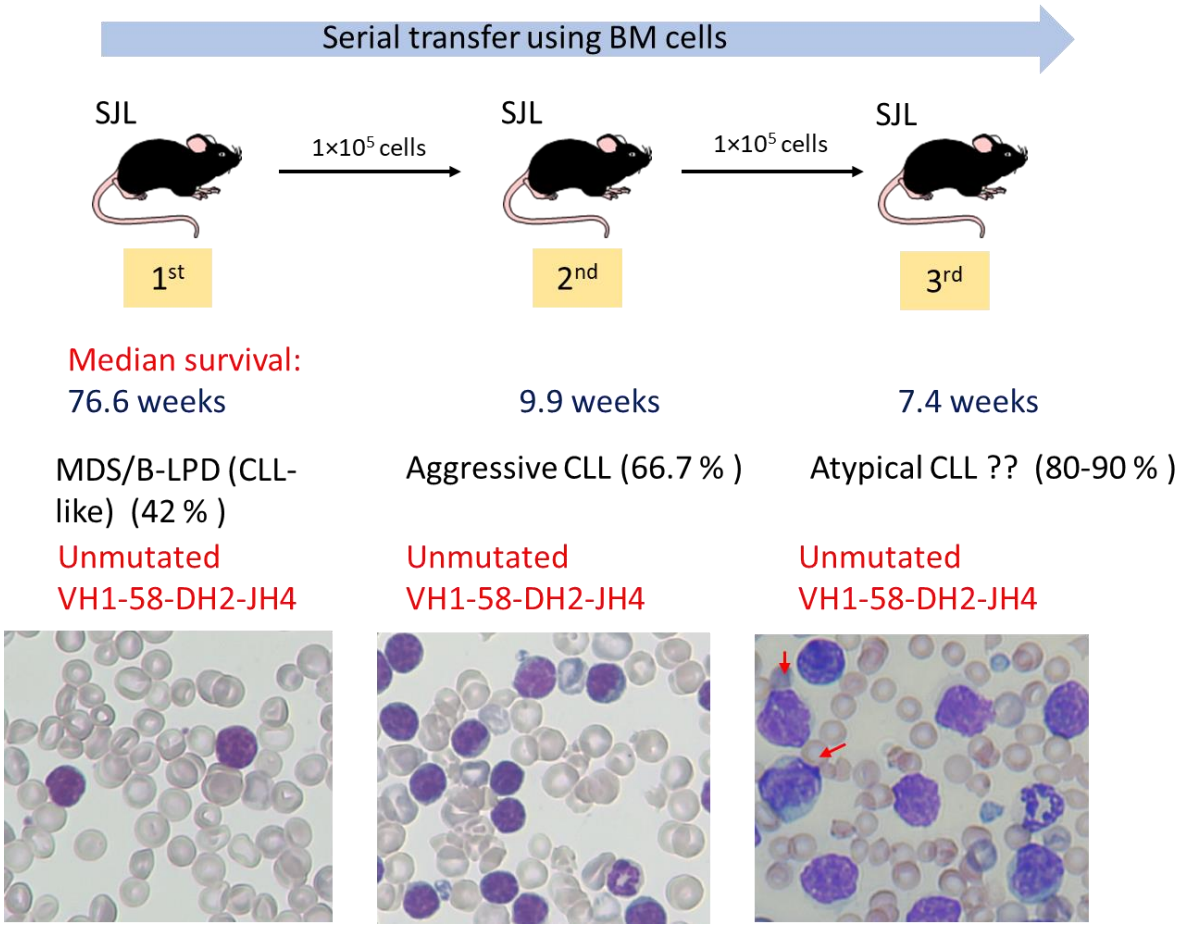

Figure 5.15. Serial transfers of *Asxl1*$^{-/-}$*Ezh2*$^{-/-}$CLL. Survival, Disease progress, penetrance and cell morphology of CLL mice in primary (1st), secondary (2nd) and tertiary (3rd) transplantation. Typical CLL cells and large cleaved CLL cells (arrows) have been shown in the MG/Giemsa staining of PB (Criel et al., 1997; Marionneaux et al., 2014).

Analysis of KEGG pathways showed differential gene enrichment in the BCR signalling pathway in BM cells from B-LPD mice, and several critical transmembrane proteins like CD19 and CD79a/b were upregulated in both single and double mutants, revealed that activated BCR signalosome might be crucial for the leukaemogenesis of Ezh2-deficient CLL (Figure 5.12). Moreover, RNA-seq profiling of BM cells from *Ezh2* single cKO mice and *Asxl1*/*Ezh2* double cKO mice exhibited significant upregulation of a prognostic marker *Zap70*, which can promote leukaemogenesis of CLL by enhancing BCR signalling (Figure

5.13) (Chen et al., 2005), and previous mouse studies show genetic inactivation of Ezh2 significantly induced expression of *Zap70* in HSPCs through decreasing the level of H3K27 methylation, suggesting that ZAP70 may be one of initial Ezh2 targets for the development of Ezh2-deficient CLL (Mochizuki-Kashio et al., 2015). Furthermore, amongst the 122 CLL-related genes, 67 genes were only significantly upregulated in *Asxl1*/*Ezh2* double cKO mice, and involved in anti-apoptosis (*Bcl-2)*, cytokine-cytokine receptor interaction (*Tnfrsf13b*, *Cxcr5)* and genome instability (*Aicda*) (Burkle et al., 2007; Heinig et al., 2014; Klein et al., 2010; Patten et al., 2012; Planelles et al., 2004; Ponader et al., 2012; Zapata et al., 2004). *Bcl-2*, for example, has been found de-repressed in CLL patients with loss of *mir15a/16-1* and crucial for driving leukaemogenesis of CLL in mouse models (Calin et al., 2005; Klein et al., 2010; Zapata et al., 2004) (Figure 5.13B and Table 5.2), and it could be epigenetically regulated by PRC2 through H3K27 methylation as well (Svotelis et al., 2011). These suggest that co-inactivation of Asxl1 and Ezh2 may further impact on the repressive function of PRC2 and derepress more crucial oncogenes such as *Bcl-2*, hence leading to a more aggressive CLL phenotype (Figure 5.16).

Although loss-of-function mutations of Asxl1 have been identified in CLL patients (Puente et al., 2015; Quesada et al., 2011), genetic inhibition of Asxl1 in haematopoietic cells is insufficient to develop any phenotypes of B-cell lymphoproliferations in previous mouse studies as well as our mouse model (Abdel-Wahab et al., 2013), and looking into the transcriptional profiling, only a limited number of genes were upregulated in BM cells from *Asxl1* cKO mice in the end point of primary experiments, revealing the marginal impact of loss of Asxl1 in CLL leukemogenesis. However, co-inactivation of Asxl1with Ezh2 considerably induced more than 900 genes including 67 genes involved in the CLL leukaemogenesis, implying Asxl1 may be more essential for the repressive function of Ezh2-defective PRC2, in which depletion of Asxl1 may profoundly disrupt the activity of

Ezh1-mediated H3K27 trimethylation and then de-repress the majority of remaining PRC2-repressed genes (Figure 5.16). To further dissect the roles of PRC2 in the alternation of transcriptional landscape, histone ChIP-seq of H3K27 trimethylation can be performed in *Asxl1*$^{-/-}$*Ezh2*$^{-/-}$ CLL cells and B cells from *Wt* mice as comparison to identify the potential CLL related genes directly regulated by PRC2.

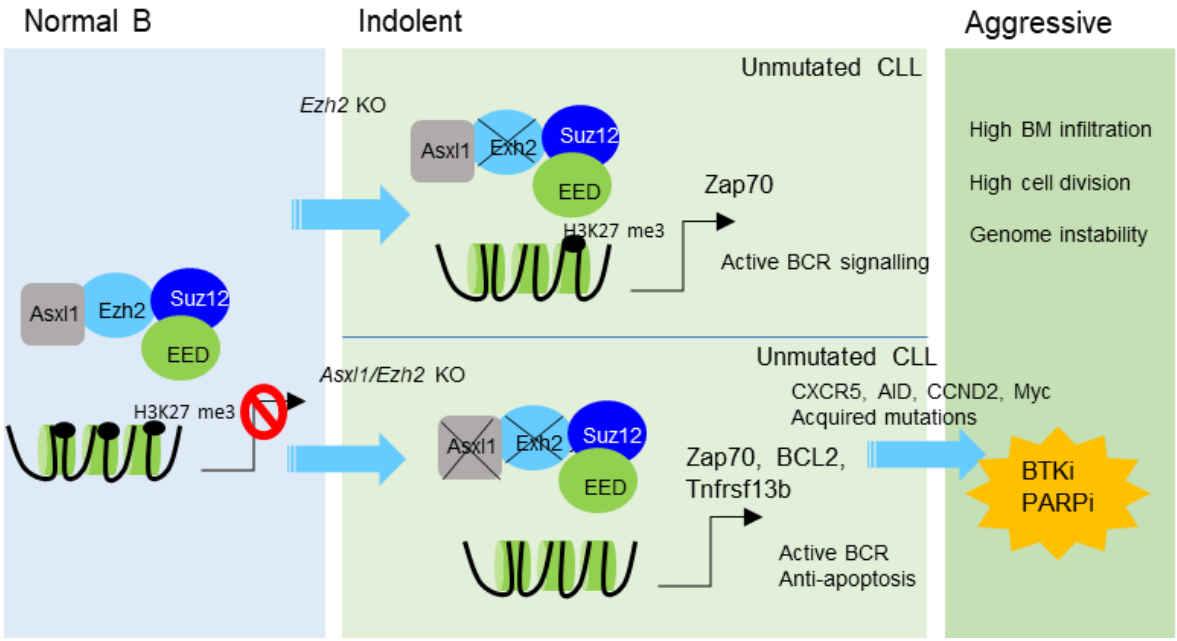

Figure 5.16. Illustration of potential molecular drivers during leukaemogenesis of CLL. In normal B1α cells, PRC2 associates with Asxl1 to repress possible pro-oncogenes related to CLL leukaemogenesis through H3K27 methylation. While levels of H3K27 methylation on a part of genes that may be compensated by Ezh1 after depletion of Ezh2, the level of H3K27me3 on potential drivers like Zap70 is reduced, thus leading to monoclonal expansion of unmutated B1α cells. Genetic co-inactivation of Asxl1 and Ezh2 further results in removal of the crucial co-activator Asxl1 from Ezh1-substituted PRC2 complex. Therefore, more CLL driving genes such BCL2 and Tnfrsf13b are derepressed directly, and genes involved in chemotaxis (CXCR5), genome instability (AID) and cell proliferation (CCND2 and Myc) might be induced subsequently in downstream reaction, ultimately transforming indolent CLL to aggressive CLL in a high-risk stage. However, the properties of high DNA base lesions and cell division may also leave the CLL cells sensitive to DDR targeting treatment such as PARP1 inhibitors as abundant DSB could be created after inhibition of PARP1.

Charter 6: Targeting PARP as a new strategy for PRC2-deficient CLL therapy

6.1. Introduction

6.1.1 Targeting PARP1 in cancer treatments

Poly ADP ribose polymerase (PARP) 1 is a crucial factor involved in BER, in which PARP1 binds to the single strand break (SSB) and converts nicotinamide adenine dinucleotide (NAD+) into ADP-ribose polymers (ARP), followed by DNA repair via initiating the assembly of XRCC1 (El-Khamisy et al., 2003; Satoh and Lindahl, 1992). Targeting PARP1 have been considered a potential remedy for cancer therapy since pioneering studies reported a decade ago that inhibition of PARP1 provides great synthetic lethality to *BRCA1/2*-defective breast and ovarian cancer through accumulating double stand break (DSB), which probably results from collapse of replication fork at the end of SSB, or trapping PARP1 into SSB sites, which may form a DNA repair intermediate and result in a more toxic lesion during replication (Bryant et al., 2005; Farmer et al., 2005; Fong et al., 2009). A functional homologous recombination (HR) is not only crucial for DSB repair but able to mediate the bypass of the PARP1-trapping obstacles (Arnaudeau et al., 2001; Helleday, 2003; Helleday, 2011). However promising it is in breast cancer and ovarian cancer, the clinical application of PARP inhibitors was not translated into a wide range of cancer therapies as the mutations of compromising DNA damage response (DDR) genes are usually rare in the other malignancies including leukaemia. Nonetheless, selectively targeting PARP1 in AML driven by chimeric oncoproteins such as AML1-ETO and PML-RARα, which initiated transcription programs with low expression of DDR genes, including

Atm, *Brca1/2*, *Rad51*, *Rpa1*, provides a new transcriptional aspect for effective use of the synthetic lethality approaches for leukaemia treatments (Esposito et al., 2015).

In addition to AML, targeting PARP1 has been evaluated in treatment of CLL patients with del (11q) or mutations of *ATM*, a crucial sensor and activator for homologous recombination. PARP1 inhibitors displayed better drug effects on *ATM*-deficient human CLL cells than *ATM*-wild type human cells in vitro and in vivo, inducing more cell death and DSB (Weston et al., 2010). Moreover, deletion of *Atm* sensitized *Eμ-TCL1* CLL mice to olaparib, reduced splenomegaly and prolonged mouse survival (Knittel et al., 2017), suggesting the crucial role of ATM for the sensitivity of PARP1 inhibitors and also revealing the possibility of compromising HR for effective PARPi treatment in CLL.

6.1.2. Roles of Ezh2 in DDR

The possible involvement of PRC2 in DNA damage response has been increasingly discussed since a proteomic study hypothesized PARP1, a crucial ADP ribosylase in BER, might be important for the recruitment of components of PRC2 to DNA damage sites (Chou et al., 2010). Ezh2 is particularly interested as it has been identified important for IR resistance in an independent shRNA screen study (Hurov et al., 2010). Proteomics screen with mass spectrometry identified the enrichments of core components of PRC2 Ezh2 and Suz12 in chromatin fractions with DNA damage after UV exposure in Hela cells while proteins known to be involved in DNA damage response such as MDC1, 53BP1, PARP2, MSH2 and MSH6 could be also recovered, which was further validated by immunofluorescence assays showing co-localization of PRC2 with γH2AX. Inhibition of PARP1 disrupted the co-localization of PRC2 and loss of 7-methylguanosine (m7G) cap nascent transcripts in the UV laser induced DNA

damage sites, further suggesting the correlation of transcriptional repression function of PRC2 with DNA damage repair. The interaction of PRC2 and PARP1 in DNA damage sites was further demonstrated using GST-pull down and Co-IP in a breast cancer study, in which instead of transcriptional repression, upon oxidative stress or alkylating DNA damage, PARP1 poly ADP-ribosylation (PARylation) dissociated PRC2 and destabilized Ezh2, therefore reducing H3K27 trimethylation. Inhibition of Ezh2 significantly improved the anti-cancer effect of PARP inhibitors in breast cancer cell line, indicating a negative function of Ezh2 in DNA damage induced cell death (Yamaguchi et al., 2018).

6.2. Results

6.2.1. Preliminary testing of PARP inhibitors in *Ezh2* cKO leukaemic cells

To investigate the role of Ezh2 in the efficacy of PARP inhibitors in leukaemia, *Ezh2* cKO AML cells were used to test the drug sensitivity with or without Ezh2 existence. Knockout of *Ezh2* significantly enhanced the cytotoxic effect of olaparib in a dose-dependent manner in MLL-AF6 AML cells through promoting cell apoptosis (Figure 6.1A-B), in which the percentage of apoptotic cells was substantially increased at 10 μM olaparib treatment. Furthermore, to examine the effect of olaparib on the colony formation capability of leukaemic cells, MLL-AF6 AML cells were seeded in semi-solid methylcellulose-based media and treated with olaparib with or without pharmacological inhibition of Ezh2. As a result, while 1 μM olaparib showed marginal effect against the colony formation of leukaemic cells, combination of olaparib with the Ezh2 inhibitor GSK126 effectively attenuated colony formation units of MLL-AF6 AML cells although the inhibition was reduced when p53, which mediates DNA damage induced cell death, was depleted (Figure 6.1C) (Yoshida and Miki, 2010). Meanwhile, looking into DNA damage response through examining the protein levels of γH2AX, genetic depletion of Ezh2 promoted PARPi-induced DNA damage while inhibition of PARP1 stabilized Ezh2 in consistency with the breast cancer study (Figure 6.2) (Yamaguchi et al., 2018), and decrease in ATM expression, further suggesting that loss of Ezh2 may compromise DNA damage response (DDR), especially homologous recombination (HR), which play a decisive roles for sensitivity of PARP inhibitors in breast cancer and leukaemia (Esposito et al., 2015; Zhao and So, 2016).

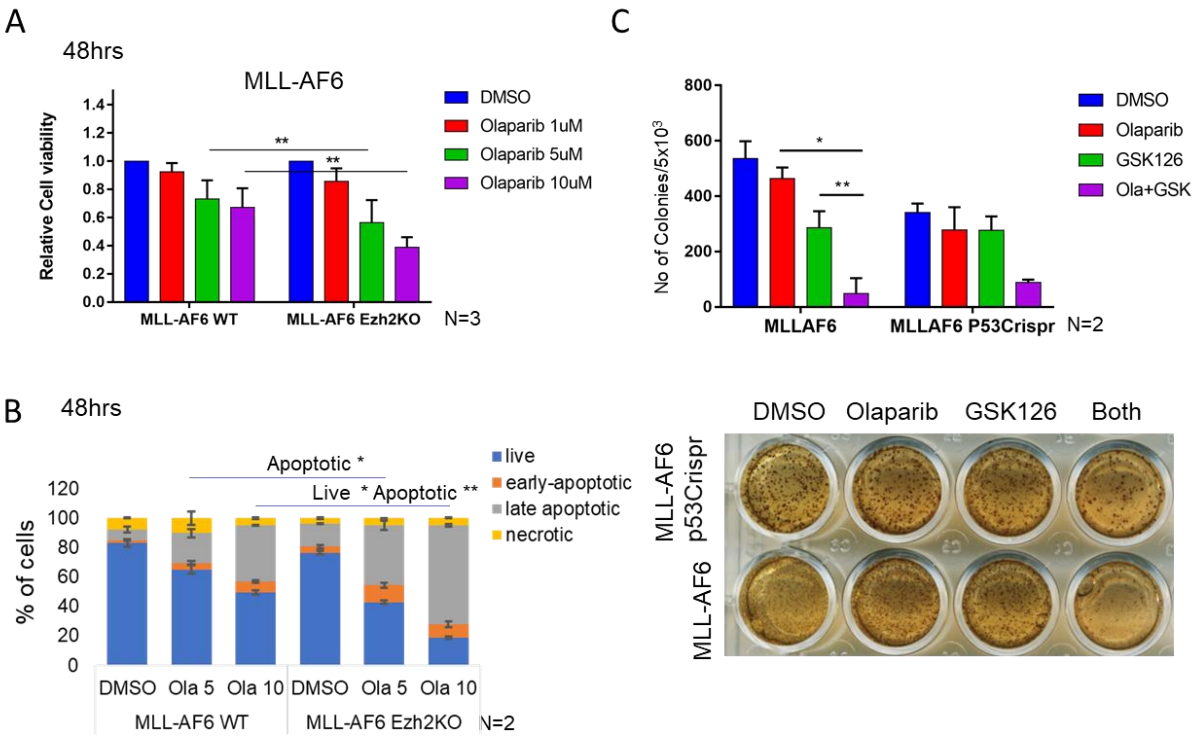

Figure 6.1. Drug effects of PARPi after inhibition of Ezh2 in MLL-AF6 AML cells. (A) MLL-AF6 *Ezh2*$^{fl/fl}$ AML cells treated with 25 nM TAM (*Ezh2* KO) or 0.1% ethanol (*Wt*) for 72hrs were subjected to 48hr olaparib treatments at indicated doses, and cell viability was analysed by MTT assay. Results were obtained from 3 independent experiments (N=3). (B) Cell apoptosis was revealed using AnnexinV/PI staining, and further distinguished into 4 groups. Live (AnnexinV-/PI-), early-apoptotic (AnnexinV+/PI-), apoptotic (AnnexinV+/PI+) and necrotic (AnnexinV-/PI+). (C) Colony formation units (CFU) of MLL-AF6 AML cells and MLL-AF6 AML cells with TP53 CRISPR/Cas9 treated with 1 μM olaparib or/and 10 μM GSK126 for 7 days. Results were obtained from 2 independent experiments (N=2). Bar graphs show mean+S.D. (*P<0.05, **P<0.01 and ***P<0.001, paired t-test).

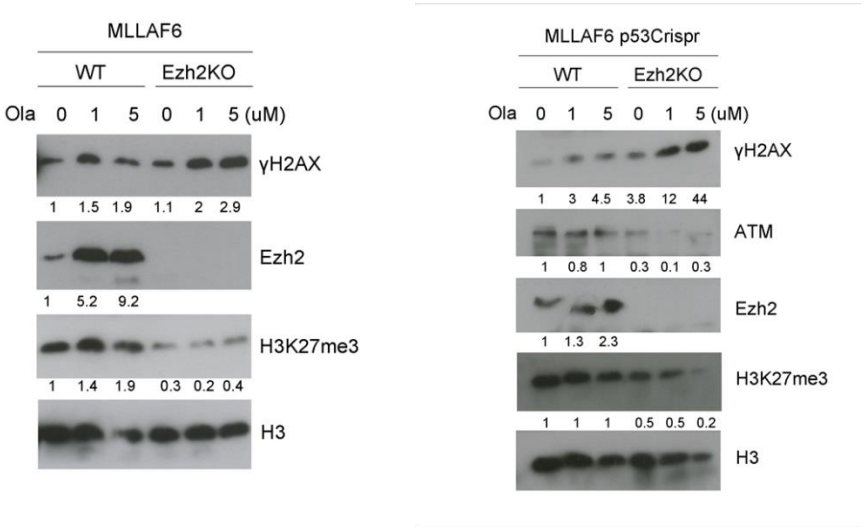

Figure 6.2. Protein levels of γH2AX after olaparib treatment in *Ezh2* cKO MLL-AF6 AML cells. Immunoblotting of total protein lysates collected from *Wt* and *Ezh2* KO AML cells with or without TP53 CRISPR/Cas9 treated with 1-10 μM olaparib for 48 hrs. Relative quantitative results are shown under each panel.

Indeed, RNA-seq profiling of *Ezh2* cKO AML cells driven by MN1 revealed loss of Ezh2 transcriptionally compromised several DDR pathways such HR, mismatch repair and nucleotide excision repair (Figure 6.3A-B). The majority of HR genes diminished after knockout of Ezh2, including ATM, Brca1, Rpa1 and Rad51 (Figure 6.3A-B), and the trend of downregulation could be seen in AML driven by MLL-fusions as well (Figure 6.3C). Furthermore, immunofluorescence staining revealed a substantial increase of γH2AX foci after Olaparib treatment, whereas Rad51 recruitment was retarded in *Ezh2* cKO AML cells with DNA damage (≥10 γH2AX foci), suggesting the importance of Ezh2 in keeping HR functional (Figure 6.4 A and 6.4 B (ii)). The preliminary results in AML together with previous studies in solid cancer consistently suggest that Ezh2 may play multiple roles in DDR through epigenetic modulation of genes encoding critical component for assembly of DDR complexes (Chou et al., 2010) .

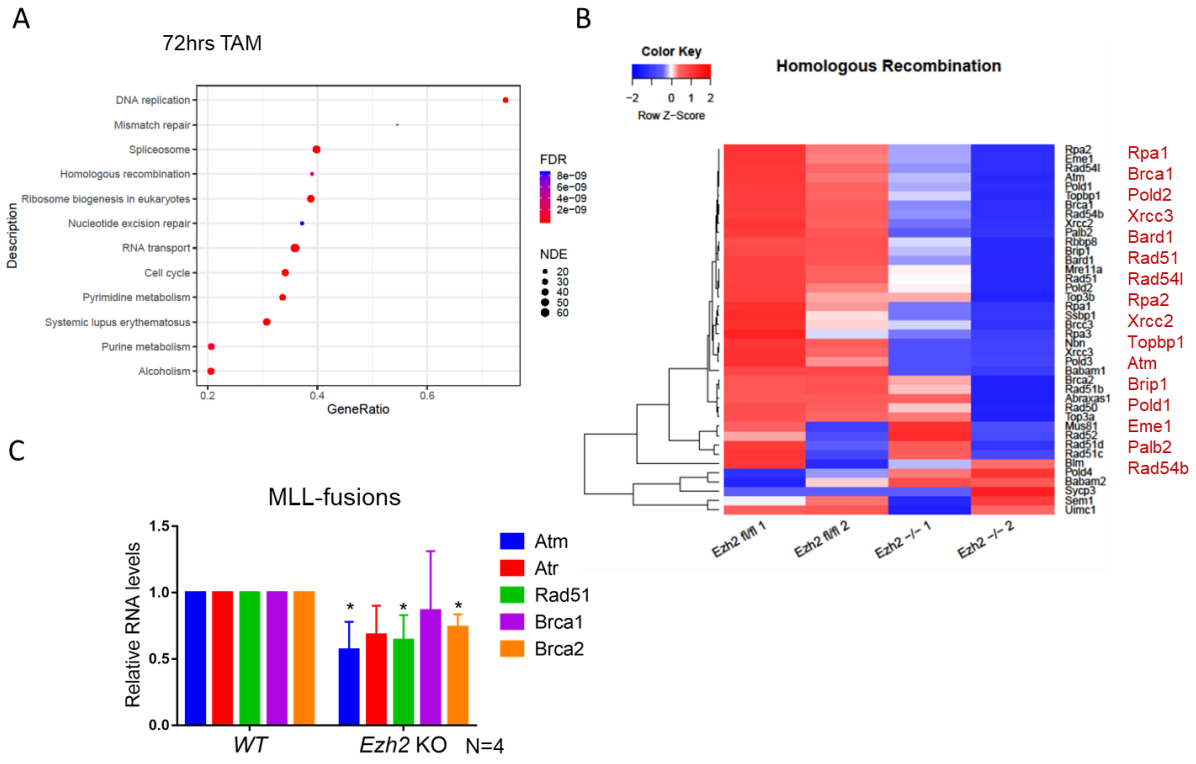

Figure 6.3. Down-regulation of DDR genes after genetic inhibition of EZH2 in AML cells. (A) The dot plot showing top KEGG pathways in MN1 *Ezh2* KO AML cells based on the downregulated differential gene list by comparison with the wild type of Ezh2. (B) The heatmap showing row normalized counts of HR genes in wild type (*Wt*) and *Ezh2* cKO MN1 AML cells, and significantly downregulated genes were pointed out on the right-hand side. (C) qRT-PCR of HR genes in *Ezh2*$^{fl/fl}$ MLL-fusions AML cells (MLL-AF6/9) treated with 25 nM TAM or 0.1% ethanol for 72hrs. Bar graphs show mean+S.D. (*P<0.05, **P<0.01 and ***P<0.001, paired t-test).

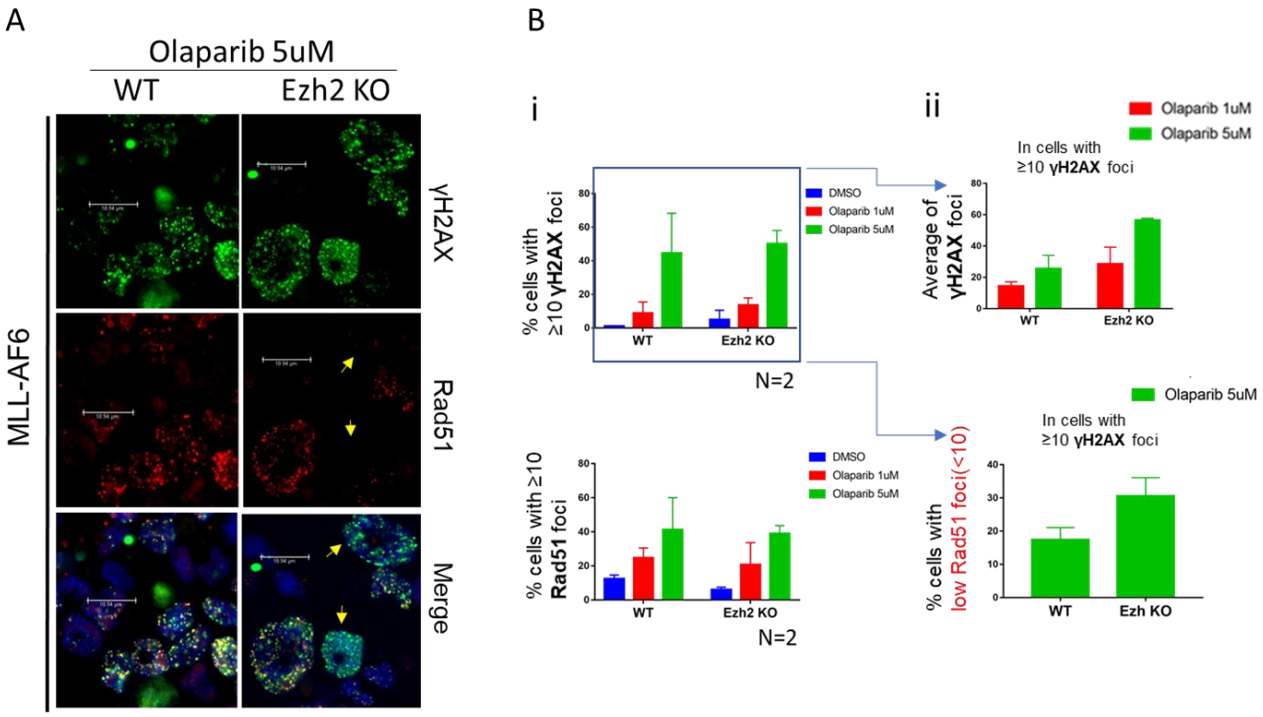

Figure 6.4. Foci of γH2AX and Rad51 recruitments after olaparib treatment in *Ezh2* KO MLL-AF6 AML cells. (A) Representative images of γH2AX, Rad51 and their merge with DAPI in MLL-AF6 *Ezh2* KO AML cells treated with 5 μM olaparib for 48hrs. (B) Bar charts showing foci counting results (N=2). (i) The percentage of cells with ≥ 10 γH2AX foci or Rad51 foci. (ii) Average foci of γH2AX (upper) and the percentage of cells with <10 Rad51 foci in cells with high levels of DNA damage (≥10 γH2AX foci). Results were obtained from 2 independent experiments (N=2). Bar graphs show mean+S.D.

6.2.2. The efficacy of PARP inhibitors in *Asxl1*/*Ezh2* cKO CLL mice

Transcriptionally active BER and overexpression of *Aicda* in RNA-seq profiling suggest a critical function of improved DDR for the survival of *Asxl1*$^{-/-}$*Ezh2*$^{-/-}$ CLL cells (Figure 6.5 and Table 5.2). Overexpression of DNA mutator *Aicda*, may create high levels of DNA base lesions and indirectly result in DSB via mismatch repair (MMR) (Stavnezer et al., 2008). However, active BER could potentially reduce the initial DNA base lesions and avoid overloaded DSB in *Asxl1*$^{-/-}$*Ezh2*$^{-/-}$ CLL cells. Theoretically, blocking BER through pharmacological inhibition of PARP1 may effectively induce

overwhelming DSB in the potential *Aicda*-expressing CLL, therefore leading to cell death and showing high drug sensitivity to PARPi.

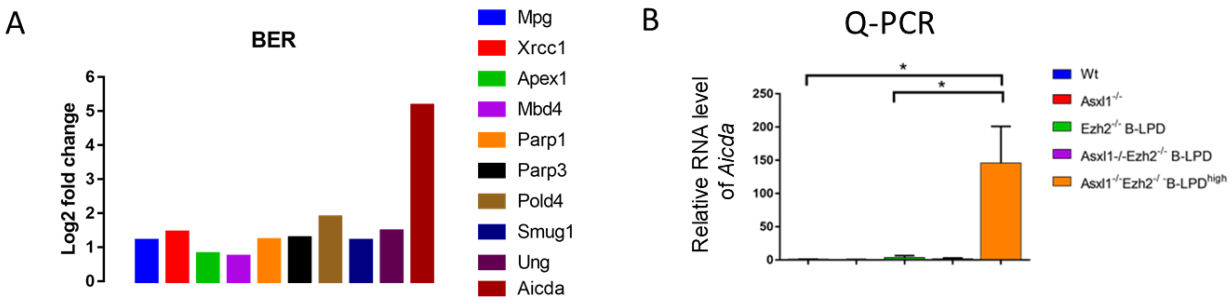

Figure 6.5. Active BER in *Asxl1*/*Ezh2* cKO CLL. (A) Fold changes of significant differential BER genes and Aicda (padj<0.05) in BM cells from *Asxl1*/*Ezh2* cKO B-LBD mice. (B) qRT-PCR of *Aicda* in BM cells from indicated mice. Bar graphs show mean+S.E.M. (*P<0.05, **P<0.01 and ***P<0.001, unpaired t-test).

To elucidate the efficacy of PARP inhibitors in A*sxl1*$^{-/-}$*Ezh2*$^{-/-}$ CLL, C57B/6 SJL mice were treated with the PARP inhibitor olaparib at 50 mg/kg one week after tertiary transplantation for 4 weeks at 5 days per week (Figure 6.6A). Meanwhile, the BTK inhibitor ibrutinib was also involved as a control to assess the clinical relevance of our mouse CLL model with unmutated CLL (Byrd et al., 2014). As a result, while a wide range of CLL counts (CD19^{+}CD5^{+}) were detected in PB after 4 week treatment of ibrutinib as BTK inhibitors can affect the homing of CLL cells from PB to lymphoid tissues (Herman et al., 2014), the restoration in RBC and haemoglobin further suggesting the recovery of haematopoiesis in BM of the CLL mice treated with ibrutinib (Figure 6.6B). On the other hand, the CLL counts significantly reduced in olaparib treatment on day35, suggesting a potential anti-proliferative effect of PARPi on A*sxl1*$^{-/-}$*Ezh2*$^{-/-}$CLL cells. (Figure 6.6B).

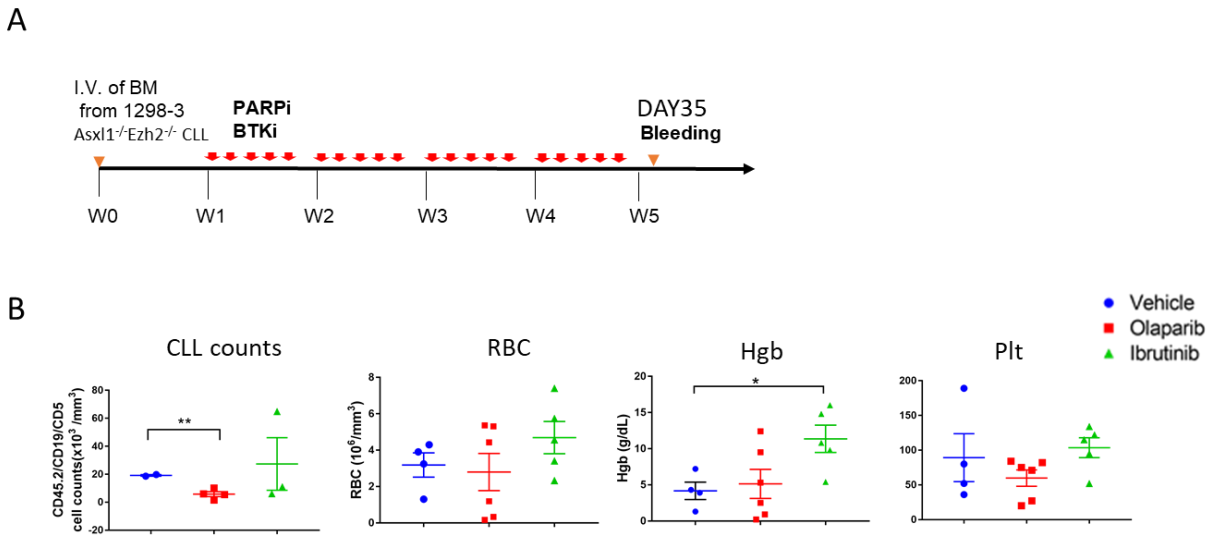

Figure 6.6. Treatments of PARPi and BTKi in the *Asxl1*$^{-/-}$*Ezh2*$^{-/-}$ CLL mouse model. (A) Recipient mice transplanted with 1×10^5 BM cells from secondary *Asxl1*$^{-/-}$*Ezh2*$^{-/-}$ CLL mice were treated with vehicles (10% HBC, N=6), 50mg/kg olaparib (N=6) and 15mg/kg ibrutinib (N=5) from week1 (W1) to week4 (W4) at 5 days per week (red arrows), and (B) absolute CLL counts (CD45.2$^+$CD19$^+$CD5$^+$) and blood counts (bottom) were analysed on day35. Dot graphs show mean+S.E.M. (*P<0.05, **P<0.01 and ***P<0.001, unpaired t-test).

Furthermore, mice treated with vehicles started coming down in week 4 with severe organomegaly and circulation of CLL cells in PB, whereas olaparib and ibrutinib delayed disease latency although only olaparib displayed a statistically significant result and reduced splenomegaly (Figure 6.7A-B). Intriguingly, while CLL cells with atypical morphology were effaced in PB after treatments (Figure 6.7C), higher numbers of circulating CLL counts were recovered and detected in a part of olabarib group and the ibrutinib treatment group when mice came down, suggesting *Asxl1*$^{-/-}$*Ezh2*$^{-/-}$ CLL cells with higher tissue invasion capacity may be preferentially targeted by the drug treatments (Figure 6.7D).

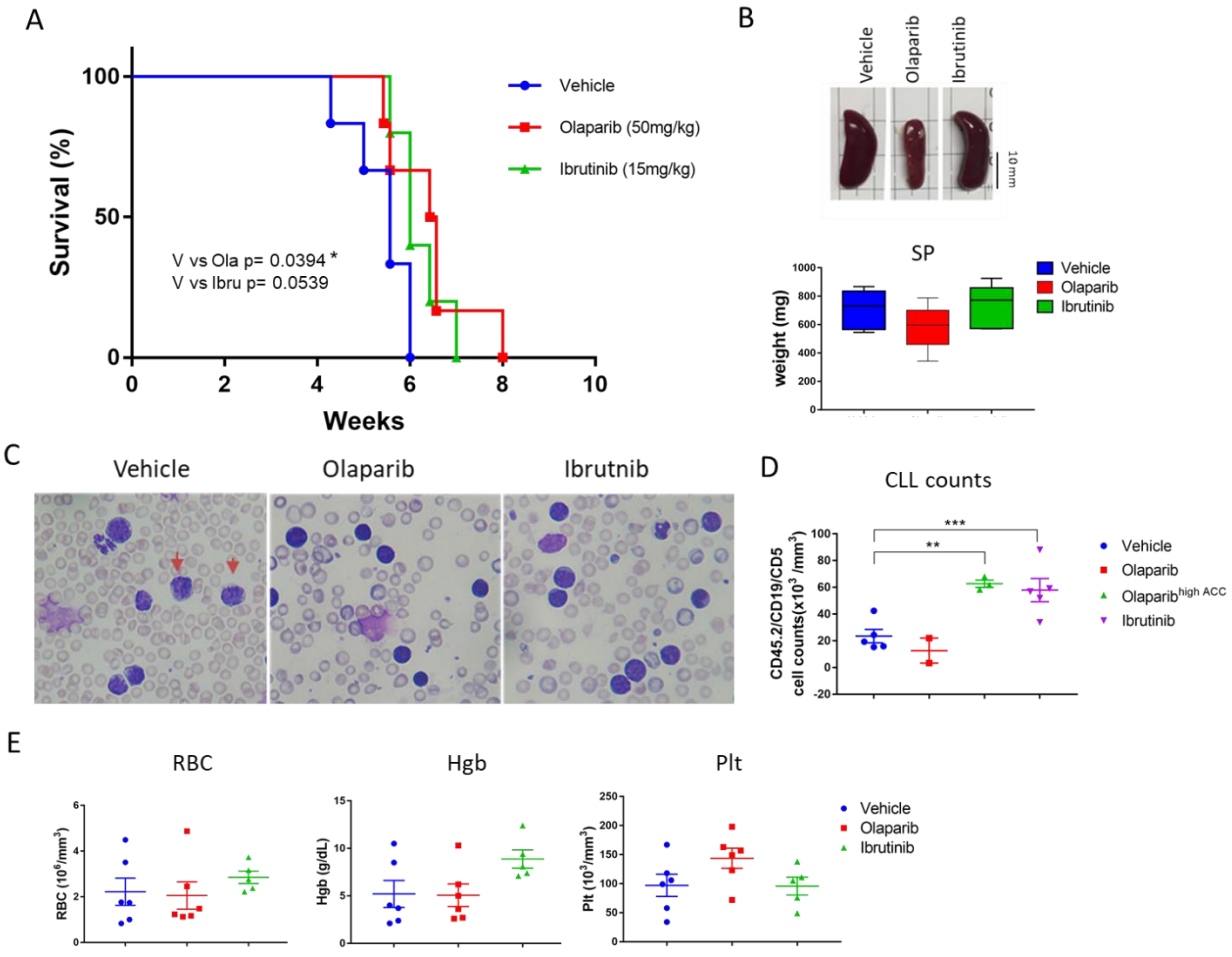

Figure 6.7. Favourable outcomes after treatments of PARPi and BTKi in *Asxl1*$^{-/-}$*Ezh2*$^{-/-}$ CLL mice. (A) Survival curves of CLL mice treated vehicles, olaparib and ibrutinib at indicated doses. (B) Representative images of spleen (upper) and weights (bottom) from CLL mice coming down. (C) Representative images of blood smears of CLL mice treated with vehicles, olaparib and ibrutinib. (D) Absolute CLL counts (ACC, CD45.2^{+}CD19^{+}CD5^{+}) and (E) blood counts from CLL mice coming down. Mice treated with olaparib showing higher numbers of CLL counts are marked as olaparib$^{\text{high ACC}}$. Dot graphs and Bar graphs show mean+S.E.M. (*P<0.05, **P<0.01 and ***P<0.001, unpaired t-test).

6.3. Discussion

It has been reported that cell senescence via retinoblastoma (RB) pathway repressed DDR genes involved in a verity of DNA repairs including NER, MMR and HR in immortalized human mammary epithelial cells as we found in AML (Collin et al., 2018) (Figure 6.3). Leukaemogenesis mediated by MLL fusions is Ezh2-dependent, and genetic removal of Ezh2 induced *CDKN2A* and reduced cell growth (Neff et al., 2012). In addition, transcriptional profiling of *Ezh2* KO AML further showed significant downregulation of genes involved in cell cycle and DNA replication (Figure 6.3A), implying cell senescence occurred after knockout of *Ezh2* and suggesting that global repression of DDR genes in *Ezh2* KO AML might be a consequence of *CDKN2A*-induced cell senescence through RB pathway (Rayess et al., 2012). The transcriptional suppression of DDR genes may create a cellular DNA damage-prone status, ultimately sensitizing the Ezh2-dependent AML cells to PARP inhibitors. Moreover, it has been demonstrated that Ezh2 and other core components of PRC2 could be Poly-ADP-ribosylated (PARsylation) by PARP1 and recruited to the UV laser irradiated DNA damage sites, which resulted in rapid loss of nascent RNA and elongating RNA polymerase. These results suggest that PRC2 may repress the transcription activity at DNA damage sites through H3K27 trimethylation, and the transcriptional repression in the vicinity of DNA lesions may be important for preventing the gigantic RNA polymerase II transcription complex from interfering the assembly of DNA repair complexes (Chou et al., 2010). Therefore, inhibition of Ezh2 may also sensitize cancer cells to PARP inhibitors by means of reducing the chromatin accessibility to DDR complexes.

However, in contrast with the Ezh2 dependency in AML, tumour suppressor genes induced after loss of Ezh2 may be subsequently compensated by Ezh1 in haematopoietic cells, and ultimately the PRC2 deficient myeloid cells and lymphoid cells developed into haematologic malignancies with proliferative features (Mochizuki-Kashio et al., 2015; Muto et al., 2013). Moreover, RNA-seq profiling showed no significant downregulation of DDR pathways in BM cells from *Ezh2* cKO and *Asxl*/*Ezh2* double cKO B-LPD mice, suggesting the cell senescence-induced transcriptional suppression of DDR should not exist in the Ezh2-deficient CLL cells. Nonetheless, BM cells from *Asxl1*/*Ezh2* KO CLL mice exhibited transcriptional profiling of high cell division, with overexpression of *Myc*, *Ccdn2*, *Bcl-2*, *Cxcr5* and *Aicda* as human CLL cells with high proliferation and class switch recombination (CSR), which contains DNA damage and genome instability due to overexpression of *Aicda* (Figure 6.5 and Table 5.2) (Palacios et al., 2010; Patten et al., 2012), and the upregulation of BER genes including PARP1 and XRCC1 further suggests the essentiality of active BER in controlling AID-induced DNA base lesions, which eventually causes DSB and leads to cell death (Figure 6.9) (Stavnezer et al., 2008). Therefore, we propose that blocking BER through PARP inhibitors might indirectly result in high levels of DSB and provide an anti-cancer effect. As a result, treatment of olaparib reduced organomegaly and significantly prolonged survival of *Asxl1*/*Ezh2* cKO CLL mice (Figure 6.7), and showing better drug effects than the BCR targeting drug ibrutinib, shedding light on use of PARP inhibitors to tackle relapsed and treatment-resistant U-CLL.

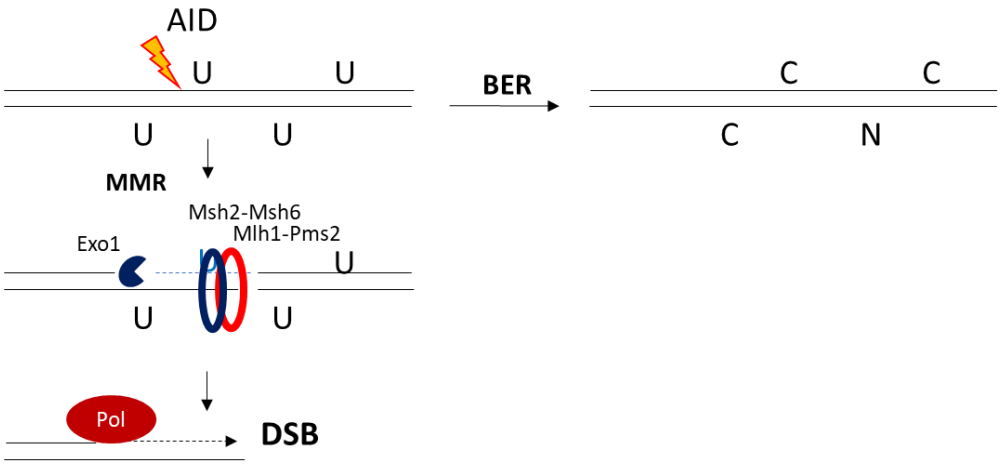

Figure 6.8. Models of AID-induced DSB. AID adds uracil (U) into DNA double strands through deamination of cytidine (C), and the DNA base lesions can be repaired by BER or mismatch repair (MMR), in which Msh2-Msh6 recognises U:G mismatches and recruits Exonuclease 1 (Exo1) along with Mlh1-Pms2, to remove the single strands toward the mismatches, thus creating the DSB indirectly.

Targeting BCR through inhibition of downstream kinase such as BTK (ibrutinib) and PI3K (idelalisib) has been approved and used for the initial treatment of high risk CLL patients, such as the clinical cases with unmutated *IGHV* or/and del (17p) (mutations of *TP53*) as well as patients with relapsed disease. These inhibitors of BCR are more effective in CLL cells with unmutated *IGHV* than CLL cells with mutated *IGHV* although the preference is still being validated in clinical trials (Kipps et al., 2017). Organomegaly and lymphadenopathy can be resolved after inhibition of BCR, which is usually accompanied with a rapid increase of absolute lymphocyte counts (lymphocytosis) in PB of CLL patients for up to 6 months likely due to impairing chemotaxis of CLL through inhibition of CXCR4/5 signalling (Herman et al., 2014; Ponader et al., 2012). In our *Asxl1/Ezh2* cKO CLL model with transcriptionally active BCR signalling (Figure 5.11-12), lymphocytosis was detected after ibrutinib treatment, followed by alleviated anaemia, and ultimately prolonged overall survival, suggesting

the correlation between the unmated CLL mouse model and clinical unmutated CLL (Figure 6.6-8).

At present, in addition to the deletion in chromosome 17p (del (17p)), which results in loss of p53 and sensitivity to chemotherapy, the mutation status of *IGHV* is another key prognostic factor to consider the type of therapeutics for CLL patients (Kipps et al., 2017). As CLL patients with del (17p) and unmutated *IGHV* (U-CLL) usually exhibit poor response rate and relatively short progress free survival (PFS) to the regimens of chemotherapy (purine analogues (fludarabine) and alkylating agents (chlorambucil)) and the treatment of anti-CD20 monoclonal antibodies (rituximab, ofatumumab), these patients are often directly subjected to the treatment of BCR inhibitors, especially the BTK inhibitor ibrutinib, which has also been used as the last line of treatment for refractory CLL (Byrd et al., 2014; Kipps et al., 2017). However, it has been reported that around 5 to 18 % of patients showing drug resistance and disease progress after the treatments of ibrutinib due to the mutations in BTK (Cys481) or PLCG2 (Ahn et al., 2017; Furman et al., 2014). While the BCL-2 inhibitor venenoclax has been approved for the treatment of relapsed and del (17p) CLL patients (Roberts et al., 2016), targeting AID-high U-CLL patients, who tend to have short PFS and overall survival (OS) (Palacios et al., 2010), with PARP inhibitors could provide a novel therapeutic avenue for the treatment of ibrutinib-resistant U-CLL.

Charter 7: Conclusion

As a result, concurrent depletion of Asxl1 with Ezh2 perturbed the haematopoiesis toward myeloid-biased differentiation, enhanced establishments of HSPCs, and ultimately contributed to high penetrance of accelerated myeloid neoplasm-like disease phenotypes, whereas loss of Ezh2 only developed mild MDS-like disease (50%), in which myelodysplastic cells such as hyposegmented neutrophils and abnormal megakaryocytes and left shift in granulocytic maturation were observed. Co-inactivation of Asxl1 with Ezh2 further provided myeloproliferative features such as splenomegaly with EMH and thrombocytosis together with myelodysplasia to *Asxl1*/*Ezh2* double mutant mice, hence leading to lethal MDS/MPN phenotypes (50%), and the results may also account for the higher frequency of cluster mutations of Asxl1 and Ezh2 in clinical MDS/MPN patients (Rinke et al., 2017; Triviai et al., 2019). Although no visual illness and myelodysplastic cells were observed in *Asxl1* cKO mice, increase in platelet numbers were also detected in two of Asxl1 single mutants, suggesting loss of Asxl1 may contribute thrombocytosis to double mutants.

Intriguingly, mono-clonal lymphoproliferation of B1α were identified and further characterized as CLL with unmutated *IGHV* (U-CLL) in both *Ezh2* single cKO mice (33%) and *Asxl1*/*Ezh2* double cKO mice (42%) (Table 4.1), in which transcriptional profiling revealed active BCR signalling and several CLL-related genes such as Zap70 crucial for CLL pathogenesis (Figure 5.12-13). Furthermore, loss of Asxl1 and Ezh2 may have additive impact on the H3K27 methylation, and ultimately derepress more genes involved in cell proliferation (Ccnd2, Myc), anti-apoptosis (Bcl-2), chemotaxis (Cxcr5) and genome instability (Aicda), therefore resulting in the high-risk CLL with high cell division, BM infiltration and genome instability (Figure 5.16). To gain insights into the mechanism for the CLL leukaemogenesis, the global landscape of H3K27

trimethylation has to be uncovered in CLL cells from *Asxl1*/*Ezh2* cKO mice to identify crucial molecular targets for the CLL leukaemogenesis.

Our high penetrance and short latency CLL transplantation models will provide a novel and powerful platform for CLL pre-clinical drug testing (Figure 5.15). Notably, over 20% of transcriptional landscape of *Asxl1*$^{-/-}$*Ezh2*$^{-/-}$ CLL overlapped with a differential gene set in human CLL cells from 98 CLL patients (Figure 5.14) (Ferreira et al., 2014), *Asxl1*$^{-/-}$*Ezh2*$^{-/-}$ CLL also displayed sensitivity to the BTK inhibitor ibrutinib (Figure 6.6-6.8), correlating the mouse CLL model with U-CLL patients, which have been reported sensitive to BCR signalling inhibitors (Byrd et al., 2014; Guo et al., 2016; Ponader et al., 2012). In addition, we also found that olaparib treatment significantly reduced organomegaly and prolonged the survival of *Asxl1*$^{-/-}$*Ezh2*$^{-/-}$ CLL mice with overexpression of Aicda and active BER. This may rise a hope for targeting BER by PARP inhibitors to tackle the treatment-resistant CLL patients with Aicda overexpression and genome instability (Figure 6.5-6.7) (Palacios et al., 2010; Patten et al., 2012). To test this hypothesis, CLL patients with unmutated *IGHV* could be classified into three subgroups with AID-high expression (++), AID-positive CLL cells (+) and AID-negative CLL cells (-) (Palacios et al., 2010), and the anti-cancer effect of olaparib can be examined in the three subgroups through analysing the cell viability, cell apoptosis, senescence and γH2AX staining to validate the role of AID in the drug sensitivity of olaparib in the CLL patients. In addition, we also showed that genetic and pharmacologic inhibition of Ezh2 compromised DDR and promoted olaparib sensitivity in AML (Figure 6.1-4), thus revealing the possibility of combination treatment of Ezh2 inhibitors with PARP inhibitors for leukaemia therapies. Finally, we also speculate that human CLL cells from U-CLL patients could benefit by combination

using Ezh2 inhibitors such as GSK126 together with olaparib, which may generate synergistic killing by inducing excessive DNA damage and epigenetic reprogramming.

Reference

Abdel-Wahab, O., M. Adli, L.M. LaFave, J. Gao, T. Hricik, A.H. Shih, S. Pandey, J.P. Patel, Y.R. Chung, R. Koche, F. Perna, X. Zhao, J.E. Taylor, C.Y. Park, M. Carroll, A. Melnick, S.D. Nimer, J.D. Jaffe, I. Aifantis, B.E. Bernstein, and R.L. Levine. 2012. ASXL1 mutations promote myeloid transformation through loss of PRC2-mediated gene repression. *Cancer cell* 22:180-193.

Abdel-Wahab, O., J. Gao, M. Adli, A. Dey, T. Trimarchi, Y.R. Chung, C. Kuscu, T. Hricik, D. Ndiaye-Lobry, L.M. Lafave, R. Koche, A.H. Shih, O.A. Guryanova, E. Kim, S. Li, S. Pandey, J.Y. Shin, L. Telis, J. Liu, P.K. Bhatt, S. Monette, X. Zhao, C.E. Mason, C.Y. Park, B.E. Bernstein, I. Aifantis, and R.L. Levine. 2013. Deletion of Asxl1 results in myelodysplasia and severe developmental defects in vivo. *The Journal of experimental medicine* 210:2641-2659.

Abdel-Wahab, O., A. Pardanani, J. Patel, M. Wadleigh, T. Lasho, A. Heguy, M. Beran, D.G. Gilliland, R.L. Levine, and A. Tefferi. 2011. Concomitant analysis of EZH2 and ASXL1 mutations in myelofibrosis, chronic myelomonocytic leukemia and blast-phase myeloproliferative neoplasms. *Leukemia* 25:1200-1202.

Aguilar-Hernandez, M.M., M.D. Blunt, R. Dobson, A. Yeomans, S. Thirdborough, M. Larrayoz, L.D. Smith, A. Linley, J.C. Strefford, A. Davies, P.M. Johnson, N. Savelyeva, M.S. Cragg, F. Forconi, G. Packham, F.K. Stevenson, and A.J. Steele. 2016. IL-4 enhances expression and function of surface IgM in CLL cells. *Blood* 127:3015-3025.

Ahn, I.E., C. Underbayev, A. Albitar, S.E. Herman, X. Tian, I. Maric, D.C. Arthur, L. Wake, S. Pittaluga, C.M. Yuan, M. Stetler-Stevenson, S. Soto, J. Valdez, P. Nierman, J. Lotter, L. Xi, M. Raffeld, M. Farooqui, M. Albitar, and A. Wiestner. 2017. Clonal evolution leading to ibrutinib resistance in chronic lymphocytic leukemia. *Blood* 129:1469-1479.

Aisenberg, A.C. 2000. Historical review of lymphomas. *British journal of haematology* 109:466-476.

Alabert, C., T.K. Barth, N. Reveron-Gomez, S. Sidoli, A. Schmidt, O.N. Jensen, A. Imhof, and A. Groth. 2015. Two distinct modes for propagation of histone PTMs across the cell cycle. *Genes & development* 29:585-590.

Anders, S., P.T. Pyl, and W. Huber. 2015. HTSeq--a Python framework to work with high-throughput sequencing data. *Bioinformatics* 31:166-169.

Arnaudeau, C., C. Lundin, and T. Helleday. 2001. DNA double-strand breaks associated with replication forks are predominantly repaired by homologous recombination involving an exchange mechanism in mammalian cells. *Journal of molecular biology* 307:1235-1245.

Awan, F.T., and J.C. Byrd. 2014. New strategies in chronic lymphocytic leukemia: shifting treatment paradigms. *Clinical cancer research : an official journal of the American Association for Cancer Research* 20:5869-5874.

Baylin, S.B., and P.A. Jones. 2011. A decade of exploring the cancer epigenome - biological and translational implications. *Nature reviews. Cancer* 11:726-734.

Bejar, R., K. Stevenson, O. Abdel-Wahab, N. Galili, B. Nilsson, G. Garcia-Manero, H. Kantarjian, A. Raza, R.L. Levine, D. Neuberg, and B.L. Ebert. 2011. Clinical effect of point mutations in myelodysplastic syndromes. *The New England journal of medicine* 364:2496-2506.

Bejar, R., K.E. Stevenson, B.A. Caughey, O. Abdel-Wahab, D.P. Steensma, N. Galili, A. Raza, H. Kantarjian, R.L. Levine, D. Neuberg, G. Garcia-Manero, and B.L. Ebert. 2012. Validation of a prognostic model and the impact of mutations in patients with lower-risk myelodysplastic syndromes. *Journal of clinical oncology : official journal of the American Society of Clinical Oncology* 30:3376-3382.

Bichi, R., S.A. Shinton, E.S. Martin, A. Koval, G.A. Calin, R. Cesari, G. Russo, R.R. Hardy, and C.M. Croce. 2002. Human chronic lymphocytic leukemia modeled in mouse by targeted TCL1 expression. *Proceedings of the National Academy of Sciences of the United States of America* 99:6955-6960.

Blackledge, N.P., N.R. Rose, and R.J. Klose. 2015. Targeting Polycomb systems to regulate gene expression: modifications to a complex story. *Nature reviews. Molecular cell biology* 16:643-649.

Bodor, C., V. Grossmann, N. Popov, J. Okosun, C. O'Riain, K. Tan, J. Marzec, S. Araf, J. Wang, A.M. Lee, A. Clear, S. Montoto, J. Matthews, S. Iqbal, H. Rajnai, A. Rosenwald, G. Ott, E. Campo, L.M. Rimsza, E.B. Smeland, W.C. Chan, R.M. Braziel, L.M. Staudt, G. Wright, T.A. Lister, O. Elemento, R. Hills, J.G. Gribben, C. Chelala, A. Matolcsy, A. Kohlmann, T. Haferlach, R.D. Gascoyne, and J. Fitzgibbon. 2013. EZH2 mutations are frequent and represent an early event in follicular lymphoma. *Blood* 122:3165-3168.

Bordoli, L., F. Kiefer, K. Arnold, P. Benkert, J. Battey, and T. Schwede. 2009. Protein structure homology modeling using SWISS-MODEL workspace. *Nature protocols* 4:1-13.

Boultwood, J., J. Perry, A. Pellagatti, M. Fernandez-Mercado, C. Fernandez-Santamaria, M.J. Calasanz, M.J. Larrayoz, M. Garcia-Delgado, A. Giagounidis, L. Malcovati, M.G. Della Porta, M. Jadersten, S. Killick, E. Hellstrom-Lindberg, M. Cazzola, and J.S. Wainscoat. 2010. Frequent mutation of the polycomb-associated gene ASXL1 in the myelodysplastic syndromes and in acute myeloid leukemia. *Leukemia* 24:1062-1065.

Bowen, D., D. Culligan, S. Jowitt, S. Kelsey, G. Mufti, D. Oscier, J. Parker, and U.M.G. Group. 2003. Guidelines for the diagnosis and therapy of adult myelodysplastic syndromes. *British journal of haematology* 120:187-200.

Boyer, L.A., K. Plath, J. Zeitlinger, T. Brambrink, L.A. Medeiros, T.I. Lee, S.S. Levine, M. Wernig, A. Tajonar, M.K. Ray, G.W. Bell, A.P. Otte, M. Vidal, D.K. Gifford, R.A. Young, and R. Jaenisch. 2006. Polycomb complexes repress developmental regulators in murine embryonic stem cells. *Nature* 441:349-353.

Bracken, A.P., N. Dietrich, D. Pasini, K.H. Hansen, and K. Helin. 2006. Genome-wide mapping of Polycomb target genes unravels their roles in cell fate transitions. *Genes & development* 20:1123-1136.

Bryant, H.E., N. Schultz, H.D. Thomas, K.M. Parker, D. Flower, E. Lopez, S. Kyle, M. Meuth, N.J. Curtin, and T. Helleday. 2005. Specific killing of BRCA2-deficient tumours with inhibitors of poly(ADP-ribose) polymerase. *Nature* 434:913-917.

Burger, J.A., M. Burger, and T.J. Kipps. 1999. Chronic lymphocytic leukemia B cells express functional CXCR4 chemokine receptors that mediate spontaneous migration beneath bone marrow stromal cells. *Blood* 94:3658-3667.

Burkle, A., M. Niedermeier, A. Schmitt-Graff, W.G. Wierda, M.J. Keating, and J.A. Burger. 2007. Overexpression of the CXCR5 chemokine receptor, and its ligand, CXCL13 in B-cell chronic lymphocytic leukemia. *Blood* 110:3316-3325.

Byrd, J.C., J.R. Brown, S. O'Brien, J.C. Barrientos, N.E. Kay, N.M. Reddy, S. Coutre, C.S. Tam, S.P. Mulligan, U. Jaeger, S. Devereux, P.M. Barr, R.R. Furman, T.J. Kipps, F. Cymbalista, C. Pocock, P. Thornton, F. Caligaris-Cappio, T. Robak, J. Delgado, S.J. Schuster, M. Montillo, A. Schuh, S. de Vos, D. Gill, A. Bloor, C. Dearden, C. Moreno, J.J. Jones, A.D. Chu, M. Fardis, J. McGreivy, F. Clow, D.F. James, P. Hillmen, and R. Investigators. 2014. Ibrutinib versus ofatumumab in previously treated chronic lymphoid leukemia. *The New England journal of medicine* 371:213-223.

Calin, G.A., M. Ferracin, A. Cimmino, G. Di Leva, M. Shimizu, S.E. Wojcik, M.V. Iorio, R. Visone, N.I. Sever, M. Fabbri, R. Iuliano, T. Palumbo, F. Pichiorri, C. Roldo, R. Garzon, C. Sevignani, L. Rassenti, H. Alder, S. Volinia, C.G. Liu, T.J. Kipps, M. Negrini, and C.M. Croce. 2005. A MicroRNA signature associated with prognosis and progression in chronic lymphocytic leukemia. *The New England journal of medicine* 353:1793-1801.

Calissano, C., R.N. Damle, G. Hayes, E.J. Murphy, M.K. Hellerstein, C. Moreno, C. Sison, M.S. Kaufman, J.E. Kolitz, S.L. Allen, K.R. Rai, and N. Chiorazzi. 2009. In vivo intraclonal and interclonal kinetic heterogeneity in B-cell chronic lymphocytic leukemia. *Blood* 114:4832-4842.

Campo, E., S.H. Swerdlow, N.L. Harris, S. Pileri, H. Stein, and E.S. Jaffe. 2011. The 2008 WHO classification of lymphoid neoplasms and beyond: evolving concepts and practical applications. *Blood* 117:5019-5032.

Cao, R., L. Wang, H. Wang, L. Xia, H. Erdjument-Bromage, P. Tempst, R.S. Jones, and Y. Zhang. 2002. Role of histone H3 lysine 27 methylation in Polycomb-group silencing. *Science* 298:1039-1043.

Carbone, M., H. Yang, H.I. Pass, T. Krausz, J.R. Testa, and G. Gaudino. 2013. BAP1 and cancer. *Nature reviews. Cancer* 13:153-159.

Chen, L., J. Apgar, L. Huynh, F. Dicker, T. Giago-McGahan, L. Rassenti, A. Weiss, and T.J. Kipps. 2005. ZAP-70 directly enhances IgM signaling in chronic lymphocytic leukemia. *Blood* 105:2036-2041.

Chen, S.S., F. Batliwalla, N.E. Holodick, X.J. Yan, S. Yancopoulos, C.M. Croce, T.L. Rothstein, and N. Chiorazzi. 2013. Autoantigen can promote progression to a more aggressive TCL1 leukemia by selecting variants with enhanced B-cell receptor signaling. *Proceedings of the National Academy of Sciences of the United States of America* 110:E1500-1507.

Chou, D.M., B. Adamson, N.E. Dephoure, X. Tan, A.C. Nottke, K.E. Hurov, S.P. Gygi, M.P. Colaiacovo, and S.J. Elledge. 2010. A chromatin localization screen reveals poly (ADP ribose)-regulated recruitment of the repressive polycomb and NuRD complexes to sites of DNA damage. *Proceedings of the National Academy of Sciences of the United States of America* 107:18475-18480.

Collin, G., A. Huna, M. Warnier, J.M. Flaman, and D. Bernard. 2018. Transcriptional repression of DNA repair genes is a hallmark and a cause of cellular senescence. *Cell death & disease* 9:259.

Criel, A., G. Verhoef, R. Vlietinck, C. Mecucci, J. Billiet, L. Michaux, P. Meeus, A. Louwagie, A. Van Orshoven, A. Van Hoof, M. Boogaerts, H. Van den Berghe, and C. De Wolf-Peeters. 1997. Further characterization of morphologically defined typical and atypical CLL: a clinical, immunophenotypic, cytogenetic and prognostic study on 390 cases. *British journal of haematology* 97:383-391.

Damle, R.N., T. Wasil, F. Fais, F. Ghiotto, A. Valetto, S.L. Allen, A. Buchbinder, D. Budman, K. Dittmar, J. Kolitz, S.M. Lichtman, P. Schulman, V.P. Vinciguerra, K.R. Rai, M. Ferrarini, and N. Chiorazzi. 1999. Ig V gene mutation status and CD38 expression as novel prognostic indicators in chronic lymphocytic leukemia. *Blood* 94:1840-1847.

Danis, E., T. Yamauchi, K. Echanique, X. Zhang, J.N. Haladyna, S.S. Riedel, N. Zhu, H. Xie, S.H. Orkin, S.A. Armstrong, K.M. Bernt, and T. Neff. 2016. Ezh2 Controls an Early Hematopoietic Program and Growth and Survival Signaling in Early T Cell Precursor Acute Lymphoblastic Leukemia. *Cell reports* 14:1953-1965.

Dey, A., D. Seshasayee, R. Noubade, D.M. French, J. Liu, M.S. Chaurushiya, D.S. Kirkpatrick, V.C. Pham, J.R. Lill, C.E. Bakalarski, J. Wu, L. Phu, P. Katavolos, L.M. LaFave, O. Abdel-Wahab, Z. Modrusan, S. Seshagiri, K. Dong, Z. Lin, M. Balazs, R. Suriben, K. Newton, S. Hymowitz, G. Garcia-Manero, F. Martin, R.L. Levine, and V.M. Dixit. 2012. Loss of the tumor suppressor BAP1 causes myeloid transformation. *Science* 337:1541-1546.

Di Croce, L., and K. Helin. 2013. Transcriptional regulation by Polycomb group proteins. *Nature structural & molecular biology* 20:1147-1155.

DiNardo, C.D., N. Daver, N. Jain, N. Pemmaraju, C. Bueso-Ramos, C.C. Yin, S. Pierce, E. Jabbour, J.E. Cortes, H.M. Kantarjian, G. Garcia-Manero, and S. Verstovsek. 2014.

Myelodysplastic/myeloproliferative neoplasms, unclassifiable (MDS/MPN, U): natural history and clinical outcome by treatment strategy. *Leukemia* 28:958-961.

Dohner, H., S. Stilgenbauer, A. Benner, E. Leupolt, A. Krober, L. Bullinger, K. Dohner, M. Bentz, and P. Lichter. 2000. Genomic aberrations and survival in chronic lymphocytic leukemia. *The New England journal of medicine* 343:1910-1916.

Doulatov, S., F. Notta, E. Laurenti, and J.E. Dick. 2012. Hematopoiesis: a human perspective. *Cell stem cell* 10:120-136.

El-Khamisy, S.F., M. Masutani, H. Suzuki, and K.W. Caldecott. 2003. A requirement for PARP-1 for the assembly or stability of XRCC1 nuclear foci at sites of oxidative DNA damage. *Nucleic acids research* 31:5526-5533.

Endo, T., M. Nishio, T. Enzler, H.B. Cottam, T. Fukuda, D.F. James, M. Karin, and T.J. Kipps. 2007. BAFF and APRIL support chronic lymphocytic leukemia B-cell survival through activation of the canonical NF-kappaB pathway. *Blood* 109:703-710.

Enzler, T., A.P. Kater, W. Zhang, G.F. Widhopf, 2nd, H.Y. Chuang, J. Lee, E. Avery, C.M. Croce, M. Karin, and T.J. Kipps. 2009. Chronic lymphocytic leukemia of Emu-TCL1 transgenic mice undergoes rapid cell turnover that can be offset by extrinsic CD257 to accelerate disease progression. *Blood* 114:4469-4476.

Ernst, T., A.J. Chase, J. Score, C.E. Hidalgo-Curtis, C. Bryant, A.V. Jones, K. Waghorn, K. Zoi, F.M. Ross, A. Reiter, A. Hochhaus, H.G. Drexler, A. Duncombe, F. Cervantes, D. Oscier, J. Boultwood, F.H. Grand, and N.C. Cross. 2010. Inactivating mutations of the histone methyltransferase gene EZH2 in myeloid disorders. *Nature genetics* 42:722-726.

Esposito, M.T., L. Zhao, T.K. Fung, J.K. Rane, A. Wilson, N. Martin, J. Gil, A.Y. Leung, A. Ashworth, and C.W. So. 2015. Synthetic lethal targeting of oncogenic transcription factors in acute leukemia by PARP inhibitors. *Nature medicine* 21:1481-1490.

Fabbri, G., S. Rasi, D. Rossi, V. Trifonov, H. Khiabanian, J. Ma, A. Grunn, M. Fangazio, D. Capello, S. Monti, S. Cresta, E. Gargiulo, F. Forconi, A. Guarini, L. Arcaini, M. Paulli, L. Laurenti, L.M. Larocca, R. Marasca, V. Gattei, D. Oscier, F. Bertoni, C.G. Mullighan, R. Foa, L. Pasqualucci, R. Rabadan, R. Dalla-Favera, and G. Gaidano. 2011. Analysis of the chronic lymphocytic leukemia coding genome: role of NOTCH1 mutational activation. *The Journal of experimental medicine* 208:1389-1401.

Fais, F., F. Ghiotto, S. Hashimoto, B. Sellars, A. Valetto, S.L. Allen, P. Schulman, V.P. Vinciguerra, K. Rai, L.Z. Rassenti, T.J. Kipps, G. Dighiero, H.W. Schroeder, Jr., M. Ferrarini, and N. Chiorazzi. 1998. Chronic lymphocytic leukemia B cells express restricted sets of mutated and unmutated antigen receptors. *The Journal of clinical investigation* 102:1515-1525.

Farmer, H., N. McCabe, C.J. Lord, A.N. Tutt, D.A. Johnson, T.B. Richardson, M. Santarosa, K.J. Dillon, I. Hickson, C. Knights, N.M. Martin, S.P. Jackson, G.C. Smith, and A. Ashworth. 2005. Targeting the DNA repair defect in BRCA mutant cells as a therapeutic strategy. *Nature* 434:917-921.

Ferrari, K.J., A. Scelfo, S. Jammula, A. Cuomo, I. Barozzi, A. Stutzer, W. Fischle, T. Bonaldi, and D. Pasini. 2014. Polycomb-dependent H3K27me1 and H3K27me2 regulate active transcription and enhancer fidelity. *Molecular cell* 53:49-62.

Ferreira, P.G., P. Jares, D. Rico, G. Gomez-Lopez, A. Martinez-Trillos, N. Villamor, S. Ecker, A. Gonzalez-Perez, D.G. Knowles, J. Monlong, R. Johnson, V. Quesada, S. Djebali, P. Papasaikas, M. Lopez-Guerra, D. Colomer, C. Royo, M. Cazorla, M. Pinyol, G. Clot, M. Aymerich, M. Rozman, M. Kulis, D. Tamborero, A. Gouin, J. Blanc, M. Gut, I. Gut, X.S. Puente, D.G. Pisano, J.I. Martin-Subero, N. Lopez-Bigas, A. Lopez-Guillermo, A. Valencia, C. Lopez-Otin, E. Campo, and R. Guigo. 2014. Transcriptome characterization by RNA sequencing identifies a major molecular and clinical subdivision in chronic lymphocytic leukemia. *Genome research* 24:212-226.

Fischle, W., Y. Wang, S.A. Jacobs, Y. Kim, C.D. Allis, and S. Khorasanizadeh. 2003. Molecular basis for the discrimination of repressive methyl-lysine marks in histone H3 by Polycomb and HP1 chromodomains. *Genes & development* 17:1870-1881.

Fisher, C.L., J. Berger, F. Randazzo, and H.W. Brock. 2003. A human homolog of Additional sex combs, ADDITIONAL SEX COMBS-LIKE 1, maps to chromosome 20q11. *Gene* 306:115-126.

Fisher, C.L., F. Randazzo, R.K. Humphries, and H.W. Brock. 2006. Characterization of Asxl1, a murine homolog of Additional sex combs, and analysis of the Asx-like gene family. *Gene* 369:109-118.

Fong, P.C., D.S. Boss, T.A. Yap, A. Tutt, P. Wu, M. Mergui-Roelvink, P. Mortimer, H. Swaisland, A. Lau, M.J. O'Connor, A. Ashworth, J. Carmichael, S.B. Kaye, J.H. Schellens, and J.S. de Bono. 2009. Inhibition of poly(ADP-ribose) polymerase in tumors from BRCA mutation carriers. *The New England journal of medicine* 361:123-134.

Furman, R.R., S. Cheng, P. Lu, M. Setty, A.R. Perez, A. Guo, J. Racchumi, G. Xu, H. Wu, J. Ma, S.M. Steggerda, M. Coleman, C. Leslie, and Y.L. Wang. 2014. Ibrutinib resistance in chronic lymphocytic leukemia. *The New England journal of medicine* 370:2352-2354.

Gao, Z., J. Zhang, R. Bonasio, F. Strino, A. Sawai, F. Parisi, Y. Kluger, and D. Reinberg. 2012. PCGF homologs, CBX proteins, and RYBP define functionally distinct PRC1 family complexes. *Molecular cell* 45:344-356.

Gelsi-Boyer, V., V. Trouplin, J. Adelaide, J. Bonansea, N. Cervera, N. Carbuccia, A. Lagarde, T. Prebet, M. Nezri, D. Sainty, S. Olschwang, L. Xerri, M. Chaffanet, M.J. Mozziconacci, N. Vey, and D. Birnbaum. 2009. Mutations of polycomb-associated gene ASXL1 in myelodysplastic syndromes and chronic myelomonocytic leukaemia. *British journal of haematology* 145:788-800.

Ghia, P., N. Chiorazzi, and K. Stamatopoulos. 2008. Microenvironmental influences in chronic lymphocytic leukaemia: the role of antigen stimulation. *Journal of internal medicine* 264:549-562.

Grasso, C.S., Y.M. Wu, D.R. Robinson, X. Cao, S.M. Dhanasekaran, A.P. Khan, M.J. Quist, X. Jing, R.J. Lonigro, J.C. Brenner, I.A. Asangani, B. Ateeq, S.Y. Chun, J. Siddiqui, L. Sam, M. Anstett, R. Mehra, J.R. Prensner, N. Palanisamy, G.A. Ryslik, F. Vandin, B.J. Raphael, L.P. Kunju, D.R. Rhodes, K.J. Pienta, A.M. Chinnaiyan, and S.A. Tomlins. 2012. The mutational landscape of lethal castration-resistant prostate cancer. *Nature* 487:239-243.

Greenberg, P.L., E. Attar, J.M. Bennett, C.D. Bloomfield, C.M. De Castro, H.J. Deeg, J.M. Foran, K. Gaensler, G. Garcia-Manero, S.D. Gore, D. Head, R. Komrokji, L.J. Maness, M. Millenson, S.D. Nimer, M.R. O'Donnell, M.A. Schroeder, P.J. Shami, R.M. Stone, J.E. Thompson, P. Westervelt, and N. National Comprehensive Cancer. 2011. NCCN Clinical Practice Guidelines in Oncology: myelodysplastic syndromes. *Journal of the National Comprehensive Cancer Network : JNCCN* 9:30-56.

Gu, Z., Y. Liu, F. Cai, M. Patrick, J. Zmajkovic, H. Cao, Y. Zhang, A. Tasdogan, M. Chen, L. Qi, X. Liu, K. Li, J. Lyu, K.E. Dickerson, W. Chen, M. Ni, M.E. Merritt, S.J. Morrison, R.C. Skoda, R.J. DeBerardinis, and J. Xu. 2019. Loss of EZH2 Reprograms BCAA Metabolism to Drive Leukemic Transformation. *Cancer discovery*

Guo, A., P. Lu, N. Galanina, C. Nabhan, S.M. Smith, M. Coleman, and Y.L. Wang. 2016. Heightened BTK-dependent cell proliferation in unmutated chronic lymphocytic leukemia confers increased sensitivity to ibrutinib. *Oncotarget* 7:4598-4610.

Guo, Y., Y. Zhou, S. Yamatomo, H. Yang, P. Zhang, S. Chen, S.D. Nimer, Z.J. Zhao, M. Xu, J. Bai, and F.C. Yang. 2019. ASXL1 alteration cooperates with JAK2V617F to accelerate myelofibrosis. *Leukemia* 33:1287-1291.

Hamblin, T.J., Z. Davis, A. Gardiner, D.G. Oscier, and F.K. Stevenson. 1999. Unmutated Ig V(H) genes are associated with a more aggressive form of chronic lymphocytic leukemia. *Blood* 94:1848-1854.

Hansen, K.H., A.P. Bracken, D. Pasini, N. Dietrich, S.S. Gehani, A. Monrad, J. Rappsilber, M. Lerdrup, and K. Helin. 2008. A model for transmission of the H3K27me3 epigenetic mark. *Nature cell biology* 10:1291-1300.

Heinig, K., M. Gatjen, M. Grau, V. Stache, I. Anagnostopoulos, K. Gerlach, R.A. Niesner, Z. Cseresnyes, A.E. Hauser, P. Lenz, T. Hehlgans, R. Brink, J. Westermann, B. Dorken, M. Lipp, G. Lenz, A. Rehm, and U.E. Hopken. 2014. Access to follicular dendritic cells is a pivotal step in murine chronic lymphocytic leukemia B-cell activation and proliferation. *Cancer discovery* 4:1448-1465.

Helleday, T. 2003. Pathways for mitotic homologous recombination in mammalian cells. *Mutation research* 532:103-115.

Helleday, T. 2011. The underlying mechanism for the PARP and BRCA synthetic lethality: clearing up the misunderstandings. *Molecular oncology* 5:387-393.

Herman, S.E., C.U. Niemann, M. Farooqui, J. Jones, R.Z. Mustafa, A. Lipsky, N. Saba, S. Martyr, S. Soto, J. Valdez, J.A. Gyamfi, I. Maric, K.R. Calvo, L.B. Pedersen, C.H. Geisler, D. Liu, G.E. Marti, G. Aue, and A. Wiestner. 2014. Ibrutinib-induced lymphocytosis in patients with chronic lymphocytic leukemia: correlative analyses from a phase II study. *Leukemia* 28:2188-2196.

Hu, D., and A. Shilatifard. 2016. Epigenetics of hematopoiesis and hematological malignancies. *Genes & development* 30:2021-2041.

Huang da, W., B.T. Sherman, and R.A. Lempicki. 2009. Bioinformatics enrichment tools: paths toward the comprehensive functional analysis of large gene lists. *Nucleic acids research* 37:1-13.

Huber, W., V.J. Carey, R. Gentleman, S. Anders, M. Carlson, B.S. Carvalho, H.C. Bravo, S. Davis, L. Gatto, T. Girke, R. Gottardo, F. Hahne, K.D. Hansen, R.A. Irizarry, M. Lawrence, M.I. Love, J. MacDonald, V. Obenchain, A.K. Oles, H. Pages, A. Reyes, P. Shannon, G.K. Smyth, D. Tenenbaum, L. Waldron, and M. Morgan. 2015. Orchestrating high-throughput genomic analysis with Bioconductor. *Nature methods* 12:115-121.

Hurov, K.E., C. Cotta-Ramusino, and S.J. Elledge. 2010. A genetic screen identifies the Triple T complex required for DNA damage signaling and ATM and ATR stability. *Genes & development* 24:1939-1950.

Illingworth, R.S., M. Moffat, A.R. Mann, D. Read, C.J. Hunter, M.M. Pradeepa, I.R. Adams, and W.A. Bickmore. 2015. The E3 ubiquitin ligase activity of RING1B is not essential for early mouse development. *Genes & development* 29:1897-1902.

Inoue, D., J. Kitaura, K. Togami, K. Nishimura, Y. Enomoto, T. Uchida, Y. Kagiyama, K.C. Kawabata, F. Nakahara, K. Izawa, T. Oki, A. Maehara, M. Isobe, A. Tsuchiya, Y. Harada, H. Harada, T. Ochiya, H. Aburatani, H. Kimura, F. Thol, M. Heuser, R.L. Levine, O. Abdel-Wahab, and T. Kitamura. 2013. Myelodysplastic syndromes are induced by histone methylation-altering ASXL1 mutations. *The Journal of clinical investigation* 123:4627-4640.

Iwama, A. 2017. Polycomb repressive complexes in hematological malignancies. *Blood* 130:23-29.

Johnson, A.J., D.M. Lucas, N. Muthusamy, L.L. Smith, R.B. Edwards, M.D. De Lay, C.M. Croce, M.R. Grever, and J.C. Byrd. 2006. Characterization of the TCL-1 transgenic mouse as a preclinical drug development tool for human chronic lymphocytic leukemia. *Blood* 108:1334-1338.

Johnson, T.A., L.Z. Rassenti, and T.J. Kipps. 1997. Ig VH1 genes expressed in B cell chronic lymphocytic leukemia exhibit distinctive molecular features. *Journal of immunology* 158:235-246.

Jones, A.V., S. Kreil, K. Zoi, K. Waghorn, C. Curtis, L. Zhang, J. Score, R. Seear, A.J. Chase, F.H. Grand, H. White, C. Zoi, D. Loukopoulos, E. Terpos, E.C. Vervessou, B. Schultheis, M. Emig, T. Ernst, E. Lengfelder, R. Hehlmann, A. Hochhaus, D. Oscier, R.T. Silver, A. Reiter, and N.C. Cross. 2005. Widespread occurrence of the JAK2 V617F mutation in chronic myeloproliferative disorders. *Blood* 106:2162-2168.

Jung, H.R., D. Pasini, K. Helin, and O.N. Jensen. 2010. Quantitative mass spectrometry of histones H3.2 and H3.3 in Suz12-deficient mouse embryonic stem cells reveals distinct, dynamic post-translational modifications at Lys-27 and Lys-36. *Molecular & cellular proteomics : MCP* 9:838-850.

Jung, H.R., S. Sidoli, S. Haldbo, R.R. Sprenger, V. Schwammle, D. Pasini, K. Helin, and O.N. Jensen. 2013. Precision mapping of coexisting modifications in histone H3 tails from embryonic stem cells by ETD-MS/MS. *Analytical chemistry* 85:8232-8239.

Kim, D., G. Pertea, C. Trapnell, H. Pimentel, R. Kelley, and S.L. Salzberg. 2013. TopHat2: accurate alignment of transcriptomes in the presence of insertions, deletions and gene fusions. *Genome biology* 14:R36.

Kipps, T.J., F.K. Stevenson, C.J. Wu, C.M. Croce, G. Packham, W.G. Wierda, S. O'Brien, J. Gribben, and K. Rai. 2017. Chronic lymphocytic leukaemia. *Nature reviews. Disease primers* 3:17008.

Klein, U., M. Lia, M. Crespo, R. Siegel, Q. Shen, T. Mo, A. Ambesi-Impiombato, A. Califano, A. Migliazza, G. Bhagat, and R. Dalla-Favera. 2010. The DLEU2/miR-15a/16-1 cluster controls B cell proliferation and its deletion leads to chronic lymphocytic leukemia. *Cancer cell* 17:28-40.

Knittel, G., T. Rehkamper, D. Korovkina, P. Liedgens, C. Fritz, A. Torgovnick, Y. Al-Baldawi, M. Al-Maarri, Y. Cun, O. Fedorchenko, A. Riabinska, F. Beleggia, P.H. Nguyen, F.T. Wunderlich, M. Ortmann, M. Montesinos-Rongen, E. Tausch, S. Stilgenbauer, P.F. L, M. Herling, C. Herling, J. Bahlo, M. Hallek, M. Peifer, R. Buettner, T. Persigehl, and H.C. Reinhardt. 2017. Two mouse models reveal an actionable PARP1 dependence in aggressive chronic lymphocytic leukemia. *Nature communications* 8:153.

Ku, M., R.P. Koche, E. Rheinbay, E.M. Mendenhall, M. Endoh, T.S. Mikkelsen, A. Presser, C. Nusbaum, X. Xie, A.S. Chi, M. Adli, S. Kasif, L.M. Ptaszek, C.A. Cowan, E.S. Lander, H. Koseki, and B.E. Bernstein. 2008. Genomewide analysis of PRC1 and PRC2 occupancy identifies two classes of bivalent domains. *PLoS genetics* 4:e1000242.

Kuzmichev, A., K. Nishioka, H. Erdjument-Bromage, P. Tempst, and D. Reinberg. 2002. Histone methyltransferase activity associated with a human multiprotein complex containing the Enhancer of Zeste protein. *Genes & development* 16:2893-2905.

Lam, K.P., R. Kuhn, and K. Rajewsky. 1997. In vivo ablation of surface immunoglobulin on mature B cells by inducible gene targeting results in rapid cell death. *Cell* 90:1073-1083.

Lanham, S., T. Hamblin, D. Oscier, R. Ibbotson, F. Stevenson, and G. Packham. 2003. Differential signaling via surface IgM is associated with VH gene mutational status and CD38 expression in chronic lymphocytic leukemia. *Blood* 101:1087-1093.

Laugesen, A., and K. Helin. 2014. Chromatin repressive complexes in stem cells, development, and cancer. *Cell stem cell* 14:735-751.

Laugesen, A., J.W. Hojfeldt, and K. Helin. 2016. Role of the Polycomb Repressive Complex 2 (PRC2) in Transcriptional Regulation and Cancer. *Cold Spring Harbor perspectives in medicine* 6:

Li, L., and H. Clevers. 2010. Coexistence of quiescent and active adult stem cells in mammals. *Science* 327:542-545.

Majumder, S., K. Thieme, S.N. Batchu, T.A. Alghamdi, B.B. Bowskill, M.G. Kabir, Y. Liu, S.L. Advani, K.E. White, L. Geldenhuys, K.K. Tennankore, P. Poyah, F.S. Siddiqi, and A. Advani. 2018. Shifts in podocyte histone H3K27me3 regulate mouse and human glomerular disease. *The Journal of clinical investigation* 128:483-499.

Margueron, R., G. Li, K. Sarma, A. Blais, J. Zavadil, C.L. Woodcock, B.D. Dynlacht, and D. Reinberg. 2008. Ezh1 and Ezh2 maintain repressive chromatin through different mechanisms. *Molecular cell* 32:503-518.

Margueron, R., and D. Reinberg. 2011. The Polycomb complex PRC2 and its mark in life. *Nature* 469:343-349.

Marionneaux, S., P. Maslak, and E.M. Keohane. 2014. Morphologic identification of atypical chronic lymphocytic leukemia by digital microscopy. *International journal of laboratory hematology* 36:459-464.

Marti, G.E., A.C. Rawstron, P. Ghia, P. Hillmen, R.S. Houlston, N. Kay, T.A. Schleinitz, N. Caporaso, and C.L.L.C. International Familial. 2005. Diagnostic criteria for monoclonal B-cell lymphocytosis. *British journal of haematology* 130:325-332.

Micol, J.B., and O. Abdel-Wahab. 2016. The Role of Additional Sex Combs-Like Proteins in Cancer. *Cold Spring Harbor perspectives in medicine* 6:

Min, J., Y. Zhang, and R.M. Xu. 2003. Structural basis for specific binding of Polycomb chromodomain to histone H3 methylated at Lys 27. *Genes & development* 17:1823-1828.

Mochizuki-Kashio, M., K. Aoyama, G. Sashida, M. Oshima, T. Tomioka, T. Muto, C. Wang, and A. Iwama. 2015. Ezh2 loss in hematopoietic stem cells predisposes mice to develop heterogeneous malignancies in an Ezh1-dependent manner. *Blood* 126:1172-1183.

Montgomery, N.D., D. Yee, A. Chen, S. Kalantry, S.J. Chamberlain, A.P. Otte, and T. Magnuson. 2005. The murine polycomb group protein Eed is required for global histone H3 lysine-27 methylation. *Current biology : CB* 15:942-947.

Montgomery, N.D., D. Yee, S.A. Montgomery, and T. Magnuson. 2007. Molecular and functional mapping of EED motifs required for PRC2-dependent histone methylation. *Journal of molecular biology* 374:1145-1157.

Moon, S., S.K. Im, N. Kim, H. Youn, U.H. Park, J.Y. Kim, A.R. Kim, S.J. An, J.H. Kim, W. Sun, J.T. Hwang, E.J. Kim, and S.J. Um. 2018. Asxl1 exerts an antiproliferative effect on mouse lung maturation via epigenetic repression of the E2f1-Nmyc axis. *Cell death & disease* 9:1118.

Morin, R.D., N.A. Johnson, T.M. Severson, A.J. Mungall, J. An, R. Goya, J.E. Paul, M. Boyle, B.W. Woolcock, F. Kuchenbauer, D. Yap, R.K. Humphries, O.L. Griffith, S. Shah, H. Zhu, M. Kimbara, P. Shashkin, J.F. Charlot, M. Tcherpakov, R. Corbett, A. Tam, R. Varhol, D. Smailus, M. Moksa, Y. Zhao, A. Delaney, H. Qian, I. Birol, J. Schein, R. Moore, R. Holt, D.E. Horsman, J.M. Connors, S. Jones, S. Aparicio, M. Hirst, R.D. Gascoyne, and M.A. Marra. 2010. Somatic mutations altering EZH2 (Tyr641) in follicular and diffuse large B-cell lymphomas of germinal-center origin. *Nature genetics* 42:181-185.

Morin, R.D., M. Mendez-Lago, A.J. Mungall, R. Goya, K.L. Mungall, R.D. Corbett, N.A. Johnson, T.M. Severson, R. Chiu, M. Field, S. Jackman, M. Krzywinski, D.W. Scott, D.L. Trinh, J. Tamura-Wells, S. Li, M.R. Firme, S. Rogic, M. Griffith, S. Chan, O. Yakovenko, I.M. Meyer, E.Y. Zhao, D. Smailus, M. Moksa, S. Chittaranjan, L. Rimsza, A. Brooks-Wilson, J.J. Spinelli, S. Ben-Neriah, B. Meissner, B. Woolcock, M. Boyle, H. McDonald, A. Tam, Y. Zhao, A. Delaney, T. Zeng, K. Tse, Y. Butterfield, I. Birol, R. Holt, J. Schein, D.E. Horsman, R. Moore, S.J. Jones, J.M. Connors, M. Hirst, R.D. Gascoyne, and M.A. Marra. 2011. Frequent mutation of histone-modifying genes in non-Hodgkin lymphoma. *Nature* 476:298-303.

Mufti, G.J. 2004. Pathobiology, classification, and diagnosis of myelodysplastic syndrome. *Best practice & research. Clinical haematology* 17:543-557.

Muller, J., C.M. Hart, N.J. Francis, M.L. Vargas, A. Sengupta, B. Wild, E.L. Miller, M.B. O'Connor, R.E. Kingston, and J.A. Simon. 2002. Histone methyltransferase activity of a Drosophila Polycomb group repressor complex. *Cell* 111:197-208.

Murati, A., M. Brecqueville, R. Devillier, M.J. Mozziconacci, V. Gelsi-Boyer, and D. Birnbaum. 2012. Myeloid malignancies: mutations, models and management. *BMC cancer* 12:304.

Muto, T., G. Sashida, M. Oshima, G.R. Wendt, M. Mochizuki-Kashio, Y. Nagata, M. Sanada, S. Miyagi, A. Saraya, A. Kamio, G. Nagae, C. Nakaseko, K. Yokote, K. Shimoda, H. Koseki, Y. Suzuki, S. Sugano, H. Aburatani, S. Ogawa, and A. Iwama. 2013. Concurrent loss of Ezh2 and Tet2 cooperates in the pathogenesis of myelodysplastic disorders. *The Journal of experimental medicine* 210:2627-2639.

Narducci, M.G., A. Stoppacciaro, K. Imada, T. Uchiyama, L. Virgilio, C. Lazzeri, C.M. Croce, and G. Russo. 1997. TCL1 is overexpressed in patients affected by adult T-cell leukemias. *Cancer research* 57:5452-5456.

Neff, T., A.U. Sinha, M.J. Kluk, N. Zhu, M.H. Khattab, L. Stein, H. Xie, S.H. Orkin, and S.A. Armstrong. 2012. Polycomb repressive complex 2 is required for MLL-AF9 leukemia. *Proceedings of the National Academy of Sciences of the United States of America* 109:5028-5033.

Nikoloski, G., S.M. Langemeijer, R.P. Kuiper, R. Knops, M. Massop, E.R. Tonnissen, A. van der Heijden, T.N. Scheele, P. Vandenberghe, T. de Witte, B.A. van der Reijden, and J.H. Jansen. 2010. Somatic mutations of the histone methyltransferase gene EZH2 in myelodysplastic syndromes. *Nature genetics* 42:665-667.

Ntziachristos, P., A. Tsirigos, P. Van Vlierberghe, J. Nedjic, T. Trimarchi, M.S. Flaherty, D. Ferres-Marco, V. da Ros, Z. Tang, J. Siegle, P. Asp, M. Hadler, I. Rigo, K. De Keersmaecker, J. Patel, T. Huynh, F. Utro, S. Poglio, J.B. Samon, E. Paietta, J. Racevskis, J.M. Rowe, R. Rabadan, R.L. Levine, S. Brown, F. Pflumio, M. Dominguez, A. Ferrando, and I. Aifantis. 2012. Genetic inactivation of the polycomb repressive complex 2 in T cell acute lymphoblastic leukemia. *Nature medicine* 18:298-301.

Oeck, S., N.M. Malewicz, S. Hurst, K. Al-Refae, A. Krysztofiak, and V. Jendrossek. 2017. The Focinator v2-0 - Graphical Interface, Four Channels, Colocalization Analysis and Cell Phase Identification. *Radiation research* 188:114-120.

Oeck, S., N.M. Malewicz, S. Hurst, J. Rudner, and V. Jendrossek. 2015. The Focinator - a new open-source tool for high-throughput foci evaluation of DNA damage. *Radiation oncology* 10:163.

Orazi, A., and U. Germing. 2008. The myelodysplastic/myeloproliferative neoplasms: myeloproliferative diseases with dysplastic features. *Leukemia* 22:1308-1319.

Orsi, G.A., S. Kasinathan, K.T. Hughes, S. Saminadin-Peter, S. Henikoff, and K. Ahmad. 2014. High-resolution mapping defines the cooperative architecture of Polycomb response elements. *Genome research* 24:809-820.

Oscier, D. 1997. Atypical chronic myeloid leukemias. *Pathologie-biologie* 45:587-593.

Oscier, D.G., A. Gardiner, and S. Mould. 1996. Structural abnormalities of chromosome 7q in chronic lymphoproliferative disorders. *Cancer genetics and cytogenetics* 92:24-27.

Palacios, F., P. Moreno, P. Morande, C. Abreu, A. Correa, V. Porro, A.I. Landoni, R. Gabus, M. Giordano, G. Dighiero, O. Pritsch, and P. Oppezzo. 2010. High expression of AID and active class switch recombination might account for a more aggressive disease in unmutated CLL patients: link with an activated microenvironment in CLL disease. *Blood* 115:4488-4496.

Pasini, D., A.P. Bracken, M.R. Jensen, E. Lazzerini Denchi, and K. Helin. 2004. Suz12 is essential for mouse development and for EZH2 histone methyltransferase activity. *The EMBO journal* 23:4061-4071.

Patnaik, M.M., R. Vallapureddy, T.L. Lasho, K.P. Hoversten, C.M. Finke, R. Ketterling, C. Hanson, N. Gangat, and A. Tefferi. 2018. EZH2 mutations in chronic myelomonocytic leukemia cluster with ASXL1 mutations and their co-occurrence is prognostically detrimental. *Blood cancer journal* 8:12.

Patten, P.E., C.C. Chu, E. Albesiano, R.N. Damle, X.J. Yan, D. Kim, L. Zhang, A.R. Magli, J. Barrientos, J.E. Kolitz, S.L. Allen, K.R. Rai, S. Roa, P.K. Mongini, T. MacCarthy, M.D. Scharff, and N. Chiorazzi. 2012. IGHV-unmutated and IGHV-mutated chronic lymphocytic leukemia cells produce activation-induced deaminase protein with a full range of biologic functions. *Blood* 120:4802-4811.

Pengelly, A.R., O. Copur, H. Jackle, A. Herzig, and J. Muller. 2013. A histone mutant reproduces the phenotype caused by loss of histone-modifying factor Polycomb. *Science* 339:698-699.

Pengelly, A.R., R. Kalb, K. Finkl, and J. Muller. 2015. Transcriptional repression by PRC1 in the absence of H2A monoubiquitylation. *Genes & development* 29:1487-1492.

Peters, A.H., S. Kubicek, K. Mechtler, R.J. O'Sullivan, A.A. Derijck, L. Perez-Burgos, A. Kohlmaier, S. Opravil, M. Tachibana, Y. Shinkai, J.H. Martens, and T. Jenuwein. 2003. Partitioning and plasticity of repressive histone methylation states in mammalian chromatin. *Molecular cell* 12:1577-1589.

Pietras, E.M., D. Reynaud, Y.A. Kang, D. Carlin, F.J. Calero-Nieto, A.D. Leavitt, J.M. Stuart, B. Gottgens, and E. Passegue. 2015. Functionally Distinct Subsets of Lineage-Biased Multipotent Progenitors Control Blood Production in Normal and Regenerative Conditions. *Cell stem cell* 17:35-46.

Planelles, L., C.E. Carvalho-Pinto, G. Hardenberg, S. Smaniotto, W. Savino, R. Gomez-Caro, M. Alvarez-Mon, J. de Jong, E. Eldering, A.C. Martinez, J.P. Medema, and M. Hahne. 2004. APRIL promotes B-1 cell-associated neoplasm. *Cancer cell* 6:399-408.

Pleasance, E.D., R.K. Cheetham, P.J. Stephens, D.J. McBride, S.J. Humphray, C.D. Greenman, I. Varela, M.L. Lin, G.R. Ordonez, G.R. Bignell, K. Ye, J. Alipaz, M.J. Bauer, D. Beare, A. Butler, R.J. Carter, L. Chen, A.J. Cox, S. Edkins, P.I. Kokko-Gonzales, N.A. Gormley, R.J. Grocock, C.D. Haudenschild, M.M. Hims, T. James, M. Jia, Z. Kingsbury, C. Leroy, J. Marshall, A. Menzies, L.J. Mudie, Z. Ning, T. Royce, O.B. Schulz-Trieglaff, A. Spiridou, L.A. Stebbings, L. Szajkowski, J. Teague, D. Williamson, L. Chin, M.T. Ross, P.J. Campbell, D.R. Bentley, P.A. Futreal, and M.R. Stratton. 2010. A comprehensive catalogue of somatic mutations from a human cancer genome. *Nature* 463:191-196.

Ponader, S., S.S. Chen, J.J. Buggy, K. Balakrishnan, V. Gandhi, W.G. Wierda, M.J. Keating, S. O'Brien, N. Chiorazzi, and J.A. Burger. 2012. The Bruton tyrosine kinase inhibitor PCI-32765 thwarts chronic lymphocytic leukemia cell survival and tissue homing in vitro and in vivo. *Blood* 119:1182-1189.

Puente, X.S., S. Bea, R. Valdes-Mas, N. Villamor, J. Gutierrez-Abril, J.I. Martin-Subero, M. Munar, C. Rubio-Perez, P. Jares, M. Aymerich, T. Baumann, R. Beekman, L. Belver, A. Carrio, G. Castellano, G. Clot, E. Colado, D. Colomer, D. Costa, J. Delgado, A. Enjuanes, X. Estivill, A.A. Ferrando, J.L. Gelpi, B. Gonzalez, S. Gonzalez, M. Gonzalez, M. Gut, J.M. Hernandez-Rivas, M. Lopez-Guerra, D. Martin-Garcia, A. Navarro, P. Nicolas, M. Orozco, A.R. Payer, M. Pinyol, D.G. Pisano, D.A. Puente, A.C. Queiros, V. Quesada, C.M. Romeo-Casabona, C. Royo, R. Royo, M. Rozman, N. Russinol, I. Salaverria, K. Stamatopoulos, H.G. Stunnenberg, D. Tamborero, M.J. Terol, A. Valencia, N. Lopez-Bigas, D. Torrents, I. Gut, A. Lopez-Guillermo, C. Lopez-Otin, and E. Campo. 2015. Non-coding recurrent mutations in chronic lymphocytic leukaemia. *Nature* 526:519-524.

Quesada, V., L. Conde, N. Villamor, G.R. Ordonez, P. Jares, L. Bassaganyas, A.J. Ramsay, S. Bea, M. Pinyol, A. Martinez-Trillos, M. Lopez-Guerra, D. Colomer, A. Navarro, T. Baumann, M. Aymerich, M. Rozman, J. Delgado, E. Gine, J.M. Hernandez, M. Gonzalez-Diaz, D.A. Puente, G. Velasco, J.M. Freije, J.M. Tubio, R. Royo, J.L. Gelpi, M. Orozco, D.G. Pisano, J. Zamora, M. Vazquez, A. Valencia, H. Himmelbauer, M. Bayes, S. Heath, M. Gut, I. Gut, X. Estivill, A. Lopez-Guillermo, X.S. Puente, E. Campo, and C. Lopez-Otin. 2011. Exome sequencing identifies recurrent mutations of the splicing factor SF3B1 gene in chronic lymphocytic leukemia. *Nature genetics* 44:47-52.

Rastelli, L., C.S. Chan, and V. Pirrotta. 1993. Related chromosome binding sites for zeste, suppressors of zeste and Polycomb group proteins in Drosophila and their dependence on Enhancer of zeste function. *The EMBO journal* 12:1513-1522.

Rayess, H., M.B. Wang, and E.S. Srivatsan. 2012. Cellular senescence and tumor suppressor gene p16. *International journal of cancer. Journal international du cancer* 130:1715-1725.

Rinke, J., J.P. Muller, M.F. Blaess, A. Chase, M. Meggendorfer, V. Schafer, N. Winkelmann, C. Haferlach, N.C.P. Cross, A. Hochhaus, and T. Ernst. 2017. Molecular characterization of EZH2 mutant patients with myelodysplastic/myeloproliferative neoplasms. *Leukemia* 31:1936-1943.

Roberts, A.W., M.S. Davids, J.M. Pagel, B.S. Kahl, S.D. Puvvada, J.F. Gerecitano, T.J. Kipps, M.A. Anderson, J.R. Brown, L. Gressick, S. Wong, M. Dunbar, M. Zhu, M.B. Desai, E. Cerri, S. Heitner Enschede, R.A. Humerickhouse, W.G. Wierda, and J.F. Seymour. 2016. Targeting BCL2 with Venetoclax in Relapsed Chronic Lymphocytic Leukemia. *The New England journal of medicine* 374:311-322.

Robinson, M.D., D.J. McCarthy, and G.K. Smyth. 2010. edgeR: a Bioconductor package for differential expression analysis of digital gene expression data. *Bioinformatics* 26:139-140.

Rocquain, J., N. Carbuccia, V. Trouplin, S. Raynaud, A. Murati, M. Nezri, Z. Tadrist, S. Olschwang, N. Vey, D. Birnbaum, V. Gelsi-Boyer, and M.J. Mozziconacci. 2010. Combined mutations of ASXL1, CBL, FLT3, IDH1, IDH2, JAK2, KRAS, NPM1, NRAS, RUNX1, TET2 and WT1 genes in myelodysplastic syndromes and acute myeloid leukemias. *BMC cancer* 10:401.

Sahtoe, D.D., W.J. van Dijk, R. Ekkebus, H. Ovaa, and T.K. Sixma. 2016. BAP1/ASXL1 recruitment and activation for H2A deubiquitination. *Nature communications* 7:10292.

Sanchez-Pulido, L., L. Kong, and C.P. Ponting. 2012. A common ancestry for BAP1 and Uch37 regulators. *Bioinformatics* 28:1953-1956.

Sashida, G., C. Wang, T. Tomioka, M. Oshima, K. Aoyama, A. Kanai, M. Mochizuki-Kashio, H. Harada, K. Shimoda, and A. Iwama. 2016. The loss of Ezh2 drives the pathogenesis of myelofibrosis and sensitizes tumor-initiating cells to bromodomain inhibition. *The Journal of experimental medicine* 213:1459-1477.

Satoh, M.S., and T. Lindahl. 1992. Role of poly(ADP-ribose) formation in DNA repair. *Nature* 356:356-358.

Scheuermann, J.C., A.G. de Ayala Alonso, K. Oktaba, N. Ly-Hartig, R.K. McGinty, S. Fraterman, M. Wilm, T.W. Muir, and J. Muller. 2010. Histone H2A deubiquitinase activity of the Polycomb repressive complex PR-DUB. *Nature* 465:243-247.

Scielzo, C., B. Apollonio, L. Scarfo, A. Janus, M. Muzio, E. Ten Hacken, P. Ghia, and F. Caligaris-Cappio. 2011. The functional in vitro response to CD40 ligation reflects a different clinical outcome in patients with chronic lymphocytic leukemia. *Leukemia* 25:1760-1767.

Shen, X., Y. Liu, Y.J. Hsu, Y. Fujiwara, J. Kim, X. Mao, G.C. Yuan, and S.H. Orkin. 2008. EZH1 mediates methylation on histone H3 lysine 27 and complements EZH2 in maintaining stem cell identity and executing pluripotency. *Molecular cell* 32:491-502.

Simonetti, G., M.T. Bertilaccio, P. Ghia, and U. Klein. 2014. Mouse models in the study of chronic lymphocytic leukemia pathogenesis and therapy. *Blood* 124:1010-1019.

Sinclair, D.A., T.A. Milne, J.W. Hodgson, J. Shellard, C.A. Salinas, M. Kyba, F. Randazzo, and H.W. Brock. 1998. The Additional sex combs gene of Drosophila encodes a chromatin protein that binds to shared and unique Polycomb group sites on polytene chromosomes. *Development* 125:1207-1216.

Sneeringer, C.J., M.P. Scott, K.W. Kuntz, S.K. Knutson, R.M. Pollock, V.M. Richon, and R.A. Copeland. 2010. Coordinated activities of wild-type plus mutant EZH2 drive tumor-associated hypertrimethylation of lysine 27 on histone H3 (H3K27) in human B-cell lymphomas. *Proceedings of the National Academy of Sciences of the United States of America* 107:20980-20985.

Stavnezer, J., J.E. Guikema, and C.E. Schrader. 2008. Mechanism and regulation of class switch recombination. *Annual review of immunology* 26:261-292.

Strati, P., and T.D. Shanafelt. 2015. Monoclonal B-cell lymphocytosis and early-stage chronic lymphocytic leukemia: diagnosis, natural history, and risk stratification. *Blood* 126:454-462.

Su, I.H., A. Basavaraj, A.N. Krutchinsky, O. Hobert, A. Ullrich, B.T. Chait, and A. Tarakhovsky. 2003. Ezh2 controls B cell development through histone H3 methylation and Igh rearrangement. *Nature immunology* 4:124-131.

Svotelis, A., S. Bianco, J. Madore, G. Huppe, A. Nordell-Markovits, A.M. Mes-Masson, and N. Gevry. 2011. H3K27 demethylation by JMJD3 at a poised enhancer of anti-apoptotic gene BCL2 determines ERalpha ligand dependency. *The EMBO journal* 30:3947-3961.

Swalm, B.M., S.K. Knutson, N.M. Warholic, L. Jin, K.W. Kuntz, H. Keilhack, J.J. Smith, R.M. Pollock, M.P. Moyer, M.P. Scott, R.A. Copeland, and T.J. Wigle. 2014. Reaction coupling between wild-type and disease-associated mutant EZH2. *ACS chemical biology* 9:2459-2464.

Swigut, T., and J. Wysocka. 2007. H3K27 demethylases, at long last. *Cell* 131:29-32.

Tanay, A., A.H. O'Donnell, M. Damelin, and T.H. Bestor. 2007. Hyperconserved CpG domains underlie Polycomb-binding sites. *Proceedings of the National Academy of Sciences of the United States of America* 104:5521-5526.

Tavares, L., E. Dimitrova, D. Oxley, J. Webster, R. Poot, J. Demmers, K. Bezstarosti, S. Taylor, H. Ura, H. Koide, A. Wutz, M. Vidal, S. Elderkin, and N. Brockdorff. 2012. RYBP-PRC1 complexes mediate H2A ubiquitylation at polycomb target sites independently of PRC2 and H3K27me3. *Cell* 148:664-678.

Tefferi, A., T.L. Lasho, and G. Gilliland. 2005. JAK2 mutations in myeloproliferative disorders. *The New England journal of medicine* 353:1416-1417; author reply 1416-1417.

ten Hacken, E., and J.A. Burger. 2014. Molecular pathways: targeting the microenvironment in chronic lymphocytic leukemia--focus on the B-cell receptor. *Clinical cancer research : an official journal of the American Association for Cancer Research* 20:548-556.

Thol, F., I. Friesen, F. Damm, H. Yun, E.M. Weissinger, J. Krauter, K. Wagner, A. Chaturvedi, A. Sharma, M. Wichmann, G. Gohring, C. Schumann, G. Bug, O. Ottmann, W.K. Hofmann, B. Schlegelberger, M. Heuser, and A. Ganser. 2011. Prognostic significance of ASXL1 mutations in patients with myelodysplastic syndromes. *Journal of clinical oncology : official journal of the American Society of Clinical Oncology* 29:2499-2506.

Tobin, G., U. Thunberg, A. Johnson, I. Eriksson, O. Soderberg, K. Karlsson, M. Merup, G. Juliusson, J. Vilpo, G. Enblad, C. Sundstrom, G. Roos, and R. Rosenquist. 2003. Chronic lymphocytic leukemias utilizing the VH3-21 gene display highly restricted

Vlambda2-14 gene use and homologous CDR3s: implicating recognition of a common antigen epitope. *Blood* 101:4952-4957.

Tobin, G., U. Thunberg, A. Johnson, I. Thorn, O. Soderberg, M. Hultdin, J. Botling, G. Enblad, J. Sallstrom, C. Sundstrom, G. Roos, and R. Rosenquist. 2002. Somatically mutated Ig V(H)3-21 genes characterize a new subset of chronic lymphocytic leukemia. *Blood* 99:2262-2264.

Triviai, I., S. Zeschke, J. Rentel, M. Spanakis, T. Scherer, R. Gabdoulline, V. Panagiota, F. Thol, M. Heuser, C. Stocking, and N. Kroger. 2019. ASXL1/EZH2 mutations promote clonal expansion of neoplastic HSC and impair erythropoiesis in PMF. *Leukemia* 33:99-109.

Vardiman, J.W., J. Thiele, D.A. Arber, R.D. Brunning, M.J. Borowitz, A. Porwit, N.L. Harris, M.M. Le Beau, E. Hellstrom-Lindberg, A. Tefferi, and C.D. Bloomfield. 2009. The 2008 revision of the World Health Organization (WHO) classification of myeloid neoplasms and acute leukemia: rationale and important changes. *Blood* 114:937-951.

Virgilio, L., C. Lazzeri, R. Bichi, K. Nibu, M.G. Narducci, G. Russo, J.L. Rothstein, and C.M. Croce. 1998. Deregulated expression of TCL1 causes T cell leukemia in mice. *Proceedings of the National Academy of Sciences of the United States of America* 95:3885-3889.

Virgilio, L., M.G. Narducci, M. Isobe, L.G. Billips, M.D. Cooper, C.M. Croce, and G. Russo. 1994. Identification of the TCL1 gene involved in T-cell malignancies. *Proceedings of the National Academy of Sciences of the United States of America* 91:12530-12534.

Wang, L., J.L. Brown, R. Cao, Y. Zhang, J.A. Kassis, and R.S. Jones. 2004. Hierarchical recruitment of polycomb group silencing complexes. *Molecular cell* 14:637-646.

Wang, L., M.S. Lawrence, Y. Wan, P. Stojanov, C. Sougnez, K. Stevenson, L. Werner, A. Sivachenko, D.S. DeLuca, L. Zhang, W. Zhang, A.R. Vartanov, S.M. Fernandes, N.R. Goldstein, E.G. Folco, K. Cibulskis, B. Tesar, Q.L. Sievers, E. Shefler, S. Gabriel, N. Hacohen, R. Reed, M. Meyerson, T.R. Golub, E.S. Lander, D. Neuberg, J.R. Brown, G. Getz, and C.J. Wu. 2011. SF3B1 and other novel cancer genes in chronic lymphocytic leukemia. *The New England journal of medicine* 365:2497-2506.

Weston, V.J., C.E. Oldreive, A. Skowronska, D.G. Oscier, G. Pratt, M.J. Dyer, G. Smith, J.E. Powell, Z. Rudzki, P. Kearns, P.A. Moss, A.M. Taylor, and T. Stankovic. 2010. The PARP inhibitor olaparib induces significant killing of ATM-deficient lymphoid tumor cells in vitro and in vivo. *Blood* 116:4578-4587.

White, H.N. 1998. Restriction-PCR fingerprinting of the immunoglobulin VH repertoire: direct detection of an immune response and global analysis of B cell clonality. *European journal of immunology* 28:3268-3279.

Widhopf, G.F., 2nd, and T.J. Kipps. 2001. Normal B cells express 51p1-encoded Ig heavy chains that are distinct from those expressed by chronic lymphocytic leukemia B cells. *Journal of immunology* 166:95-102.

Woloschak, G.E., and C.J. Krco. 1987. Regulation of kappa/lambda immunoglobulin light chain expression in normal murine lymphocytes. *Molecular immunology* 24:751-757.

Woyach, J.A., E. Bojnik, A.S. Ruppert, M.R. Stefanovski, V.M. Goettl, K.A. Smucker, L.L. Smith, J.A. Dubovsky, W.H. Towns, J. MacMurray, B.K. Harrington, M.E. Davis, S. Gobessi, L. Laurenti, B.Y. Chang, J.J. Buggy, D.G. Efremov, J.C. Byrd, and A.J. Johnson. 2014. Bruton's tyrosine kinase (BTK) function is important to the development and expansion of chronic lymphocytic leukemia (CLL). *Blood* 123:1207-1213.

Yamaguchi, H., Y. Du, K. Nakai, M. Ding, S.S. Chang, J.L. Hsu, J. Yao, Y. Wei, L. Nie, S. Jiao, W.C. Chang, C.H. Chen, Y. Yu, G.N. Hortobagyi, and M.C. Hung. 2018. EZH2 contributes to the response to PARP inhibitors through its PARP-mediated poly-ADP ribosylation in breast cancer. *Oncogene* 37:208-217.

Yan, X.J., E. Albesiano, N. Zanesi, S. Yancopoulos, A. Sawyer, E. Romano, A. Petlickovski, D.G. Efremov, C.M. Croce, and N. Chiorazzi. 2006. B cell receptors in TCL1 transgenic mice resemble those of aggressive, treatment-resistant human chronic lymphocytic leukemia. *Proceedings of the National Academy of Sciences of the United States of America* 103:11713-11718.

Yang, Y., H. Akada, D. Nath, R.E. Hutchison, and G. Mohi. 2016. Loss of Ezh2 cooperates with Jak2V617F in the development of myelofibrosis in a mouse model of myeloproliferative neoplasm. *Blood* 127:3410-3423.

Yap, D.B., J. Chu, T. Berg, M. Schapira, S.W. Cheng, A. Moradian, R.D. Morin, A.J. Mungall, B. Meissner, M. Boyle, V.E. Marquez, M.A. Marra, R.D. Gascoyne, R.K. Humphries, C.H. Arrowsmith, G.B. Morin, and S.A. Aparicio. 2011. Somatic mutations at EZH2 Y641 act dominantly through a mechanism of selectively altered PRC2 catalytic activity, to increase H3K27 trimethylation. *Blood* 117:2451-2459.

Yoshida, K., and Y. Miki. 2010. The cell death machinery governed by the p53 tumor suppressor in response to DNA damage. *Cancer science* 101:831-835.

Zanesi, N., R. Aqeilan, A. Drusco, M. Kaou, C. Sevignani, S. Costinean, L. Bortesi, G. La Rocca, P. Koldovsky, S. Volinia, R. Mancini, G. Calin, C.P. Scott, Y. Pekarsky, and C.M. Croce. 2006. Effect of rapamycin on mouse chronic lymphocytic leukemia and the development of nonhematopoietic malignancies in Emu-TCL1 transgenic mice. *Cancer research* 66:915-920.

Zapata, J.M., M. Krajewska, H.C. Morse, 3rd, Y. Choi, and J.C. Reed. 2004. TNF receptor-associated factor (TRAF) domain and Bcl-2 cooperate to induce small B cell lymphoma/chronic lymphocytic leukemia in transgenic mice. *Proceedings of the National Academy of Sciences of the United States of America* 101:16600-16605.

Zee, B.M., R.S. Levin, B. Xu, G. LeRoy, N.S. Wingreen, and B.A. Garcia. 2010. In vivo residue-specific histone methylation dynamics. *The Journal of biological chemistry* 285:3341-3350.

Zeisig, B.B., A.G. Kulasekararaj, G.J. Mufti, and C.W. So. 2012. SnapShot: Acute myeloid leukemia. *Cancer cell* 22:698-698 e691.

Zenz, T., D. Mertens, R. Kuppers, H. Dohner, and S. Stilgenbauer. 2010. From pathogenesis to treatment of chronic lymphocytic leukaemia. *Nature reviews. Cancer* 10:37-50.

Zhao, L., and C.W. So. 2016. PARP-inhibitor-induced synthetic lethality for acute myeloid leukemia treatment. *Experimental hematology* 44:902-907.

Zhou, T., M.C. Kinney, L.M. Scott, S.S. Zinkel, and V.I. Rebel. 2015. Revisiting the case for genetically engineered mouse models in human myelodysplastic syndrome research. *Blood* 126:1057-1068.